

Relative Timing of Uplift along the Zagros Mountain Front Flexure (Kurdistan Region of Iraq): Constrained by Geomorphic Indices and Landscape Evolution Modelling, Kurdistan Region of Iraq

Mjahid Zebari^{1,2}, Christoph Grützner¹, Payman Navabpour¹, Kamil Ustaszewski¹

5 ¹Institute of Geological Sciences, Friedrich-Schiller-University Jena, Jena, 07749, Germany

²Geology Department, Salahaddin University-Erbil, Erbil, 44002, Kurdistan Region of Iraq

Correspondence to: Mjahid Zebari (mjahid.zebari@uni-jena.de)

Abstract. The Mountain Front Flexure marks a dominant topographic step in the frontal part of the Zagros Fold-Thrust Belt. It is characterized by numerous active anticlines atop of ~~an underlying~~ a basement fault. So far, little is known about the relative activity of the anticlines, about their evolution, and about how crustal deformation migrates over time. We assessed the relative landscape maturity of three along-strike anticlines (from SE to NW: Harir, Perat, and Akre) located on the hanging wall of the Mountain Front Flexure in the Kurdistan Region of Iraq to identify the most active structures and to get insights into the evolution of the ~~fault-and-fold~~-thrust belt. Landscape maturity was evaluated using geomorphic indices such as hypsometric curves, hypsometric integral, surface roughness, and surface index. Subsequently, numerical landscape evolution models were run to estimate the relative time difference between the onset of growth of the ~~three~~ anticlines, using the present-day topography of the Harir Anticline as a base model. A stream power equation was used to introduce fluvial erosion, and a hillslope diffusion equation was applied to account for colluvial sediment transport. For different time steps of model evolution, we calculated the geomorphic indices generated from the base model. While Akre Anticline shows deeply incised valleys and advanced erosion, Harir and Perat anticlines have relatively smoother surfaces and are supposedly younger than the Akre Anticline. The landscape maturity level decreases from NW to SE. A comparison of the geomorphic indices of the model output to those of the present-day Akre Anticline topography revealed that it would take the Harir Anticline ~~70±10~~ about 80-100 kyr and 160-200±20 kyr to reach the maturity level of the Perat and Akre anticlines, respectively, assuming erosion under constant erosion conditions and constant rock uplift rates along the three anticlines. Since the factors controlling geomorphology (lithology, structural setting and climate) are similar for all three anticlines, and under the assumption of constant growth and erosion ~~rates~~ conditions, we infer that uplift of the Akre Anticline started ~~25-160-200±20~~ 160-200±20 kyr before that of the Harir Anticline, with the Perat Anticline showing an intermediate age. A NW-ward propagation of the Harir Anticline itself implies that the uplift has been independent within different segments ~~rather than being continuous from NW to SE~~. Our method of estimating the relative age difference can be applied to many other anticlines in the Mountain Front Flexure region to construct a model of temporal evolution of this belt.

30

1 Introduction

The Zagros Fold-Thrust Belt is an active orogen that resulted from the collision between the Arabian and Eurasian plates and contains the deformed portions of the NE part of the former Arabian passive margin (Fig. 1; ~~Alavi, 2007~~; Berberian, 1995; Mouthereau et al., 2012). Many aspects of the structural configuration and the evolution of the Zagros Fold-Thrust Belt are by now satisfactorily constrained, but the detailed spatial and temporal distribution of deformation across the belt is not yet well understood. This concerns especially in the NW part of the belt in the Kurdistan Region of Iraq (KRI) due to a lack of comprehensive studies and for geopolitical reasons that make access to the field challenging. The style, timing, and relative activity of front thrusts, deformation propagation, and along-strike variations have not been sufficiently studied, ~~and neither~~ It is it-not well-known well-known which structures are currently the most active ones either.

One of the morphologically most conspicuous structural elements of the Zagros Fold-Thrust Belt is the Mountain Front Flexure (MFF), which separates the High Folded Zone and the Foothill Zone (known in Iran as the Zagros Simply Folded Belt and Zagros Foredeep, respectively; Figs. 1 and 2; ~~Alavi, 2007~~; Berberian, 1995; Jassim and Goff, 2006; McQuarrie, 2004; Mouthereau et al., 2012; Vergés et al., 2011). In most parts of the Zagros, the MFF marks a pronounced topographic step, separating folds with high amplitudes, narrow wavelengths, and higher topography in the High Folded Zone from folds with relatively low amplitudes, long wavelengths, and lower topography in the Foothill Zone (Fig. 2). The MFF is characterized by numerous active anticlines atop of fault strands emerging from a basement fault. It was suggested that the onset of the MFF activity in the NW Zagros was about 5 ± 1 Ma based on low temperature thermochronology (Koshnaw et al., 2017). The timing of this activity is expected to differ along-strike the belt and, hence, the initiation of uplift of the anticlines on the hanging wall of the MFF is the key to understand this temporal and spatial evolution. In the neighbouring Iranian part, the MFF was a relatively long-lived structure active from 8.1 to 7.2 Ma to about the Pliocene-Pleistocene boundary. After that, only the southwesternmost anticline remained active in front of the MFF. This was inferred from progressive unconformities and magnetostratigraphy (Hessami et al., 2001, 2006; Homke et al., 2004).

In active orogens, the main factor that contributes to building up topography is ongoing convergence (Bishop, 2007; Burbank and Anderson, 2012; Whittaker, 2012). Recent advancements in the availability of high-resolution digital elevation models (DEMs) and GIS software allowed to quantitatively analyse the landscape (Bishop, 2007; Tarolli, 2014; ~~Waleott and Summerfield, 2008~~). Tectonic geomorphology approaches and landscape maturity studies have been used extensively and proven to be efficient in studying the relative tectonic activity of different areas in contractional settings (~~Allen et al., 2013~~; Cheng et al., 2012; Mahmood and Gloaguen, 2012; Ramsey et al., 2008; Regard et al., 2009). Nevertheless, the NW part of the Zagros lacks modern studies on tectonic geomorphology with few exceptions. Bretis et al. (2011) detected sets of wind gaps (i.e. segments of river valleys abandoned due to lateral and vertical fold growth) in the High Folded Belt, NE of the MFF, suggesting that larger folds grew by linkage of smaller, shorter folds. Zebari and Burberry (2015) performed detailed analyses of various geomorphic indices for numerous anticlines in the High Folded Zone, concluding that the combination of clearly asymmetric drainage patterns and the mountain front sinuosity index (Bull, 2007; Keller et al., 1999) is a valuable tool for

identifying putatively active fault-related folds. Obaid and Allen (2017) studied the landscape maturity of various anticlines within the Zagros Foothill Zone and constrained the order of deformation of these anticlines by proposing an out-of-sequence propagation of underlying faults into the foreland. They proposed that the Zagros Deformation Front was among the earliest faults that have been reactivated within the Foothill Zone.

5 In an active orogen such as the Zagros, a better understanding of the temporal and spatial distribution of deformation due to ongoing tectonics can be achieved with landscape modelling. In the last two decades, numerical models have been extensively used to study landscape evolution (Chen et al., 2014; Tucker and Hancock, 2010; ~~Valters, 2016; van der Beek, 2013~~) and several software packages were specifically developed for this purpose (~~Hancock et al., 2010; e.g.~~ Hancock and Willgoose, 2002; Hobley et al., 2017; Refice et al., 2012; Salles and Hardiman, 2016; Tucker et al., 2001). Most of these models include
10 algorithms for bedrock fluvial incision and hillslope creep as input parameters. Several studies have constrained the landscape evolution with the involvement of the corresponding tectonics and structures [elsewhere](#) (Collignon et al., 2016; Cowie et al., 2006; ~~Langston et al., 2015; Miller et al., 2007; Refice et al., 2012; Robl et al., 2008~~).
15 In this study, we assessed variations in the landscape maturity of three anticlines (from SE to NW, the Harir, Perat and Akre anticlines) located on the hanging wall of the MFF by quantitatively analysing landscape indices (hypsometric curve, hypsometric integral, surface roughness, and surface index) in order to distinguish more mature segments from less mature ones, and to reconstruct the relative variation of uplift time and/or rates along these anticlines. We then computed the difference in the onset of uplift between more mature anticlines and less mature ones using a landscape evolution model. The ~~present day~~[present-day](#) topography of the least mature anticline served as an input model for computing the time that it takes this anticline to reach the same state as the most mature ones. Also, three structural cross-sections were constructed across the
20 three anticlines to delineate their structural style and to link it with their landscape maturity.

2 Geological Setting

The Zagros Fold-Thrust Belt is the result of the collision between the Arabian and Eurasian plates (Fig. 1; ~~Alavi, 2007~~; Berberian, 1995; Mouthereau et al., 2012). Continental collision started in the Early Miocene following the progressive subduction of Neo-Tethyan oceanic lithosphere underneath Eurasia (Agard et al., 2011; Csontos et al., 2012; Koshnaw et al.,
25 2017; Mouthereau et al., 2012). The Zagros Fold-Thrust Belt extends for about 2000 km from the Strait of Hormuz in southern Iran to the KRI and further into SE Turkey. Since the onset of collision, the deformation front has propagated 250-350 km southwestward, involving the northeastern margin of the Mesopotamian foreland basin and the Persian Gulf into a largely NW-SE-trending foreland fold-thrust belt (Mouthereau, 2011; Mouthereau et al., 2007). The shortening across different sectors of the Zagros Fold-Thrust Belt is estimated to range between 10% and 32% (Blanc et al., 2003; McQuarrie, 2004; Molinaro et al.,
30 2005; Mouthereau et al., 2007; Vergés et al., 2011). GPS-derived horizontal velocities between Arabia and Eurasia show present-day convergence rates between 19 and 23 mm/yr (McClusky et al., 2003). It is suggested that deformation partitioning occurs between the external and internal portions of the Iranian part of the Zagros Fold-Thrust Belt. While the internal Zagros

Fold-Thrust Belt currently accommodates 3-4 mm/yr of right-lateral displacement along the Main Recent Fault (Fig. 1; Reilinger et al., 2006; Vernant et al., 2004), the external part accommodates 7-10 mm/yr of shortening by thrusting and folding (Hessami et al., 2006; Vernant et al., 2004), 2-4 mm/yr of which is taken up by the MFF in the Fars Arc (Oveisi et al., 2009). However, no such estimates are available for the Iraqi segment of the Zagros Mountains. It is hence not known how much of the total Arabia-Eurasia plate convergence is being accommodated across the Iraqi part of the Zagros Fold-Thrust Belt.

The NW segment of the Zagros Fold-Thrust Belt in the KRI is subdivided into several NE-trending morphotectonic zones. These zones from NE to SW are: (i) Zagros Suture, (ii) Imbricated Zone, (iii) High Folded Zone and (iv) Foothill Zone (Figs. 1 and 2; Jassim and Goff, 2006). These zones are bounded by major faults in the area. The faults include Main Zagros Thrust separating the Zagros Suture from the Imbricated Zone, High Zagros Fault that separates the Imbricate Zone from the High Folded Zone, and the Mountain Front Flexure that separates the High Folded Zone from the Foothill Zone (Figs. 1 and 2; Berberian, 1995; Jassim and Goff, 2006).

The deformed sedimentary succession is composed of 8 - 12 km thick Paleozoic to Cenozoic strata that rest on the Precambrian crystalline basement (Aqrabi et al., 2010; Jassim and Goff, 2006). The thick sedimentary cover consists of various competent and incompetent rock successions separated by detachment horizons. The infra-Cambrian Hormuz salt, which acts as a basal detachment in much of the Southern and Central Zagros Mountains in Iran, pinches out towards northwest (Hinsch and Bretis, 2015; Kent, 2010). Other intermediate detachment horizons influence the structural style of Central Zagros in Iran (e.g., Sherkati et al., ~~2005~~, 2006; Sepehr et al., 2006), but their behaviour is uncertain in NW Zagros due to limitations in outcrops and insufficient seismic profiles southwest of the Main Zagros Thrust. Some proposed detachment levels include Ordovician and Silurian shales (Aqrabi et al., 2010; ~~De Vera et al., 2009~~), Triassic-Jurassic anhydrites (Aqrabi et al., 2010; Hinsch and Bretis, 2015; ~~De Vera et al., 2009~~; Zebari, 2013; Zebari and Burberry, 2015), and ~~Early~~ Lower Miocene anhydrite (Aqrabi et al., 2010; Csontos et al., 2012; Jassim and Goff, 2006; Kent, 2010; Zebari and Burberry, 2015).

The exposed geological units within the High Folded Zone are limited to c. 5 km thick Upper Triassic to Recent rocks (Fig. ~~2~~; 2; Jassim and Goff, 2006; Law et al., 2014). Most anticlines are made up of Cretaceous carbonate rocks, while Upper Triassic-Lower Cretaceous strata are only exposed in the core of some anticlines. The Tertiary clastic rocks are preserved within the adjacent synclines. Within the studied structures, the Upper Jurassic-Lower Cretaceous Chia Gara and Lower Cretaceous Sarmord formations only crop out in ~~the core of~~ Bekhme and Zinta gorges ~~only~~ and consist of medium to thick bedded marly limestone, dolomitic limestone, and shale (Figs. 2 and 3). The Lower Cretaceous succession of Qamchuqa and Upper Cretaceous Bekhme and Aqra formations consist of thick bedded and massive reef limestone, dolomitic limestone, and dolomite. These units are generally rigid and resistant to erosion. Thus, they build the raised cores of anticlines. The Upper Cretaceous-Tertiary succession consists primarily of clastic rocks, which are mostly denuded, and alternating Upper Paleocene and Upper Eocene limestone of Khurmala and Pila Spi formations, respectively. They form a ridge surrounding the anticlines (Figs. 2 and 3). Unconsolidated Quaternary sediments in the study area consist of slope deposits, residual soil, alluvial fan deposits, and river terraces.

There is no agreement concerning the overall structural style of the NW Zagros in KRI. Several authors (Al-Qayim et al., 2012; Ameen, 1991; Fouad, 2014; Jassim and Goff, 2006; Numan, 1997; ~~De Vera et al., 2009~~) suggested that the Iraqi part of the Zagros Fold-Thrust Belt reveals a combination of both thin- and thick-skinned deformation. Partly relying on reflection seismic data, it was also suggested that contraction has been localized on inherited passive-margin normal faults in the basement, which were inverted during the late stage of deformation since c. 5 Ma (Abdulnaby et al., 2014; Burberry, 2015; Koshnaw et al., 2017). The structural relief across the MFF (Fig. 2) is likely linked to blind thrusts in the basement (Al-Qayim et al., 2012; Ameen, 1991, 1992; Fouad, 2014; Koshnaw et al., 2017; Numan, 1997; ~~De Vera et al., 2009~~). The same linkage between structural relief and a regional basement blind thrust is also documented in the Iranian Zagros (Blanc et al., 2003; Emami et al., 2010; Leturmy et al., 2010; Sherhati et al., 2006). Alternatively, Hinsch and Bretis (2015) argued that the structural relief in the hanging wall of the MFF is related to an underlying duplex structure that is linked to a stepped detachment horizon rooting in ~~an early~~ a Lower Paleozoic detachment in the internal parts of the orogen. The relief has been attributed to the accumulation of the Hormuz salt in the Iranian Zagros (McQuarrie, 2004). Even though the MFF is believed to be a major blind thrust in the basement (Berberian, 1995), it is usually mapped along the southwestern limb of the last high anticline where the Pila Spi limestones or the Bekhme and Aqra limestones crop out (Fouad, 2014; Jassim and Goff, 2006; Numan, 1997). Given that landforms in the vicinity of the MFF indicate ongoing tectonic deformation, we suspect that these blind faults might be active at present. Unfortunately, however, instrumental seismicity in the entire region is too diffusely distributed to be attributed to any particular faults (Jassim and Goff, 2006).

Structurally, this segment of Zagros Fold-Thrust Belt is dominated by ~~NENW-SWSE~~ trending fault-related folds, the trend of folds changes to nearly E-W to the west of the Greater Zab River (Fig 2). The folds are usually S-verging and the related faults emerge to the surface within both Imbricated Zone and High Folded Zone, while they remain blind within the Foothill Zone (Fouad, 2014; Hinsch and Bretis, 2015). ~~This is also seen within the studied anticlines, which have thrust fault in their forelimb. The Perat Anticline has a thrust in its back limb as well (Fig 4).~~

3 Data and Methods

We calculated and analysed landscape indices from DEMs for the studied anticlines and built a landscape evolution model that simulates progressive uplift and erosion of the landscape. We also constructed structural cross-section across these anticlines based on literature data and our own field observations.

3.1 Geomorphic Indices

The present-day relief in the study area resulted from a competition between rock uplift triggered by horizontal contraction and erosion destroying it. Parameters controlling these competing processes are the rate of tectonic accretion, rock erodibility and climate (Bishop, 2007; Burbank and Anderson, 2012).

In order to quantitatively analyse the landscape for the Harir, Perat and Akre anticlines (Figs. 2 and 4), we calculated hypsometric curves and determined ~~four~~three geomorphic indices: (i) hypsometric ~~curve~~, (ii) ~~hypsometric~~-integral, (iii) surface roughness, and (iv) ~~iii~~ surface index. These are considered proxies for the relative maturity of a particular landscape. The hypsometric curve and ~~the hypsometric~~-integral ~~highlight raised and flat surfaces.~~refer to the distribution of surface area of a landscape with respect to the elevation (Strahler, 1952). The surface roughness value is mainly sensitive to incision (Andreani et al., 2014; Andreani and Gloaguen, 2016; Pike and Wilson, 1971); the surface index is a measure for the amount of erosion. When referring to the results obtained by using this set of geomorphic indices, we colloquially refer to them as “landscape maturity” parameters.

3.1.1 Hypsometric ~~curve~~Curve

The hypsometric curve for a basin is the frequency distribution of elevation of the watershed area below a given height (Strahler, 1952). Convex-shaped hypsometric curves represent ~~less mature~~relatively youthful stages of the basin ~~while, s-shaped and~~ concave ~~shaped~~ curves ~~represent older~~refer to more mature and old stages (Ohmori, 1993; Pérez Peña et al., 2009)Strahler, 1952). Hypsometric curves are usually calculated for a specific drainage basin. ~~However, in~~In this study, we calculated ~~them~~the weighted mean of the hypsometric curves for ~~entire~~basins with areas > 0.25 km² within each anticlinal ~~ridges, restricting~~ridge, weighted by the basin area within the anticline. We restricted our ~~considerations~~analyses to those ~~areas~~basins where Upper Cretaceous carbonates are exposed (Fig. 54). This allowed us to make realistic comparisons between the three anticlines, neglecting the differences in rock erodibility that arise when varying lithologies are included. Wind gaps and water gaps as well as the plunging crests of the anticlines were also excluded from the calculation.

3.1.2 Hypsometric ~~integral~~Integral

The hypsometric integral (HI) ~~illustrates the distribution of landmass and it marks the isolated upraised mass above a relatively plain surfaces of low values from poorly eroded, broad and plain surface of high values.~~is the ratio of area under the hypsometric curve (Strahler, 1952). It is used to highlight the erosional stage of a landscape with high values corresponding to less mature landscapes and low values indicating advanced stages of erosion. The hypsometric integral is computed for a certain area by the following equation (Pike and Wilson, 1971):

$$HI = \frac{h_{mean} - h_{min}}{h_{max} - h_{min}}, \quad (1)$$

where h_{mean} , h_{min} and h_{max} are the mean, minimum and maximum elevations [m] of the examined area.

3.1.3 Surface roughness ~~Roughness~~

The surface roughness (SR) measures how much an area deviates from being totally flat. It differentiates flat planar surfaces with values close to 1 from irregular surfaces with higher values. It increases with the increase in incision by streams. The surface roughness is calculated using the following equation (Grohmann, 2004):

$$5 \quad SR = \frac{TS}{FS}, \quad (2)$$

where TS and FS are the areas [m²] of the actual topographic surface and the corresponding projection of that surface onto a planar surface, respectively.

3.1.4 Surface index ~~Index~~

10 The surface index (SI; Andreani et al., 2014) combines elevations, hypsometric integral and surface roughness to map simultaneously preserved and eroded portions of an elevated landscape. It is calculated using equation 3 (Andreani and Gloaguen, 2016):

$$SI = (N_{HI} * N_h) - N_{SR}, \quad (3)$$

15 where N_{HI}, N_h and N_{SR} are the normalized ~~elevations~~, hypsometric integral, elevations, and surface roughness values, respectively. Elevated and poorly incised landscapes with high hypsometric integral and low surface roughness show positive surface index values. Highly dissected landscapes with a high surface roughness yield negative surface index values. This means that the surface index is also sensitive to elevation.

3.1.5.2 Digital ~~elevation~~ Elevation models ~~Models~~

20 The geomorphic indices for this study were calculated from the 12 m resolution TanDEM-X DEM (Krieger et al., 2007) obtained from the German Aerospace Center (DLR) and the 30 m resolution SRTM1 DEM (NASA JPL, 2013); these two inputs were used since different DEM inputs give slightly different geomorphic results (Andreani et al., 2014; Koukouvelas et al., 2018; Obaid and Allen, 2017). Geomorphic indices were calculated using both the TanDEM-X and the SRTM1 data. However, the TanDEM-X data revealed numerous artefacts and voids, which made calculations unstable and results unreliable. (also see the comparison in the supplementary material). All results of the geomorphic indices and ~~all~~ subsequent calculations presented in the following sections were calculated from a 100 ~~x~~ 100 pixel cell (3 ~~x~~ 3 km) moving window on the 30 m resolution SRTM1 data. A larger moving window makes the obtained measurements smoother and vice versa. The size of the moving window must be chosen based on the scale of the target; here we targeted anticlines with wavelengths varying from 5 to 8 km. A 3 km moving window covered almost an entire limb of an anticline. ~~The calculations within the moving window were performed using the neighbourhood toolset in ESRI ArcGIS 10.4 software~~ We also tested the method proposed by Pérez-Peña et al. (2009) in order to account for the neighbouring cells in the calculation of the geomorphic indices. Rather than using a moving window, this approach uses a spatial autocorrelation of neighbouring cells and maps clusters of high and low values

30

of indices using Moran's I statistic (Moran, 1950) and G_i^* statistics (Ord and Getis, 1995). We have tested the same method here by calculating the HI for a 500 * 500 m grid of the SRTM data. We applied a hot spot analysis using G_i^* statistics with a distance of 1.5 km to define neighbour cells. Then, we resampled the HI map calculated from a 100 * 100 cell (3 * 3 km) moving window to 500 * 500 m grid from SRTM data. The calculations were performed using the focal and zonal toolsets in ESRI ArcGIS 10.4 software. In addition, the SRTM DEMs with 30 m resolution were used to extract topographic profiles, drainage networks, watersheds, stream slopes, and upstream drainage areas wherever required.

3.23 Modelling Landscape Evolution Model

We built a landscape evolution model to quantify the time difference in between the maturity level of the Akre and Harir anticlines by comparing the geomorphic indices of the evolved landscape with those of both anticlines based upon the open-source Landlab toolkit (Hobley et al., 2017; <http://landlab.github.io>).

We used two components in our model: one simulating erosion due to fluvial action and another simulating sediment transport along slopes due to ~~soil-creep~~ hillslope diffusion processes. Chen et al. (2014) showed that consideration of only these two components is sufficient for many landscapes but cannot model fluvial sedimentation. However, from field observations and from satellite imagery, we know that no significant fluvial sedimentation takes place on the slopes of the analysed anticlines. In On slopes on-of anticline flanks, the detachment-limited erosion due to the fluvial system tends to be the dominant process (Howard, 1994). To detect changes in the landscape due to fluvial erosion through time, we applied the commonly accepted idea that the rate of stream incision is directly proportional to the hydraulic shear stress of a stream (Braun and Willett, 2013). Consequently, we used the stream power incision law (Sklar and Dietrich, 1998; Whipple and Tucker, 1999):

$$\frac{\partial z}{\partial t} = KA^m S^n, \quad (4)$$

where $\partial z/\partial t$ is the erosion rate [myr^{-1}]; K is an erodibility coefficient [$\text{yr}^{-1}\text{m}^{(1-2m)}$] that encompasses the influence of climate, lithology, and sediment transport processes; A is the upstream drainage area [m^2] and is typically taken as a proxy for discharge (Wobus et al., 2006); $S = \partial z/\partial x$ is the local channel slope [m/m]; z is the elevation [m]; and m and n are the area and slope exponents, respectively. The stream power incision law (Eq. 4) is derived since the upstream drainage area A scales with channel discharge and channel width. The magnitude of the sediment flux in the channel is assumed to equal unity in the standard detachment-limited stream power model (Perron, 2017; Whipple, 2002). In the model, an incision threshold (C) was included, below which no incision occurs (Hobley et al., 2017).

To account for the provision of sediment due to ~~soil-creep~~ hillslope diffusion processes from slopes outside the river system, we used the hillslope diffusion equation (Culling, 1963; Tucker and Bras, 1998):

$$\frac{\partial z}{\partial t} = K_d \nabla^2 z, \quad (5)$$

where K_d is the diffusivity coefficient [m^2yr^{-1}], z is the elevation [m], and ∇^2 is the Laplace operator, i.e. the divergence of the gradient.

Finally, the overall evolution of the landscape in different time steps was calculated as the uplift rate ~~minus~~ subtracted by the changes due to both fluvial erosion and the hillslope diffusion (Temme et al., 2017):

$$Y \frac{\partial z}{\partial t} = U - KA^m S^n - K_d \nabla^2 z, \quad (6)$$

where U is the uplift rate [myr^{-1}].

5 A DEM raster grid of the present-day Harir Anticline and the surrounding basins (Fig. [6a5a](#)) served as model input. The advantage of using Harir Anticline was that the evolved drainage network overprinted the pre-existing one. The boundary conditions were set as closed on all sides except in pre-existing outlets in the input grid. The basins surrounding Harir Anticline were also included in the input grid to minimize the effect of the boundary conditions on the Harir Anticline itself. In the input raster grid, a flow route of each cell was connected with neighbouring cells both diagonally and orthogonally. This means that
10 each cell had the possibility to be linked with eight surrounding cells across its sides and corners (Hobley et al., 2017; Tucker et al., 2016).

Concerning the parameter used in the model, the value of m/n, n, and K were found following the methodology described ~~in~~ by (Harel et al., (2016), ~~;~~ Mudd et al., (2014), and; Perron and Royden, (2013), and by comparison with data from Harel et al. (2016). The value of m/n was found by plotting the elevation against X (elevation-X plot) for streams in the input grid (Fig.

15 [6a5a](#)), where X is found following the equation described by (Perron and Royden, 2013):

$$X = \int_{x_b}^x \left(\frac{A_0}{A(x)} \right)^{m/n} dx, \quad (7)$$

where A_0 is the reference drainage area [m^2] of 166160 m^2 and x is the horizontal upstream distance [m]. In this approach, we ascribed values for m/n range from zero to one, and X was calculated for each time ~~step~~ from Eq. 7. The value of m/n with maximum regression (R^2) value in the elevation-X plot was taken as the best-fitting value, which was 0.41 in our case for the
20 present-day Harir Anticline's drainages (Fig. [6b5b](#)). This value of m/n is located within the theoretically predicted values of m/n, which ranges from 0.3 to 0.7, ~~from~~ based on the stream power incision model (Kwang and Parker, 2017; Temme et al., 2017; Whipple and Tucker, 1999).

In the model, $n = 1.7$ and $K = 3.0\text{E-}6 \text{ yr}^{-1}\text{m}^{-0.4}$ were used; these values were estimated as mean of K and n in Harel et al. (2016) for those areas that are comparable with our study area in aspect of lithology, climate, and precipitation. The value of m was
25 0.7. We used an incision threshold of $C = 1.0\text{E-}5\text{myr}^{-1}$, which is widely adopted for erosion of an upland landscape (Hobley et al., 2017). A present-day annual mean precipitation of c. 0.7 myr^{-1} was used through the time due to the lack of nearby paleoclimate data with good quality. The average of the modelled precipitation anomaly data for Lake Van in SE Turkey (200 km to the NNW of the studied anticlines) is close to zero (Stockhecke et al. 2016). The current elevation of the Bekhme and Aqra formations in the crest of Harir Anticline is about 1500 m above sea level. Above that, ~~2072-2070~~ 2072-2070 m of Upper Cretaceous-
30 Miocene units (Law et al., 2014) and 300 m of LateUpper Miocene Lower Bakhtiari were exhumed before exposure of the Bekhme and Aqra formations. If we consider that the Lower Bakhtiari have been deposited close to sea level before onset of

the MFF c. 5 Ma, there would be 3872 m of rock uplift at a rate of ~ 0.000770007 myr⁻¹, which was used in the model. Since soil (regolith) is rare and very thin when present on the slopes, a low diffusivity coefficient of $K_d = 0.001$ m²yr⁻¹ was used (Fernandes and Dietrich, 1997).

There are minor variations in lithology ~~of~~ between the three anticlines (they consist of a thick pile of ~~Late~~ dominantly Cretaceous carbonate) and no variation in climate can be expected ~~in~~ on such a relatively local scale. Therefore, no significant variances are expected in the used parameters. Lastly, the parameters were calibrated by comparing the nature of the evolved landscape to other anticlines within the High Folded Zone that are cored by ~~the~~ Cretaceous carbonates and more mature than the Harir Anticline to evaluate how realistic the evolved landscape is.

4 Results

4.1 ~~Geomorphic Indices~~ Landscape Maturity

The three studied anticlines are composed of ~~Late~~ the raised Cretaceous carbonates ridges arising in their crests, ~~where~~ whereas the Tertiary clastic rocks have been denuded, but conserved ~~and now compose the sedimentary filling~~ in the adjacent synclines. The three anticlines are dissected by rivers that form water gaps across them. Bekhme and Zinta gorges cut the Perat and Akre anticlines, respectively. We also observed wind gaps, such as those in the NW end of Harir Anticline (Zebari and Burberry, 2015). Therefore, neither the location of these water and wind gaps nor the plunging tips of anticlines have been considered in interpreting the geomorphic indices as proxies for relative landscape maturity.

The anticlines reach up to c. 1500 m asl, ~~the~~ The minimum altitude is ~~c. 400 m in the Greater Zab river course and~~ c. 700 in the adjacent synclines and c. 400 m in the Greater Zab river course. The hypsometric curves for the three anticlines are presented in Fig. ~~7~~ 6. Harir Anticline's curve is more convex, and its shape is close to the youthful stage of Strahler's diagram (Ohmori, 1993; Strahler, 1952) with ~~68~~ 78% of the area above the mean elevation, while Akre Anticline is less convex and close to a mature stage with only ~~39~~ 50% of the area above the mean elevation. Perat Anticline's values are located in between and closer to the Harir Anticline curve with ~~60~~ 64% of its area above the mean elevation.

The ~~next~~ three calculated geomorphic indices (HI, SR, and SI) seem to be substantially influenced by the local structure, and wind and water gaps (Fig. ~~8~~ 7). Hypsometric integral values vary between 0.2 and 0.77, with lower values in the adjacent synclines and higher values in the crest of the anticlines. The HI values decrease toward the plunging ends of the anticlines and at ~~water gaps~~ gorges, e.g. Perat Anticline's HI values are ~~maximum~~ minimum at the Greater Zab River. In general, Harir Anticline shows higher values (≤ 0.77) than the other two anticlines. Harir Anticline has a broad crest and has been incised by narrow valleys. This makes the mean elevation within the moving window in the calculation close to the maximum elevation and, thus, causes higher values of the hypsometric integral. Perat Anticline shows high values of ≤ 0.66 HI on its crest to the west of Bekhme Gorge. Among the three anticlines, Akre Anticline shows the lowest values of ≤ 0.56 ~~to the east of the Zinta Gorge where it links with the Perat Anticline. In~~ HI in its central part ~~the HI values are~~ ≤ 0.51 , which is due to presence of more

incised and wider valleys. Elevation drops rapidly from the hinge of the anticline toward the limbs, which ~~cause~~causes the mean elevation within the window to fall.

The surface roughness values range between 1 and 1.33 in the area. The lowest values of the SR are also present in the adjacent synclines and in the plunging tips of the anticlines. The highest values are associated with the location of water gaps. These are areas where rivers deeply incised at both at Bekhme (≤ 1.33) and Zinta (≤ 1.32) gorges. Harir Anticline has lowest surface roughness values ~~of ≤ 1.14 in the SE. They decrease to ≥ 1.03 in the central part and to ≥ 1.04 in the NW.~~ Perat Anticline shows the highest value of ~~≤ 1.21 SR~~ especially in its northern limb. Akre Anticline has moderate SR values ≤ 1.16 in its central segment and ~~≤ 1.19 in western side where~~ a wind gap ~~at the western side~~ is present.

The results of the surface index range between -0.04 to 0.70 in the three anticlines studied. Few locations show negative values.

These are associated partly with adjacent synclines and with Bekhme Gorge (~~≥ 0.04~~). Apart from these locations, the area shows positive surface indices. Harir Anticline exhibits higher values on its broad crest (~~≤ 0.70~~). SI. Perat Anticline shows moderate values reach ≥ 0.49 of SI on the its crest of Perat Anticline to the west and east of Bekhme Gorge and ≤ 0.58 to the west of the gorge. The For Akre Anticline, SI values reach to ≤ 0.54 are lower than in both Harir and Perat anticlines, with highest values on the its crest of Akre Anticline east of Zinta Gorge and ≤ 0.38 east of the gorge. These high values of SI highlight the flat areas with high elevation and high hypsometric integral. The surface index values also highlight the Pila Spi and Khurmala limestone ridges encircling the anticlines with values close to zero.

~~The~~ In our calculation, the results of geomorphic indices vary depending on the resolution of the DEM and the change with changing the size of the moving window (and the resolution of the input data (see supplementary material). This was also detected by Andreani et al., (2014) and Obaid and Allen, (2017). Andreani et al. (2014) found that the DEM resolution does not affect the hypsometric integral, but it affects the surface roughness, while the size of the moving window affects both hypsometric integral and surface roughness. The results become smoother with an increasing size of the moving window. In our case, the results also change with changing the size of the moving window and resolution of the input data (see supplementary material). Since our main aim is to constrain relative maturity levels along the studied anticlines with 6-7 km width, Here, we found that it is reasonable to use a ~~100x100~~ 100 * 100 cell (3x3 * 3 km) moving window, which covers approximately ~~a one~~ one limb of the anticline each time and with 6-7 km width. It therefore highlights the desirable signal. ~~A smaller window resolves smaller local features rather than~~ The cluster map for the HI Gi* statistics was calculated following the approach by Pérez-Peña et al. (2009) for the 500 * 500 m grid. We obtained results similar to the HI map calculated from a 100 * 100 cell (3 * 3 km) moving window and resampled to 500 * 500 m grid in terms of highlighting the anticlines as cluster of high and low HI values (Fig. S19 a whole and b in supplementary material). This comparison proves that our method is equally applicable and valid, and a larger window does not resolve the main anticlines themselves. We therefore ran all analyses based on the 100 * 100 cell moving window as described above.

~~Based on~~ According to these the hypsometric curves and the geomorphic indices of the three anticlines, we ~~conclude~~ found that there is a measurable difference in landscape maturity between ~~them~~ the three anticlines. We classified our anticlines as relatively mature (Akre Anticline), moderately mature (Perat Anticline), and less mature (Harir Anticline). The difference in

the maturity level must be due to a difference in one or more of the factors tectonics, climate, or rock erodibility. No variation in the climate is expected ~~for along~~ the scale of these ~~anticlines studied area~~, therefore its impact on the landscape maturity can be neglected. The three anticlines show essentially the same lithology (Figs. 2 and 3), ~~i.e. similar lateral rock type and erodibility~~. Thus, the only factors that may vary along the anticlines are uplift rate or onset time of the uplift. This can be interpreted with one of the following scenarios: either the anticlines started to uplift in the order (1) Akre, (2) Perat and (3) Harir from west to east, or all of them started at the same time but with different rates. In the latter case, the uplift rate would have been highest at Akre and lowest at Harir, exposing Akre to erosion earlier than Harir.

4.2 Landscape Evolution Model

The aged landscape from the model run (Figs. 8 and 9) is the result of fluvial erosion and hillslope diffusion on the one hand, and uplift due to folding on the other hand. In the landscape modelling, various simulations with different parameters and time spans were performed. (supplementary material S24-S27). Harir Anticline was used as an input model and the landscape evolution model was run for a time span of 10 kyr up to 100 kyr and then it was run for a time span of 20 kyr. The evolving drainage system overprints the pre-existing one in the input and gradually becomes more deeply incised from the anticline flanks curving-carving toward its core (Fig. 98). Harir Anticline is a box-shaped anticline with a wide and plain flat crest area. With ongoing incision towards the core of the anticline, this plain crest narrowed gradually and finally became a sharp ridge that divided the drainage basins ~~on-of~~ the SW flank from those ~~in-of~~ the NE.

We compared the hypsometric curves of the model outputs to the present-day curves of the anticlines. The hypsometric curves were calculated first as total weighted mean for basins within the anticline and later calculated for the entire anticlinal ridges (Fig. 109). Statistically, (with minimum RMS), the hypsometric curve of Harir Anticline was closest to the present-day Perat Anticline after ~~70~~100 kyr and 80 kyr of erosion: when using total weighted mean and entire anticlinal ridge, respectively, in calculation of the hypsometric curves. The output curve after 160 kyr and 200 kyr matched best with present-day Akre Anticline ~~(with minimum RMS)~~, when using total weighted mean and entire anticlinal ridge, respectively, in calculation of the hypsometric curves. We conclude that it will take Harir Anticline roughly about ~~70~~80 to 100 kyr to reach the maturity level of Perat Anticline and about 160 to 200 kyr to reach the level of Akre Anticline based on our model and comparison of the hypsometric curves if the uplift rates of the three anticlines were the same. The other possibility is that the anticlines started to grow at the same time but with different uplift rates. In this case, it is not possible to find the difference in uplift rates via our landscape modelling. Since the factors that control geomorphology (lithology, structural setting, and climate) were similar for all three anticlines, and under the assumption of constant growth and ~~erosion rates~~erosional conditions, we infer that uplift of Akre and Perat anticlines started respectively 160-200+20 kyr and ~~70~~80-100 kyr before Harir started to grow if their uplift rates were the same.

4.3 Geometry of the Studied Anticlines

The structural cross-sections for the three anticlines (Fig. 10) constructed from field data and literature (Syan, 2014) shows that the anticlines are box-shaped with broad crests. They are asymmetrical verging toward the SW with a nearly vertical or overturned forelimb. The three anticlines are thrust-related, in accordance with published studies of the area (Csontos et al. 2012), and have a thrust in their forelimb. Perat Anticline additionally exhibits a back thrust in its NE limb. The shortening across the three anticlines was calculated using line-length balancing. We found 26%, 28% and 29% shortening for Harir, Perat and Akre anticlines, respectively, and conclude that there is no significant variation. A difference in the fold amplitude between the three anticlines can be discerned in the cross-sections. The amplitude of Perat Anticline is higher than that of both Harir and Akre anticlines. Another difference concerns the thickness of the Upper Cretaceous - Middle Eocene clastic succession, which dwindles toward the Akre Anticline. The whole Miocene succession, however, is the thickest in the Akre Anticline. Both the Upper Cretaceous - Middle Eocene and Miocene successions consist of highly erodible clastic rocks, and the thicker Miocene succession in the Akre Anticline counterbalances the thinner Upper Cretaceous - Middle Eocene succession. Therefore, it is not expected that these variations in the structural geometry and stratigraphic thickness have a great impact on the variation of the landscape maturity in the three anticlines and the landscape model.

15 **5 Discussion**

5.1 Rock Erodibility

As described in section 2.2 and Fig. 3, the stratigraphic column in the area consists of rocks with different erodibility. In general, the Cretaceous carbonate units of Qamchuqa, Bekhme, and Aqra formations and the Paleogene carbonates of Sinjar, Khurmala, and Pila Spi formations are more resistant to erosion and form outstanding ridges. The Upper Cretaceous Tertiary elastic rocks are less resistant to erosion. The latter units have been eroded to the ground level where they crop out, except in some areas where they form a badland landscape (e.g. Bakhtiari group). The progress of erosion along with the uplift due to folding can be separated into several stages that reflect the resistance of the exposed rock units to erosion (Figs. 2 and 11): first, the area is covered by Quaternary sediments in unfolded, very wide synclines in between anticlines, especially in the Foothill Zone (e.g. in Akre Plain to the south of Akre Anticline). Next, the Neogene Fars and Bakhtiari units expose in the next stage of folding and produce badland landforms without a prominent relief. Their surrounding areas do not exceed 500 m asl (e.g. in Sarta Anticline; Fig. 11). Then, Paleogene carbonates expose in the core of the anticlines and form outstanding whale-shaped anticlinal ridges with relief exceeding 750 m (e.g. Pirmam anticline; Figs. 2 and 11). In the next erosional step, the Cretaceous carbonates expose in the core of anticlines and form anticlinal ridge also with relief exceeding 2 km (e.g. many anticlines within the High Folded Zone including the three studied anticlines). Finally, the Upper Triassic-Lower Cretaceous evaporites, shale, and bedded limestone units are exposed where the Cretaceous carbonates have been eroded down to the cores of the anticlines, especially in those that are located to the north and northeast close to the High Zagros Fault.

Currently, the studied anticlines are in the stage in which the Cretaceous carbonates form the main anticline body. The maturity level along these anticlines therefore represents the level when these carbonates cropped out in their latest stage.

5.2 5.1 Landscape Maturity and Modelling

Any relative change in the base level induced by tectonics or climate leads to the change of erosion rates. A relict landscape survives when its uplift is not completely counterbalanced by erosion (Andreani and Gloaguen, 2016; Burbank and Anderson, 2012; Pérez-Peña et al., 2015). The relative relict landscape and its distribution on these three anticlines atop the MFF reveal clues about underlying tectonics since there is no significant variation in climate and lithology.

Within the three studied anticlines, the geomorphic indices effectively highlighted their incision. ~~The locations dissected by rivers show high surface roughness.~~ The surface index which combines both hypsometric integral and surface roughness, sets apart relict landscapes of positive and high values from transient landscapes of negative values that are preferentially incised (Andreani et al., 2014). There is a notable relative ~~declination~~ deviation in areas where anticlines are crossed by rivers e.g. Bekhme and Zinta gorges, which show a high surface roughness. Also, variations in surface index are found in comparable areas in the three anticlines. Focussing on the crest of the anticlines, we ~~see~~ observe that Harir Anticline shows higher values than the two others. The lowest values are found in Akre Anticline. Harir has low incision at elevated surfaces while Akre has more incised uneven landscapes ~~and the~~ because erosion ~~has waves have functioned~~ worked deeper into the core of the anticline. This can also be ~~seen~~ inferred from the valley shapes. We observe a ~~narrow-tight~~ V-shape valleys in the flanks of Harir and a ~~wide-open~~ V-shape valleys in Akre (Figs. ~~12a~~ 11a and ~~12b~~). ~~The same effect is visible in swath topographic profiles (Figs. 12c and 12d): in Harir Anticline, there is a clear topographic step with a higher slope angle, while in Akre Anticline the slope is gentler and more linear.~~ 11b). We relate this difference to the ~~underlying tectonics. This~~ tectonic uplift and to the effects of longer erosion acting on Akre. The observation can be interpreted with one of ~~these~~ the following two premises: either ~~both~~ the anticlines started to uplift successively (first Akre, then Perat, and finally Harir), or all of them started at the same time but with different uplift and exhumation rates (Akre the fastest, Harir the slowest). In other words, the Cretaceous carbonates in Harir Anticline were exposed to the erosion later than in Akre Anticline and, consequently, incised less.

The current landscape of these anticlines exposes Cretaceous carbonates of the Qamchuqa, Bekhme and Aqra formations, which became exposed to erosion only after unroofing of the entire Palaeogene ~~to~~ Neogene succession. The Upper Miocene-Pliocene Bakhtiari Group, which is the youngest stratigraphic unit in the area, is affected by folding ~~is the Upper Miocene-Pliocene Bakhtiari group~~, as observed from growth strata (Csontos et al., 2012). This has also been observed in the Upper Bakhtiari (Pliocene-Pleistocene) close to the MFF (Koshnaw et al., 2017). In between Bekhme and Aqra and the Upper Bakhtiari formations, 2.37 km of the Upper Cretaceous ~~to~~ Miocene clastic rocks interbedded with thin units of limestone (Law et al., 2014) have been exhumed due to successive rock uplift in the crest of the studied anticlines, triggered by shortening and erosion. They are only preserved in the adjacent synclines. The Cretaceous carbonates themselves have been exposed in the crests of Akre, Perat, and Harir anticlines for c. 0.9 km above the level of the other exhumed units. Based on the thickness, the amount of the exposed ~~Upper~~ Cretaceous carbonate makes c. 28 % of the total exhumed and exposed thickness in the crest

of the anticlines. Therefore, with both scenarios (different uplift time or different uplift rate) and with assumption of constant (linear) rock uplift rate through time, the ~~Upper~~-Cretaceous carbonate in Harir Anticline was exposed to erosion later than in the Akre Anticline (Fig. ~~13a~~-~~12a~~).

The steeper valley flanks in Harir Anticline compared to those of Akre also support higher uplift rates of the Harir Anticline.

5 Furthermore, the relationship between stream slope and upstream drainage area at any given point ~~for of~~ streams in the Harir Anticline is positive (Fig. ~~13b~~), ~~which means~~ 12b). This means that the streams have a convex shape and the streams' segments with steeper slopes are still located in the flanks of the anticline. In the Akre Anticline, this relationship is negative (Fig. ~~13b~~ 12b), which means that the streams have a concave shape and the segments with steeper slopes have migrated toward the core of the anticline. This implies that tectonic activity in the Harir Anticline is younger than in the Akre Anticline. Therefore, 10 the premise of having Harir Anticline starting its uplift later than Akre Anticline is most likely. This is our preferred scenario in the model for the successive tectonic evolution of the study area presented below.

The geomorphic indices have been widely used to assess the landscape maturity and, subsequently, active tectonics (Andreani and Gloaguen, 2016; Mahmood and Gloaguen, 2012; Pérez-Peña et al., 2009). The challenging aspect of landscape maturity modelling is to obtain an absolute quantification of tectonics and the relevant time spans. The same holds true with using a 15 landscape evolution model to estimate the relative time difference between two landscapes, because it is difficult to compare two landscapes in terms of maturity by absolute means. The results of the landscape modelling approach yielded a numerically derived estimate on the relative age difference between the studied anticlines but without absolute growth ages.

~~Since the Upper Cretaceous carbonates in Harir Anticline were exposed later than in Akre Anticline, a landscape evolution model is a viable approach to estimate the exposure time difference. Here the model is built for the first premise of different~~ 20 ~~onsets of uplift. Even if the second premise of different uplift rates is correct, the estimated time difference of the carbonate exposure will only be 28% less than that for the first scenario. As described in section 4.2, the calculated uplift time difference between Akre and Harir anticline is 200±20 kyr, and if the second scenario is correct, the time difference of the carbonate exposure would be 144±14.4 kyr.~~

In the model, various parameters and two well-known landscape evolution equations for the fluvial erosion and hillslope 25 diffusion were used, but in general it is impossible to mimic nature perfectly. The relative time ~~variation~~ difference of landscape evolution of these anticlines was ~~measured~~ estimated from the model assuming that the climate ~~did~~ has not changed much during the evolution of the landscape ~~due to lack of paleoclimate~~ since there was not much variation in the precipitation based 30 on the modelled data (Stockhecke et al. 2016) and for the sake of simplicity, ~~acknowledging~~ admitting that climatic change has a significant impact on the landscape. In addition, neither rock fall nor karstification were included in the model for simplicity.

Field observations suggest that karstification does not have a significant impact on the landscape. Overall, the evolved landscape from the model seems to be plausible in comparison with the other anticlines that surround Harir Anticline, and the landscape models are more mature with respect to the developed topography ~~that developed~~ and to the overall drainage patterns.

5.3.2 Structural Style and ~~regional tectonics~~ Regional Tectonics

~~We constructed structural cross sections for the three anticlines from field data and literature (Fig. 4; Syan, 2014). These crosssections show thrust related folds in accordance with published studies of the area (Csontos et al. 2012). The anticlines are box shaped with broad hinge zones and doubly plunging. All three anticlines show a thrust fault in their forelimb. The Perat Anticline has a thrust in its backlimb, as well. The anticlines have a steeper forelimb which is nearly vertical, and the strata become overturned within the Pila Spi, Sinjar, and Khurmala formations. Using line length balancing, the shortening of the Upper Cretaceous strata is measured from the constructed cross sections to be 26%, 31%, and 29% in the Harir, Perat and Akre anticlines, respectively. The cross sections show variations in the stratigraphic thickness in between the three anticlines, especially in the thickness of the Late Cretaceous Tertiary clastic rocks. The clastic rocks are less resistant to erosion and the raised body of the anticlines is entirely made up of Cretaceous carbonates. Therefore, it is not expected that these variations in the structural geometry and stratigraphic thickness have much impact on the variation of the landscape maturity in the three anticlines.~~

An orogenic bend is depicted in the area where the trend of structures changes across the Greater Zab River from NW-SE at the eastern side of the river to nearly E-W at its western side. The course of the Greater Zab River is suggested to overlie a NE-trending transversal basement fault with right-lateral displacement (Ameen, 1992; Burberry, 2015; Jassim and Goff, 2006; Omar, 2005) ~~and there is~~ evidenced by an offset of the High Folded Zone propagation foreland-ward. At the eastern side of the river the deformation has propagated for about 25 km further than on its western side (Figs. 1 and 2). The origin of this fault reaches back to the Late Proterozoic tectonic history of the Arabian Plate, ~~and t~~ The ~~is~~ is fault has been reactivated later in subsequent tectonic events (Ameen, 1992; Aqrawi et al., 2010; Burberry, 2015; Jassim and Goff, 2006). This can also be noticed in the thickness of the sedimentary cover, which is thinner to the west of the Greater Zab River (Ameen, 1992; Zebari and Burberry, 2015). This change in thickness is ~~most likely due~~ attributed to a series of uplift events and erosional/non-depositional gaps during the Mesozoic (Ameen, 1992; Aqrawi et al., 2010), which in turn may have ~~influences~~ influenced the foreland-ward propagation of deformation (Marshak and Wilkerson, 1992). The deference in propagation of deformation may also be due to the convergence being accommodated differently across the curved fold-thrust belt ~~rotation of the belt trend as the convergence direction changed~~ (Csontos et al., 2012) from NW-SE in the eastern side where the convergence is accommodated ~~by~~ through belt-normal slip and right-lateral strike-slip across the eastern NW-SE trending part, and to nearly E-W in the west where the convergence is mostly aecommodated by belt-normal slip across the western E-W trending segment (Reilinger et al., 2006).

Zebari and Burberry (2015) found that anticlines to the east of the Greater Zab River (Harir, Shakrok and Safin anticlines) demonstrate pronounced NW-ward propagation based on their geomorphic criteria, and the start point of the NW-ward propagation of the Harir Anticline is close to its SE end ~~(their Figs 16 and 20)~~. This implies that progressing uplift in the hanging wall of the MFF was not gradually continuing from the Akre Anticline towards the Perat Anticline and further ~~SEward~~ SE-ward to the Harir Anticline. The uplift progress is probably rather partitioned into segments along the belt. In

addition, other anticlines to the south (Safin Anticline) and to the southwest (Shakrok Anticline) of Harir Anticline are more mature than Harir Anticline itself, based on their hypsometric curves (Fig. ~~14~~13) and geomorphic indices (supplementary material; S1-S18), implying that the foreland-ward propagation of the deformation was also out-of-sequence in this part of the High Folded Zone. This has also been noted in the Foothill Zone based on thermochronological dating (Koshnaw et al., 2017) and landscape maturity (Obaid and Allen, 2017). Thus, the most plausible scenario is that deformation in the Harir segment started sometime after that in Akre segment (160-200 kyr according to our landscape evolution modelling). Harir Anticline uplift would also postdate Perat Anticline uplift (~~70~~80-100 kyr) to the west and the onset of Safin and Shakrok anticlines to the south and southeast, which are not included in the model (Fig. ~~15~~14). As discussed by Csontos et al., (2012), the fold relay corresponds to the change in strain partitioning and rotation of the horizontal stress direction from ~~the~~NE-SW to N-S in Late Pliocene (Navabpour et al., 2008; Navabpour and Barrier, 2012). During the latest stage of the N-S convergence, a right-lateral shear and superposed folding along the NW-SE trending anticlines (Csontos et al., 2012) can be observed from the relay of the Shakrok, Harir and Perat anticlines (Figs. 2 and ~~15~~14). Applying this concept requires a comprehensive paleostress analysis investigation especially within these studied anticlines, which is beyond the scope of this paper.

6 Conclusions

The geomorphic indices used in this study allowed us to quantitatively differentiate between variably degraded landforms in the frontal Zagros Mountain of NE Iraq. This area is characterized by active folding due to ongoing convergence between the Eurasian and Arabian plates. Three active thrust-related anticlines that are aligned along-strike the MFF were studied in detail. While the Akre Anticline shows deeply incised valleys indicative of advanced erosion, the Harir and Perat anticlines have relatively smooth surfaces and ~~are~~ show younger landscape than Akre. We related this difference to the underlying tectonics. This can be interpreted with one of the following concepts: either anticlinal growth started at different times or all of them started to grow at the same time, but with different surface uplift and exhumation rates.

A comparison of the geomorphic indices values of the model output with those of the present-day Akre Anticline topography revealed that it will take Harir Anticline about 160-200±20 kyr to reach the maturity level of today's Akre Anticline, and ~~70±10~~about 80-100 kyr to reach the maturity level of the Perat Anticline assuming constant uplift rates along the three anticlines. Due to similarity in the lithology, structural setting and climate along the three anticlines and by assuming constant growth and erosion ~~rates~~conditions, we infer that Akre Anticline started to grow 160-200±20 kyr before Harir Anticline. The onset of growth of Perat Anticline lies ~~closer to~~in between that of Harir and Akre anticlines. A NW-ward propagation of Harir Anticline itself implies that the uplift has been independent within different segments rather than having been continuous from the NW to the SE. Our method of estimating relative age differences in variously degraded anticlines can be applied to many other anticlines along the MFF and could eventually develop into a model of the temporal evolution of this fold and thrust belt.

7 Acknowledgments

The German Academic Exchange Service (DAAD) is acknowledged for providing a scholarship (Research Grants – Doctoral Programmes in Germany, 2016/17; 57214224) to the first author to conduct this PhD research in Germany. The authors express their gratitude to the German Research Foundation (DFG) project no. 393274947 for providing financial [research](#) support. The German Aerospace Agency (DLR) and Mr. Thomas Busche in particular are thanked for providing TanDEM-X digital elevation models. [We also thank two anonymous peers for their partly very thorough reviews that helped us to further clarify and improve numerous aspects of our work.](#)

References

- Abdulnaby, W., Mahdi, H., Numan, N. M. S. and Al-Shukri, H.: Seismotectonics of the Bitlis–Zagros Fold and Thrust Belt in Northern Iraq and Surrounding Regions from Moment Tensor Analysis, *Pure & Appl. Geophys.*, 171(7), 1237–1250, [https://doi: 10.1007/s00024-013-0688-4](https://doi.org/10.1007/s00024-013-0688-4), 2014.
- 5 Agard, P., Omrani, J., Jolivet, L., Whitechurch, H., Vrielynck, B., Spakman, W., Monié, P., Meyer, B. and Wortel, R.: Zagros orogeny: A subduction-dominated process, *Geol. Mag.*, 148(5–6), 692–725, [https://doi:10.1017/S001675681100046X](https://doi.org/10.1017/S001675681100046X), 2011.
- Al-Qayim, B., Omer, A. and Koyi, H.: Tectonostratigraphic overview of the Zagros Suture Zone, Kurdistan Region, Northeast Iraq, *GeoArabia*, 17(4), 109–156, 2012.
- Alavi, M.: Structures of the Zagros fold-thrust belt in Iran, *Am. J. Sci.*, 307(9), 1064–1095, [https://doi:10.2475/09.2007.02](https://doi.org/10.2475/09.2007.02),
10 2007.
- ~~Allen, G. H., Barnes, J. B., Pavelsky, T. M. and Kirby, E.: Lithologic and tectonic controls on bedrock channel form at the northwest Himalayan front, *J. Earth Surf.*, 118(3), 1806–1825, [https://doi:10.1002/jgrf.20113](https://doi.org/10.1002/jgrf.20113), 2013.~~
- Ameen, M. S.: Possible forced folding in the Taurus–Zagros Belt of northern Iraq, *Geol. Mag.*, 128(6), 561–584, [https://doi:10.1017/S0016756800019695](https://doi.org/10.1017/S0016756800019695), 1991.
- 15 Ameen, M. S.: Effect of basement tectonics on hydrocarbon generation, migration, and accumulation in Northern Iraq, *Am. Assoc. Pet. Geol. Bull.*, 76(3), 356–370, 1992.
- Andreani, L. and Gloaguen, R.: Geomorphic analysis of transient landscapes in the Sierra Madre de Chiapas and Maya Mountains (northern Central America): Implications for the North American-Caribbean-Cocos plate boundary, *Earth Surf. Dyn.*, 4(1), 71–102, [https://doi:10.5194/esurf-4-71-2016](https://doi.org/10.5194/esurf-4-71-2016), 2016.
- 20 Andreani, L., Stanek, K. P., Gloaguen, R., Krentz, O. and Domínguez-González, L.: DEM-based analysis of interactions between tectonics and landscapes in the ~~ore mountains~~[Ore Mountains](#) and ~~eger rift~~[Eger Rift](#) (East Germany and NW Czech Republic), *Remote Sens.*, 6(9), 7971–8001, [https://doi:10.3390/rs6097971](https://doi.org/10.3390/rs6097971), 2014.
- Aqrawi, A. A. M., Goff, J. C., Horbury, A. D. and Sadooni F. N.: *The Petroleum Geology of Iraq*, Scientific Press, Beaconsfield., 2010.
- 25 Berberian, M.: Master “blind” thrust faults hidden under the Zagros folds: active basement tectonics and surface morphotectonics, *Tectonophysics*, 241(3–4), [https://doi:10.1016/0040-1951\(94\)00185-C](https://doi.org/10.1016/0040-1951(94)00185-C), 1995.
- Bishop, P.: Long-term landscape evolution: linking tectonics and surface processes, *Earth Surf. Process. Landforms*, 32(3), 329–365, <https://doi.org/10.1002/esp.1493>, 2007.
- Blanc, E. J.-P., Allen, M. B., Inger, S. and Hassani, H.: Structural styles in the Zagros Simple Folded Zone, Iran, *J. Geol. Soc. London.*, 160(3), 401–412, [https://doi:10.1144/0016-764902-110](https://doi.org/10.1144/0016-764902-110), 2003.
- 30 Braun, J. and Willett, S. D.: A very efficient O(n), implicit and parallel method to solve the stream power equation governing fluvial incision and landscape evolution, *Geomorphology*, 180–181, 170–179, [https://doi:10.1016/j.geomorph.2012.10.008](https://doi.org/10.1016/j.geomorph.2012.10.008), 2013.

- Bretis, B., Bartl, N. and Grasemann, B.: Lateral fold growth and linkage in the Zagros fold and thrust belt (Kurdistan, NE Iraq), *Basin Res.*, 23(6), 615–630, <https://doi:10.1111/j.1365-2117.2011.00506.x>, 2011.
- Bull, W. B.: *Tectonic Geomorphology of Mountains: A New Approach to Paleoseismology*, Wiley-Blackwell, Oxford, 2007.
- Burbank, D. and Anderson, R.: *Tectonic Geomorphology*, 2nd Ed, Wiley-Blackwell, Chichester, UK, 2012.
- 5 Burberry, C. M.: The effect of basement fault reactivation on the ~~Frassie~~ Triassic-Recent Geology of Kurdistan, North Iraq, *J. Pet. Geol.*, 38(37–58), 37–58, <https://doi.org/10.1111/jpg.12597>, 2015.
- Chen, A., Darbon, J. Ô. and Morel, J. M.: Landscape evolution models: A review of their fundamental equations, *Geomorphology*, 219, 68–86, <https://doi:10.1016/j.geomorph.2014.04.037>, 2014.
- Cheng, K. Y., Hung, J. H., Chang, H. C., Tsai, H. and Sung, Q. C.: Scale independence of basin hypsometry and steady state
10 topography, *Geomorphology*, 171–172, 1–11, <https://doi:10.1016/j.geomorph.2012.04.022>, 2012.
- Collignon, M., Yamato, P., Castelltort, S. and Kaus, B. J. P.: Modeling of wind gap formation and development of sedimentary basins during fold growth: application to the Zagros Fold Belt, Iran, *Earth Surf. Process. Landforms*, 41(11), 1521–1535, <https://doi:10.1002/esp.3921>, 2016.
- Cowie, P. A., Attal, M., Tucker, G. E., Whittaker, A. C., Naylor, M., Ganas, A. and Roberts, G. P.: Investigating the surface
15 process response to fault interaction and linkage using a numerical modelling approach, *Basin Res.*, 18(3), 231–266, <https://doi:10.1111/j.1365-2117.2006.00298.x>, 2006.
- Csontos, L., Sasvári, Á., Pocsai, T., Kósa, L., Salae, A. T. and Ali, A.: Structural evolution of the northwestern Zagros, Kurdistan Region, Iraq: Implications on oil migration, *GeoArabia*, 17(2), 81–116, 2012.
- Culling, W. E. H.: Soil Creep and the Development of Hillside Slopes, *J. Geol.*, 71(2), 127–161, 1963.
- 20 ~~De Vera, J., Gines, J., Oehlers, M., McClay, K. and Doski, J.: Structure of the Zagros fold and thrust belt in the Kurdistan Region, northern Iraq, *Trab. Geol.*, 29, 213–217, 2009.~~
- Emre, Ö., Duman, T. Y., Özalp, S., Elmacı, H., Olgun, Ş. and Şaroğlu, F.: *Active Fault Map of Turkey with an Explanatory Text*. 1:1,250,000 Scale, General Directorate of Mineral Research and Exploration, Ankara., 2013.
- Emami, H., Vergés, J., Nalpas, T., Gillespie, P., Sharp, I., Karpuz, R., Blanc, E. P. and Goodarzi, M. G. H.: Structure of the
25 Mountain Front Flexure along the Anaran anticline in the Pusht-e Kuh Arc (NW Zagros, Iran): insights from sand box models, *Geol. Soc. London, Spec. Publ.*, 330(1), 155–178, <https://doi:10.1144/SP330.9>, 2010.
- Fernandes, N. F. and Dietrich, W. E.: Hillslope evolution by diffusive processes: The timescale for equilibrium adjustments, *Water Resour. Res.*, 33(6), 1307–1318, <https://doi:10.1029/97WR00534>, 1997.
- Fouad, S. F. A.: Western Zagros Fold – Thrust Belt, Part II: The High Folded Zone, *Iraqi Bull. Geol. Min., Special Iss.* (6),
30 53–71, 2014.
- Grohmann, C. H.: Morphometric analysis in geographic information systems: Applications of free software GRASS and R, *Comput. Geosci.*, 30(9–10), 1055–1067, <https://doi:10.1016/j.cageo.2004.08.002>, 2004.
- ~~Hancock, G., Lowry, J., Coulthard, T., Evans, K. and Moliere, D.: A catchment scale evaluation of the SIBERIA and CAESAR landscape evolution models, *Earth Surf. Process. Landforms*, 35(8), 863–875, <https://doi:10.1002/esp.1863>, 2010.~~

- Hancock, G. R. and Willgoose, G. R.: The use of a landscape simulator in the validation of the Siberia landscape evolution model: Transient landforms, *Earth Surf. Process. Landforms*, 27(12), 1321–1334, <https://doi:10.1002/esp.414>, 2002.
- Harel, M. A., Mudd, S. M. and Attal, M.: Global analysis of the stream power law parameters based on worldwide ¹⁰Be denudation rates, *Geomorphology*, 268, 184–196, <https://doi:10.1016/j.geomorph.2016.05.035>, 2016.
- 5 Hessami, K., Koyi, H. A., Talbot, C. J., Tabashi, H. and Shabaniyan, E.: Progressive unconformities within an evolving foreland fold-thrust belt, Zagros Mountains, *J. Geol. Soc. London.*, 158(6), 969–981, <https://doi:10.1144/0016-764901-007>, 2001.
- Hessami, K., Nilforoushan, F. and Talbot, C. J.: Active deformation within the Zagros Mountains deduced from GPS measurements, *J. Geol. Soc. London.*, 163(1), 143–148, <https://doi:10.1144/0016-764905-031>, 2006.
- Hinsch, R. and Bretis, B.: A semi-balanced section in the northwestern Zagros region: Constraining the structural architecture
10 of the Mountain Front Flexure in the Kirkuk Embayment, Iraq, *GeoArabia*, 20(4), 41–62, 2015.
- Hobley, D. E. J., Adams, J. M., Siddhartha Nudurupati, S., Hutton, E. W. H., Gasparini, N. M., Istanbuloglu, E. and Tucker, G. E.: Creative computing with Landlab: An open-source toolkit for building, coupling, and exploring two-dimensional numerical models of Earth-surface dynamics, *Earth Surf. Dyn.*, 5(1), 21–46, <https://doi:10.5194/esurf-5-21-2017>, 2017.
- Homke, S., Vergés, J., Garcés, M., Emami, H. and Karpuz, R.: Magnetostratigraphy of Miocene-Pliocene Zagros foreland
15 deposits in the front of the Push-e Kush Arc (Lurestan Province, Iran), *Earth Planet. Sci. Lett.*, 225(3–4), 397–410, <https://doi:10.1016/j.epsl.2004.07.002>, 2004.
- Howard, A. D.: A detachment limited model of drainage basin evolution, *Water Resour. Res.*, 30(7), 2261–2285, <https://doi:10.1029/94WR00757>, 1994.
- Jassim, S. Z. and Goff, J. C.: *Geology of Iraq*, Dolin, Prague and Moravian Museum, Brno, Czech Rep., 2006.
- 20 Keller, E. A., Gurrola, L. and Tierney, T. E.: Geomorphic criteria to determine direction of lateral propagation of reverse faulting and folding, *Geology*, 27(6), 515–518, [https://doi.org/10.1130/0091-7613\(1999\)027<0515:GCTDDO>2.3.CO;2](https://doi.org/10.1130/0091-7613(1999)027<0515:GCTDDO>2.3.CO;2), 1999.
- Kent, W. N.: Structures of the Kirkuk Embayment, northern Iraq: Foreland structures or Structures of the Kirkuk Embayment, northern Iraq: Foreland structures or Zagros Fold Belt structures?, *GeoArabia*, 15(4), 147–157, 2010.
- 25 Koshnaw, R. I., Horton, B. K., Stockli, D. F., Barber, D. E., Tamar-Agha, M. Y. and Kendall, J. J.: Neogene shortening and exhumation of the Zagros fold-thrust belt and foreland basin in the Kurdistan region of northern Iraq, *Tectonophysics*, 694, 332–355, <https://doi:10.1016/j.tecto.2016.11.016>, 2017.
- Koukouvelas, I. K., Zygouri, V., Nikolakopoulos, K. and Verroios, S.: Treatise on the tectonic geomorphology of active faults: The significance of using a universal digital elevation model, *J. Struct. Geol.*, 116(June), 241–252,
30 <https://doi:10.1016/j.jsg.2018.06.007>, 2018.
- Krieger, G., Moreira, A., Fiedler, H., Hajnsek, I., Werner, M., Younis, M., and Zink, M.: TanDEM-X: A satellite formation for high-resolution SAR interferometry, *IEEE Trans. Geosci. Remote Sens.*, 45, 3317–3341, <https://doi:10.1109/TGRS.2007.900693>, 2007.

- Kwang, J. S. and Parker, G.: Landscape evolution models using the stream power incision model show unrealistic behavior when m/n equals 0.5, *Earth Surf. Dyn.*, 5(4), 807–820, <https://doi:10.5194/esurf-5-807-2017>, 2017.
- ~~Langston, A., Law, A., Munn, D., Symms, A., Wilson, D., Hattingh, S., Bobolecki, R., Marci, K. Al, Chernik, P., Parry, D. and Ho, J.: Competent Person's Report on Certain Petroleum Interests of Gulf Keystone Petroleum and its Subsidiaries in Kurdistan, Iraq, Gulf keystone Petroleum., 2014.~~
- 5
- Leturmy, P., Molinaro, M. and de Lamotte, D. F.: Structure, timing and morphological signature of hidden reverse basement faults in the Fars Arc of the Zagros (Iran), *Geol. Soc. London, Spec. Publ.*, 330(1), 121–138, <https://doi:10.1144/SP330.7>, 2010.
- Mahmood, S. A. and Gloaguen, R.: Appraisal of active tectonics in Hindu Kush: Insights from DEM derived geomorphic indices and drainage analysis, *Geosci. Front.*, 3(4), 407–428, <https://doi:10.1016/j.gsf.2011.12.002>, 2012.
- 10
- Marshak, S. and Wilkerson, M. S.: Effect of overburden thickness on thrust belt geometry and development, *Tectonics*, 11(3), 560–566, <https://doi:10.1029/92TC00175>, 1992.
- McClusky, S., Reilinger, R., Mahmoud, S., Ben Sari, D. and Tealeb, A.: GPS constraints on Africa (Nubia) and Arabia plate motions, *Geophys. J. Int.*, 155(1), 126–138, <https://doi:10.1046/j.1365-246X.2003.02023.x>, 2003.
- 15
- McQuarrie, N.: Crustal scale geometry of the Zagros fold-thrust belt, Iran, *J. Struct. Geol.*, 26(3), 519–535, <https://doi:10.1016/j.jsg.2003.08.009>, 2004.
- Miller, S. R., Slingerland, R. L. and Kirby, E.: Characteristics of steady state fluvial topography above fault-bend folds, *J. Geophys. Res. Earth Surf.*, 112(4), 1–21, <https://doi:10.1029/2007JF000772>, 2007.
- Molinaro, M., Leturmy, P., Guezou, J. C., Frizon de Lamotte, D. and Eshraghi, S. A.: The structure and kinematics of the southeastern Zagros fold-thrust belt, Iran: From thin-skinned to thick-skinned tectonics, *Tectonics*, 24(3), 1–19, <https://doi:10.1029/2004TC001633>, 2005.
- 20
- [Moran, P.P.: Notes on continuous stochastic phenomena, *Biometrika*, 37\(1–2\), 17–23, https://doi:10.1093/biomet/37.1-2.17.1950.](https://doi:10.1093/biomet/37.1-2.17.1950)
- Mouthereau, F.: Timing of uplift in the Zagros belt/Iranian plateau and accommodation of late Cenozoic Arabia-Eurasia convergence, *Geol. Mag.*, 148(5–6), 726–738, <https://doi:10.1017/S0016756811000306>, 2011.
- 25
- Mouthereau, F., Tensi, J., Bellahsen, N., Lacombe, O., De Boissgrollier, T. and Kargar, S.: Tertiary sequence of deformation in a thin-skinned/thick-skinned collision belt: The Zagros Folded Belt (Fars, Iran), *Tectonics*, 26(5), <https://doi:10.1029/2007TC002098>, 2007.
- Mouthereau, F., Lacombe, O. and Vergés, J.: Building the Zagros collisional orogen: Timing, strain distribution and the dynamics of Arabia/Eurasia plate convergence, *Tectonophysics*, 532–535, 27–60, <https://doi:10.1016/j.tecto.2012.01.022>, 2012.
- 30
- Mudd, S. M., Attal, M., Milodowski, D. T., Grieve, S. W. D. and Valters, D. A.: A statistical framework to quantify spatial variation in channel gradients using the integral method of channel profile analysis, *J. Geophys. Res. Earth Surf.*, 119(2), 138–152, <https://doi:10.1002/2013JF002981>, 2014.

- NASA JPL: NASA Shuttle Radar Topography Mission Global 1 arc second [Data set]. NASA EOSDIS Land Processes DAAC. <http://doi:10.5067/MEaSURES/SRTM/SRTMGL1.003>, 2013.
- Navabpour, P., Angelier, J. and Barrier, E.: Stress state reconstruction of oblique collision and evolution of deformation partitioning in W-Zagros (Iran, Kermanshah), *Geophys. J. Int.*, 175(2), 755–782, <https://doi:10.1111/j.1365246X.2008.03916.x>, 2008.
- 5 [Navabpour, P. and Barrier, E.: Stress states in the Zagros fold-and-thrust belt from passive margin to collisional tectonic setting. In: Gudmundsson, A. & Bergerat, F. \(eds\) *Crustal Stresses, Fractures, and Fault Zones: The Legacy of Jacques Angelier*. *Tectonophysics*, 581, 76–83, doi: 10.1016/j.tecto.2012.01.011, 2012.](#)
- Numan, N. M. S.: A plate tectonic scenario for the phanerozoic succession in Iraq, *J. Geol. Soc. Iraq*, 30(2), 85–110, 1997.
- 10 Obaid, A. K. and Allen, M. B.: Landscape maturity, fold growth sequence and structural style in the Kirkuk Embayment of the Zagros, northern Iraq, *Tectonophysics*, 717, 27–40, <https://doi:10.1016/j.tecto.2017.07.006>, 2017.
- Ohmori, H.: Changes in the hypsometric curve through mountain building resulting from concurrent tectonics and denudation, *Geomorphology*, 8(4), 263–277, [https://doi:10.1016/0169-555X\(93\)90023-U](https://doi:10.1016/0169-555X(93)90023-U), 1993.
- ~~Omar, A. A.: An Integrated Structural and Tectonic Study of the Bina Bawi Safin Bradost Region, PhD thesis, Salahaddin University Erbil, 2005.~~
- 15 [Ord, J. K., and Getis, A: Local Spatial Autocorrelation Statistics, Distributional Issues and Application. *Geogr. Anal.*, 27\(4\), 286–306. <https://doi.org/10.1111/j.1538-4632.1995.tb00912.x>, 1995.](#)
- Oveisi, B., Lavé, J., Van Der Beek, P., Carcaillet, J., Benedetti, L. and Aubourg, C.: Thick- and thin-skinned deformation rates in the central Zagros simple folded zone (Iran) indicated by displacement of geomorphic surfaces, *Geophys. J. Int.*, 176(2), 20 627–654, <https://doi:10.1111/j.1365-246X.2008.04002.x>, 2009.
- ~~Pérez Peña, J. V., Azañón, J. M. and Azor, A.: CalHypso: An ArcGIS extension to calculate hypsometric Geophys. curves and their statistical moments. Applications to drainage basin analysis in SE Spain, *Comput. Geosci.*, 35(6), 1214–1223, <https://doi:10.1016/j.cageo.2008.06.006>, 2009.~~
- 25 [-Pe´rez-Peña, J. V., Azañón, J. M., Booth-Rea, G., Azor, A., and Delgado, J.: Differentiating geology and tectonics using a spatial autocorrelation technique for the hypsometric integral, *J. Geophys. Res.*, 114\(F02018\), <https://doi:10.1029/2008JF001092>, 2009.](#)
- Pérez-Peña, J. V., Azañón, J. M., Azor, A., Booth-Rea, G., Galve, J. P., Roldán, F. J., Mancilla, F., Giaconia, F., Morales, J. and Al-Awabdeh, M.: Quaternary landscape evolution driven by slab-pull mechanisms in the Granada Basin (Central Betics), *Tectonophysics*, 663, 5–18, <https://doi:10.1016/j.tecto.2015.07.035>, 2015.
- 30 Perron, J. T.: Climate and the Pace of Erosional Landscape Evolution, *Annu. Rev. Earth Planet. Sci.*, 45(1), annurev-earth5 060614-105405, <https://doi:10.1146/annurev-earth-060614-105405>, 2017.
- Perron, J. T. and Royden, L.: An integral approach to bedrock river profile analysis, *Earth Surf. Process. Landforms*, 38(6), 570–576, <https://doi:10.1002/esp.3302>, 2013.

- Pike, R. J. and Wilson, S. E.: Elevation-relief ratio, hypsometric integral, and geomorphic area-altitude analysis, *Bull. Geol. Soc. Am.*, 82(4), 1079–1084, [https://doi.org/10.1130/0016-7606\(1971\)82\[1079:ERHIAG\]2.0.CO;2](https://doi.org/10.1130/0016-7606(1971)82[1079:ERHIAG]2.0.CO;2), 1971.
- Ramsey, L. A., Walker, R. T. and Jackson, J.: Fold evolution and drainage development in the Zagros mountains of Fars province, SE Iran, *Basin Res.*, 20(1), 23–48, <https://doi:10.1111/j.1365-2117.2007.00342.x>, 2008.
- 5 Refice, A., Giachetta, E. and Capolongo, D.: SIGNUM: A Matlab, TIN-based landscape evolution model, *Comput. Geosci.*, 45, 293–303, <https://doi:10.1016/j.cageo.2011.11.013>, 2012.
- Regard, V., Lagnous, R., Espurt, N., Darrozes, J., Baby, P., Roddaz, M., Calderon, Y. and Hermoza, W.: Geomorphic evidence for recent uplift of the Fitzcarrald Arch (Peru): A response to the Nazca Ridge subduction, *Geomorphology*, 107(3–4), 107–117, <https://doi:10.1016/j.geomorph.2008.12.003>, 2009.
- 10 Reilinger, R., McClusky, S., Vernant, P., Lawrence, S., Ergintav, S., Cakmak, R., Ozener, H., Kadirov, F., Guliev, I., Stepanyan, R., Nadariya, M., Hahubia, G., Mahmoud, S., Sakr, K., ArRajehi, A., Paradissis, D., Al-Aydrus, A., Prilepin, M., Guseva, T., Evren, E., Dmitrova, A., Filikov, S. V., Gomez, F., Al-Ghazzi, R. and Karam, G.: GPS constraints on continental deformation in the Africa-Arabia-Eurasia continental collision zone and implications for the dynamics of plate interactions, *J. Geophys. Res. Solid Earth*, 111(5), 1–26, <https://doi:10.1029/2005JB004051>, 2006.
- 15 ~~Robl, J., Hergarten, S. and Stüwe, K.: Morphological analysis of the drainage system in the Eastern Alps, *Tectonophysics*, 460(1–4), 263–277, <https://doi:10.1016/j.tecto.2008.08.024>, 2008.~~
- Salles, T. and Hardiman, L.: Badlands: An open-source, flexible and parallel framework to study landscape dynamics, *Comput. Geosci.*, 91, 77–89, <https://doi:10.1016/j.cageo.2016.03.011>, 2016.
- Sepehr, M., Cosgrove, J. and Moieni, M.: The impact of cover rock rheology on the style of folding in the Zagros fold-thrust belt, *Tectonophysics*, 427(1–4), 265–281, <https://doi:10.1016/j.tecto.2006.05.021>, 2006.
- ~~Sherkati, S., Molinaro, M., Frizon de Lamotte, D. and Letouzey, J.: Detachment folding in the Central and Eastern Zagros fold belt (Iran): Salt mobility, multiple detachments and late basement control, *J. Struct. Geol.*, 27(9), 1680–1696, 30 <https://doi:10.1016/j.jsg.2005.05.010>, 2005.~~
- 25 Sherkati, S., Letouzey, J. and De Lamotte, D. F.: Central Zagros fold-thrust belt (Iran): New insights from seismic data, field observation, and sandbox modeling, *Tectonics*, 25(4), 1–27, <https://doi:10.1029/2004TC001766>, 2006.
- Sissakian, V. K.: Geological Map of ~~IArbeel~~[Arbeel](#) and Mahabad Quadrangles Sheets NJ-38- 14 and NJ-38-15, Scale 1:250.000, 1997.
- Sklar, L. and Dietrich, W. E.: River Longitudinal Profiles and Bedrock Incision Models: Stream Power and the Influence of Sediment Supply, in *Rivers Over Rock: Fluvial Processes in Bedrock Channels*, edited by K. J. Tinkler and E. E. Wohl, pp. 237–260, American Geophysical Union., 1998.
- 30 [Stockhecke, M., Timmermann, A., Kipfer, R., Haug, G., Kwiecien, O., Friedrich, T., Menviel, L., Litt, T., Pickarski, N., Anselmetti, F. S.: Millennial to orbital-scale variations of drought intensity in the eastern Mediterranean, *Quaternary Science Reviews*, 133, 77–95. <https://doi.org/10.1016/j.quascirev.2015.12.016>, 2016.](https://doi.org/10.1016/j.quascirev.2015.12.016)

- Strahler, A.: Hypsometric (Area-Altitude) Analysis of Erosional Topography, *GSA Bull.*, 63(11), 1117–1142, [https://doi.org/10.1130/0016-7606\(1952\)63\[1117:HAAOET\]2.0.CO;2](https://doi.org/10.1130/0016-7606(1952)63[1117:HAAOET]2.0.CO;2), 1952.
- Syan, S. H. A.: Tectonic Criteria from Shortening Estimation in different geological time and space using Balancing Cross Sections in the Harir and Khatibian Anticlines, Zagros Fold-Thrust Belt, Kurdistan of Iraq, MSc. Thesis, Salahaddin University-Erbil., 2014.
- Tarolli, P.: High-resolution topography for understanding Earth surface processes: Opportunities and challenges, *Geomorphology*, 216, 295–312, <https://doi:10.1016/j.geomorph.2014.03.008>, 2014.
- Temme, A. J. A. M., Armitage, J., Attal, M., van Gorp, W., Coulthard, T. J. and Schoorl, J. M.: Developing, choosing and using landscape evolution models to inform field-based landscape reconstruction studies, *Earth Surf. Process. Landforms*, 42(13), 2167–2183, <https://doi:10.1002/esp.4162>, 2017.
- Tucker, G. E. and Bras, R. L.: Hillslope processes, drainage density, and landscape morphology, *Water Resour. Res.*, 34(10), 2751–2764, <https://doi:10.1029/98WR01474>, 1998.
- Tucker, G. E. and Hancock, G. R.: Modelling landscape evolution, *Earth Surf. Process. Landforms*, 35(1), 28–50, <https://doi.org/10.1002/esp.1952>, 2010.
- 15 Tucker, G., Lancaster, S., Gasparini, N., and Bras, R.: The channel hillslope integrated landscape development model (CHILD), in: *Landscape erosion and evolution modeling*, edited by: Harmon, R. S. and Doe III, W. W., 349–388, Kluwer Academic/Plenum Publishers, New York, USA, 2001.
- Tucker, G. E., Hobbey, D. E. J., Hutton, E., Gasparini, N. M., Istanbuluoglu, E., Adams, J. M. and Siddartha Nudurupati, S.: CellLab-CTS 2015: Continuous-time stochastic cellular automaton modeling using Landlab, *Geosci. Model Dev.*, 9(2), 823–
20 839, <https://doi:10.5194/gmd-9-823-2016>, 2016.
- ~~Valters, D. A.: Modelling geomorphic systems: landscape evolution, in: *Geomorphological Techniques*, edited by: Cook, S.J., Clarke, L.E. and Nield, J.M., British Society for Geomorphology, London, UK, Chap. 5, Sec. 6.12, 2016.~~
- ~~van der Beek, P.: Modelling landscape evolution, in: *Environmental Modelling*, edited by: Wainwright, J., and Mulligan, M., Wiley and Sons, Ltd, 309–331, <https://doi:10.1002/9781118351475.ch19>, 2013.~~
- 25 Vergés, J., Saura, E., Casciello, E., Fernández, M., Villaseñor, A., Jiménez-Munt, I. and García-Castellanos, D.: Crustal-scale cross-sections across the NW Zagros belt: Implications for the Arabian margin reconstruction, *Geol. Mag.*, 148(5–6), 739–761, <https://doi:10.1017/S0016756811000331>, 2011.
- Vernant, P., Nilforoushan, F., Hatzfeld, D., Abbassi, M. R., Vigny, C., Masson, F., Nankali, H., Martinod, J., Ashtiani, A., Bayer, R., Tavakoli, F. and Chéry, J.: Present-day crustal deformation and plate kinematics in the Middle East constrained by
30 GPS measurements in Iran and northern Oman, *Geophys. J. Int.*, 157(1), 381–398, <https://doi:10.1111/j.1365246X.2004.02222.x>, 2004.
- ~~Walcott, R. C. and Summerfield, M. A.: Scale dependence of hypsometric integrals: An analysis of southeast African basins, *Geomorphology*, 96(1–2), 174–186, <https://doi:10.1016/j.geomorph.2007.08.001>, 2008.~~

Whipple, K. X.: Implications of sediment-flux-dependent river incision models for landscape evolution, *J. Geophys. Res.*, 107(B2), 2039, <https://doi:10.1029/2000JB000044>, 2002.

Whipple, K. X. and Tucker, G. E.: Dynamics of the stream-power river incision model: Implications for height limits of mountain ranges, landscape response timescales, and research needs, *J. Geophys. Res. Solid Earth*, 104(B8), 17661–17674, <https://doi:10.1029/1999JB900120>, 1999.

Whittaker, A. C.: How do landscapes record tectonics and climate? *Lithosphere*, 4(2), 160–164, <https://doi:10.1130/RF.L003.1>, 2012.

Wobus, C., Whipple, K. X., Kirby, E., Snyder, N., Johnson, J., Spyropolou, K., Crosby, B. and Sheehan, D.: Tectonics from topography: procedures, promise, and pitfalls, *Geol. Soc. Am. Spec. Pap.*, 398(04), 55–74, [https://doi:10.1130/2006.2398\(04\)](https://doi:10.1130/2006.2398(04)), 2006.

Zebari, M.: Geometry and Evolution of Fold Structures within the High Folded Zone: Zagros Fold-Thrust Belt, Kurdistan Region-Iraq, University of Nebraska-Lincoln., 2013.

Zebari, M. M. and Burberry, C. M.: 4-D evolution of anticlines and implications for hydrocarbon exploration within the Zagros Fold- Thrust Belt, Kurdistan Region, Iraq, *GeoArabia*, 20(1), 161–188, 2015.

15

Figures

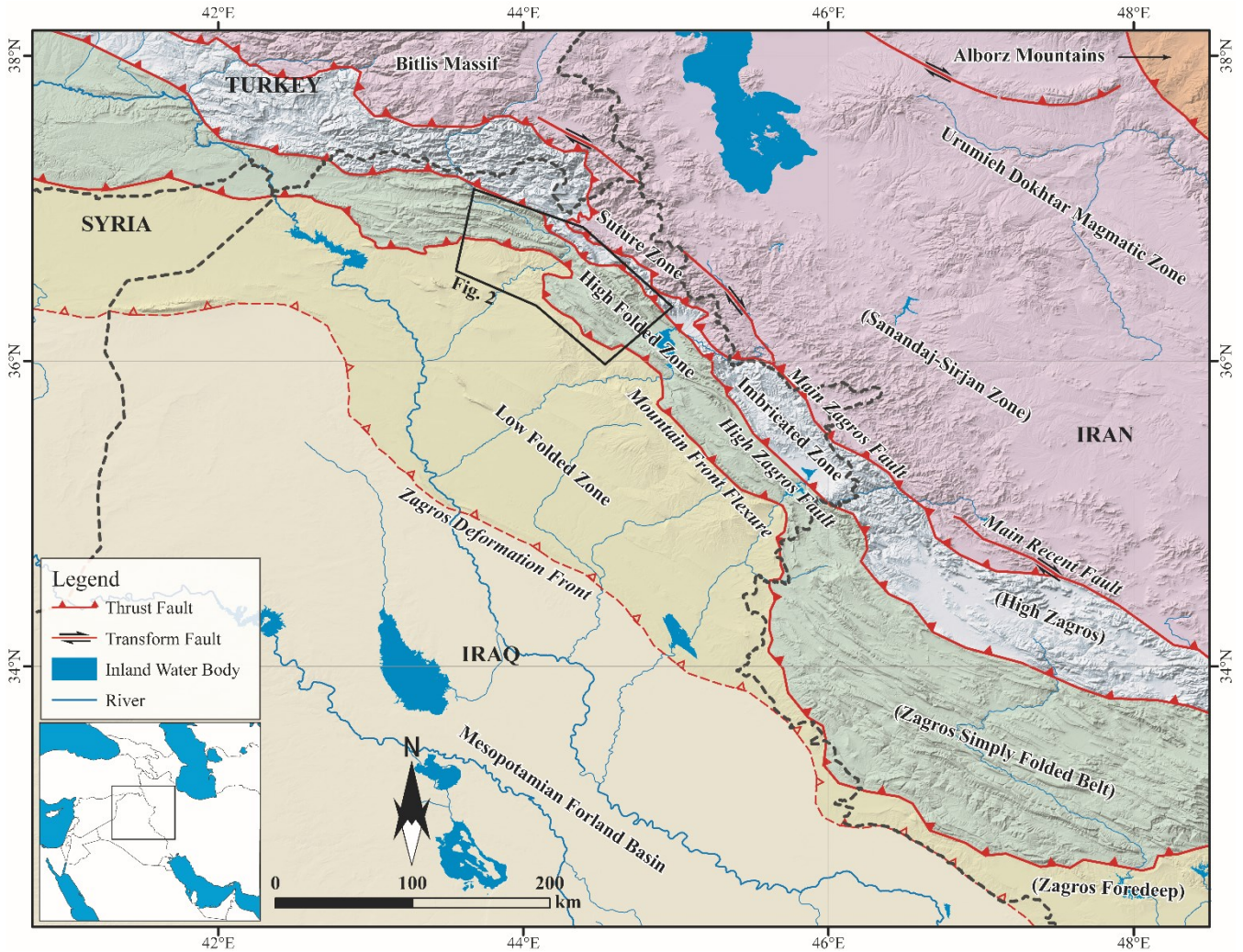
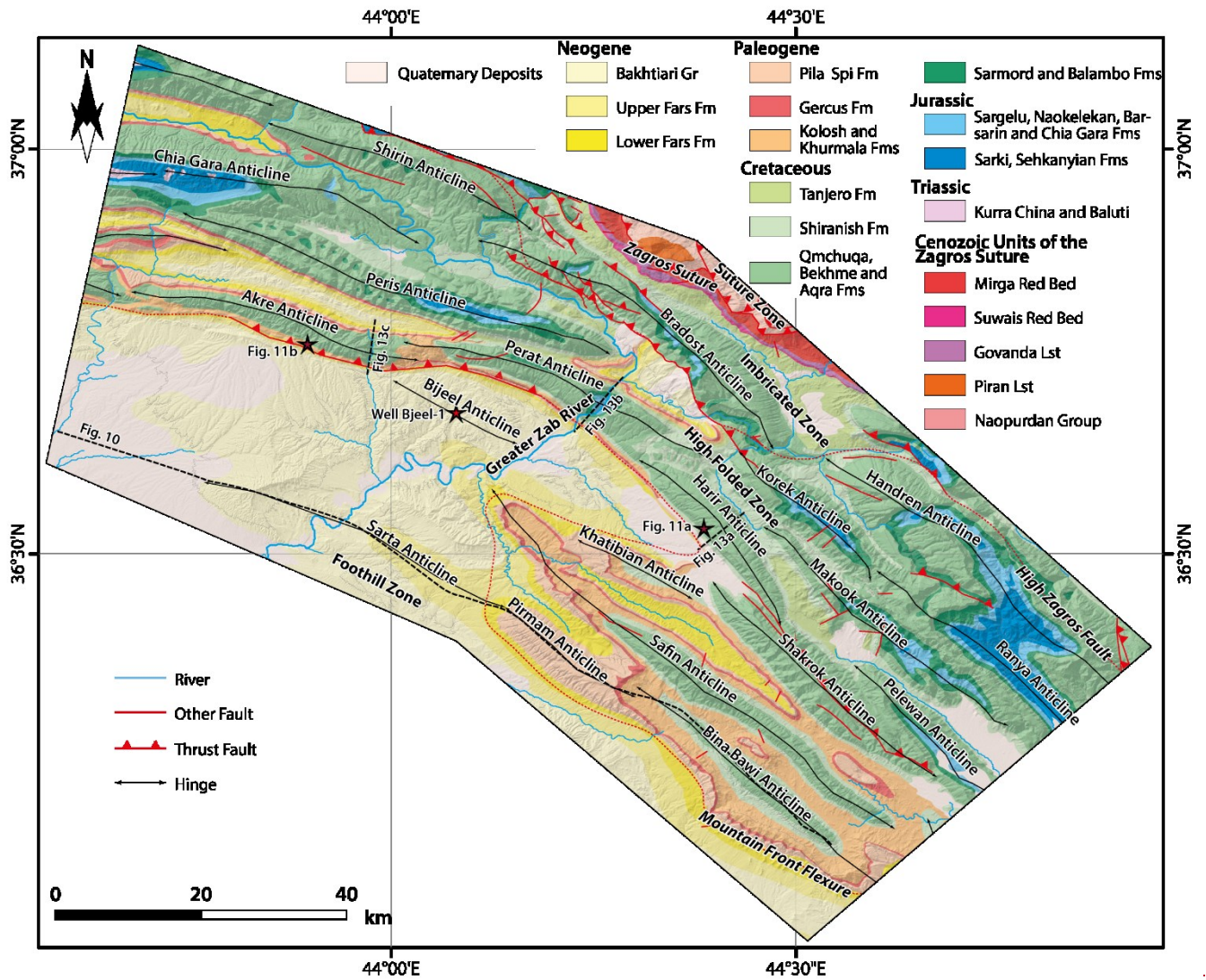


Figure 1: Tectonic subdivision of the NW segment of the Zagros Fold-Thrust Belt (modified after Berberian, 1995; Emre et al., 2013;

5 Koshnaw et al., 2017; Zebari and Burberry, 2015). Names within the parentheses are known in the Iranian part of Zagros.



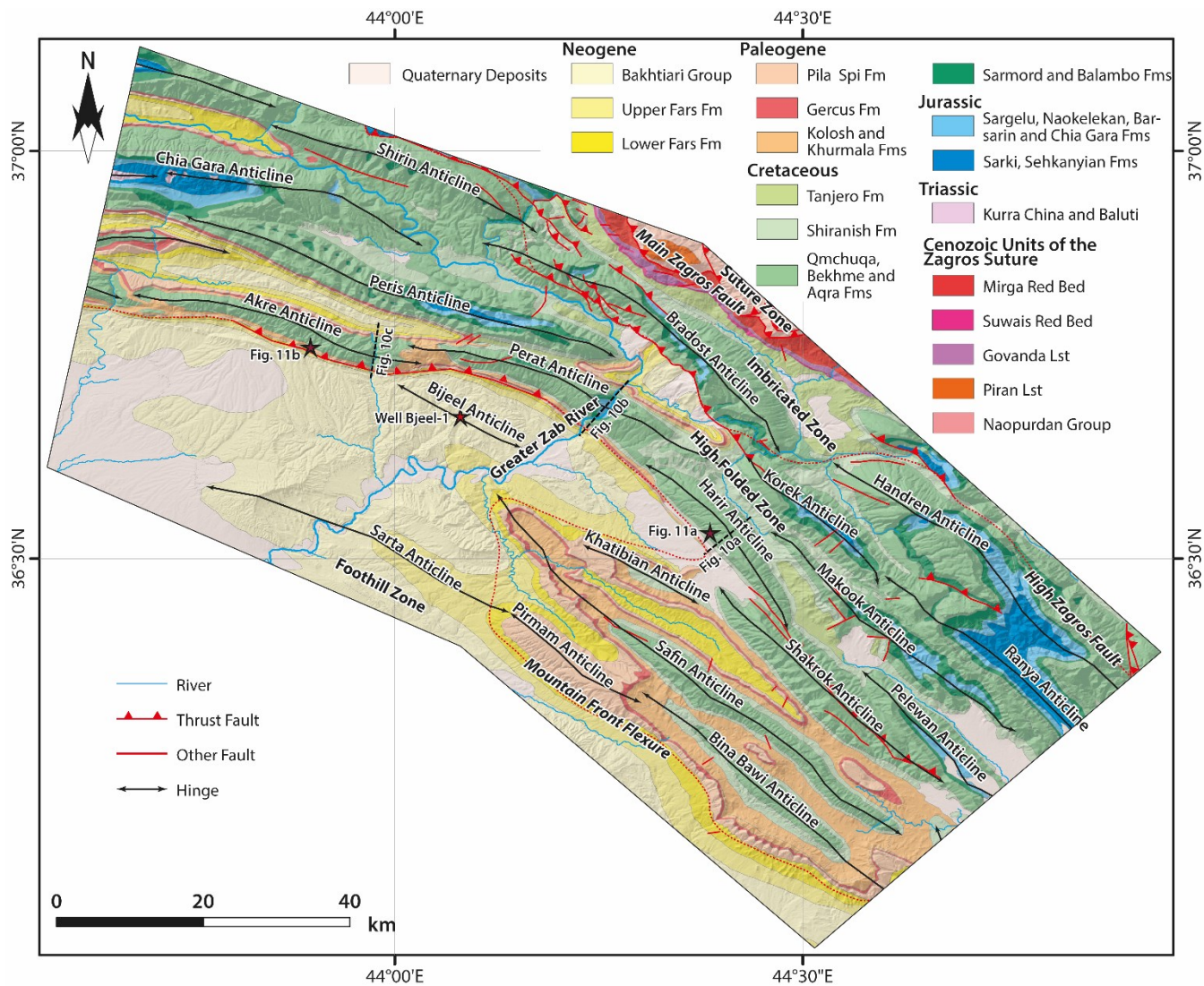
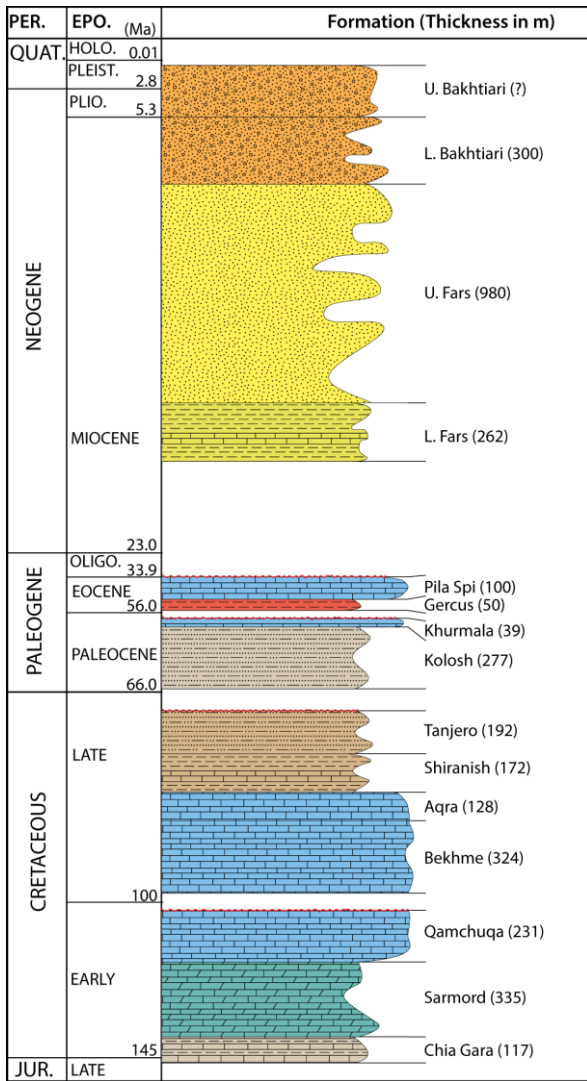


Figure 2: Geological map of the Zagros belt in KRI showing the location of the three anticlines Harir, Perat, and Akre with respect to the MFF that separates the High Folded Zone from the Foothill Zone (modified after Csontos et al., 2012; Sissakian, 1997; Zebari and Burberry, 2015).



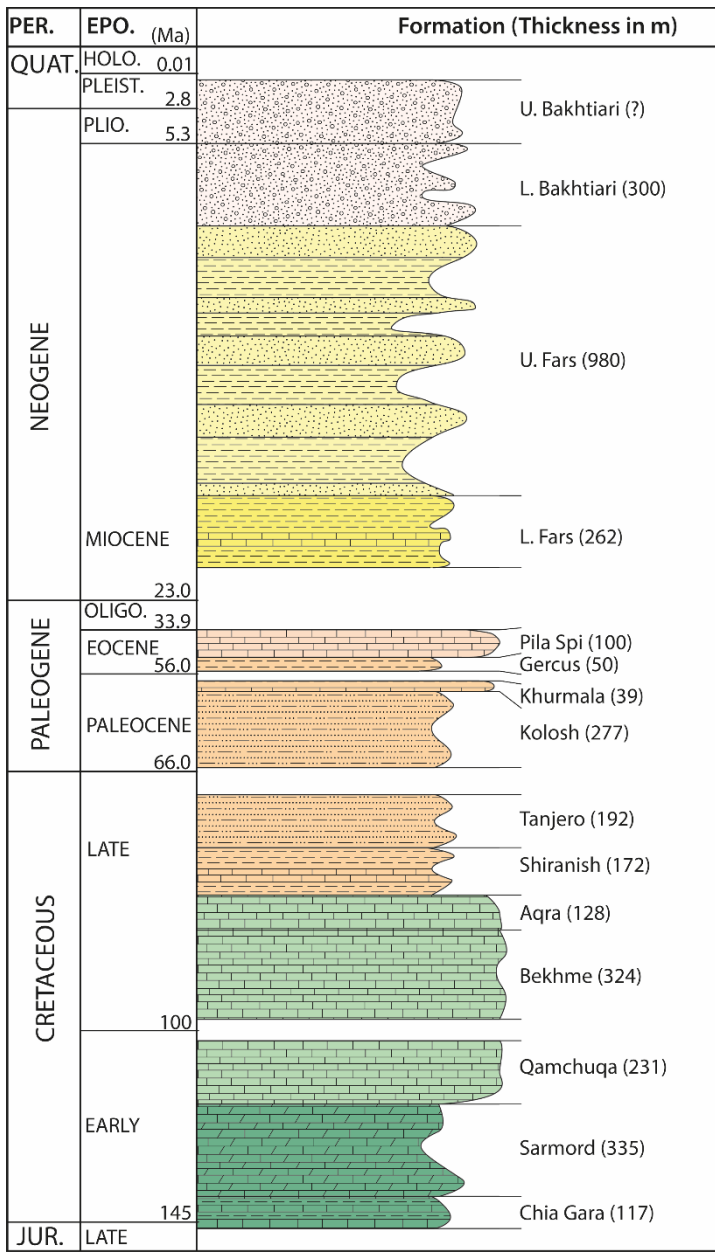


Figure 3: Stratigraphic column of the exposed rock units in the area. Thicknesses are given as in well Bijeel-1 (Fig. 2), which is located 5 km to the south of Perat Anticline (modified after Law et al., 2014). The column is scaled to the stratigraphic thicknesses.

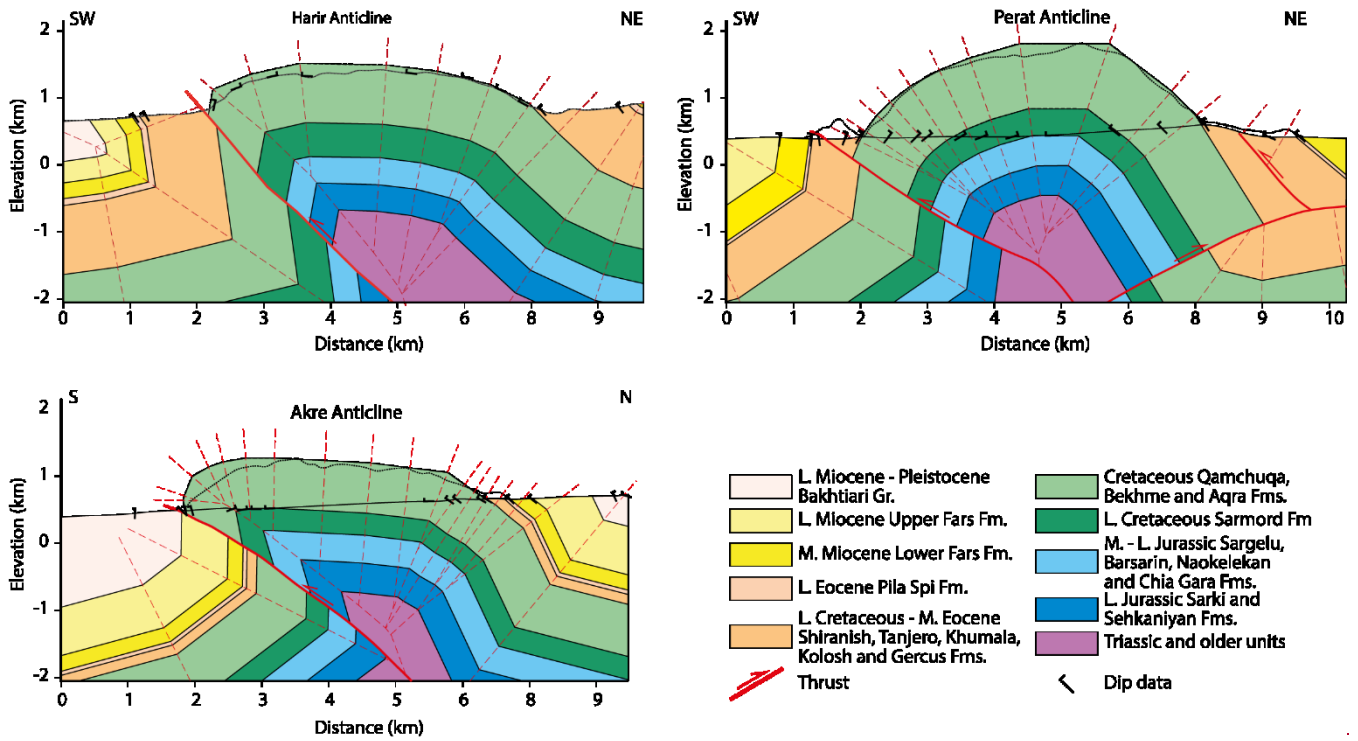


Figure 4: Structural cross-section across the three studied anticlines; a) Harir section (modified after Syan, 2014), b) Perat section constructed from field data and thrusts inferred from an interpreted seismic line by Csonotos et al. (2012), c) Akre section constructed from field data (see Figure 2 for the locations).

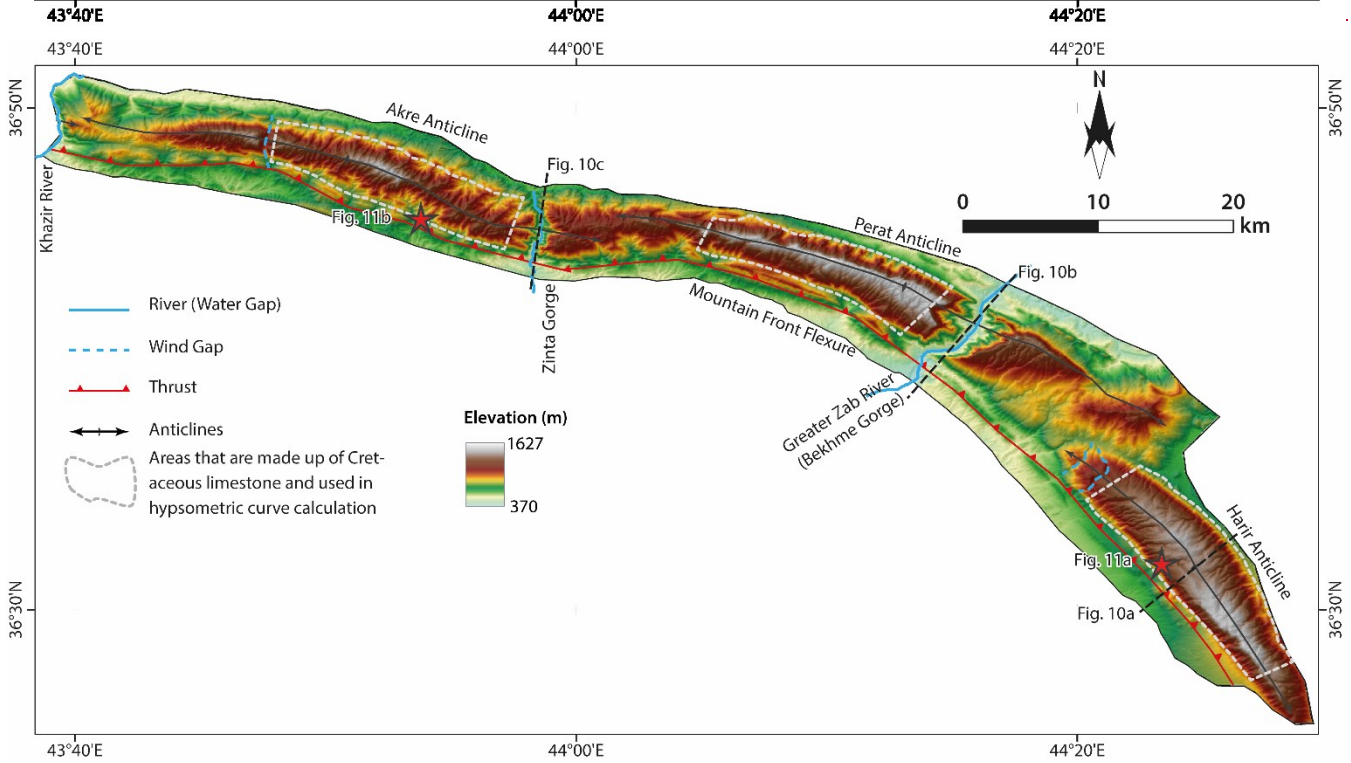
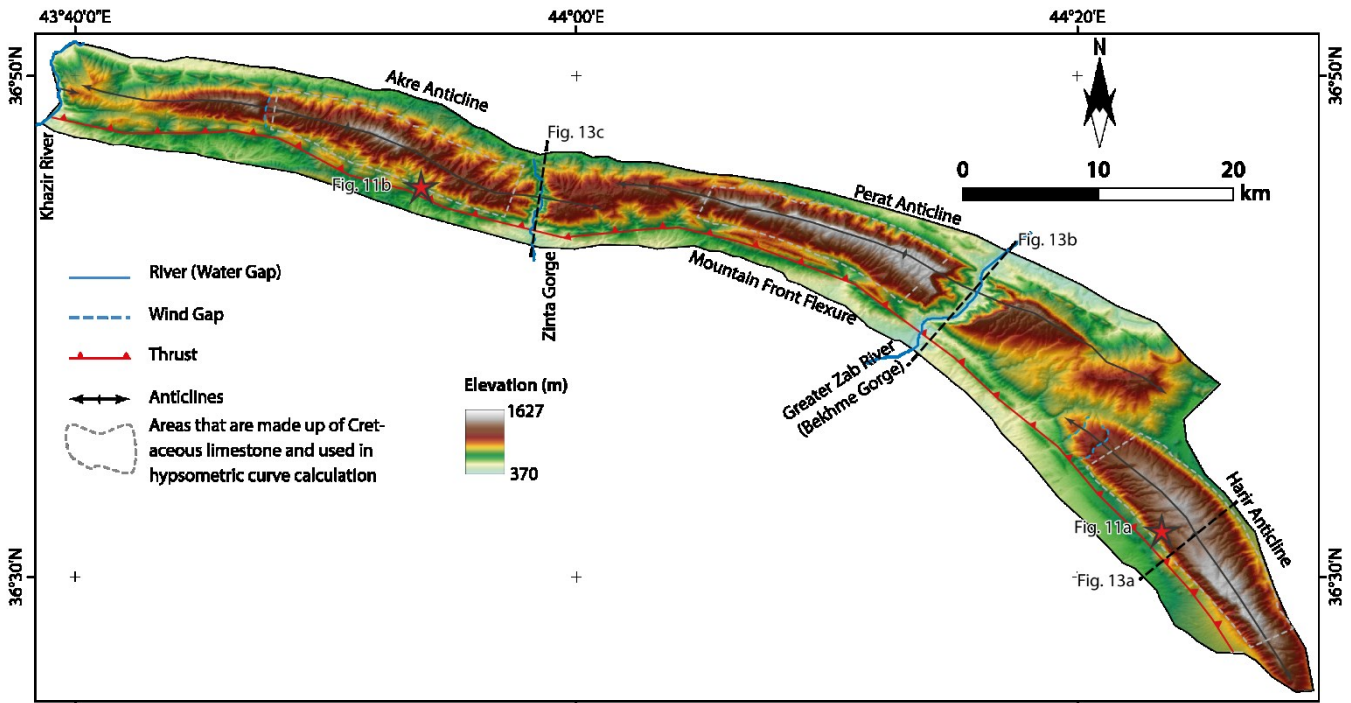
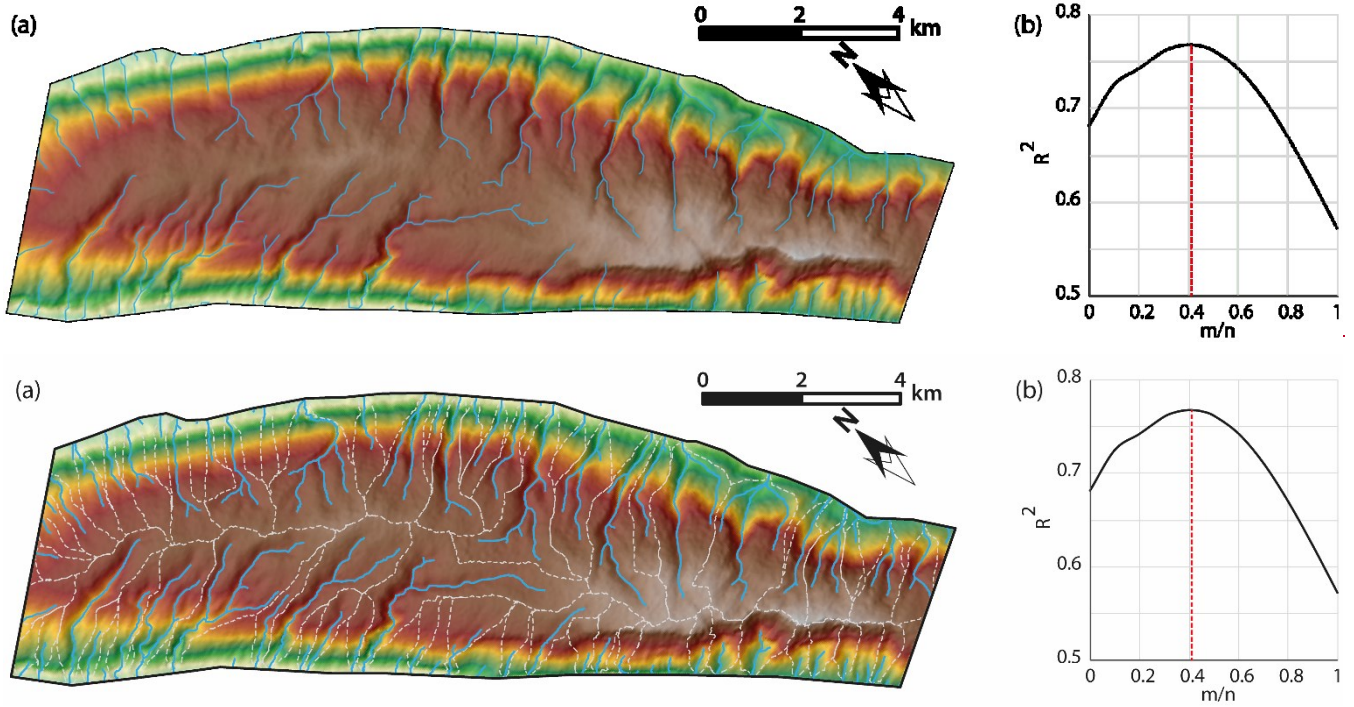


Figure 54: Topography of the studied anticlines obtained from 30 m resolution SRTM1 DEM data showing the location of water and wind gaps across these anticlines.



5

Figure 65: a) DEM grid, and drainage network and basins for the present-day Harir Anticline that is used as an input for the model. White lines are basin divides; b) m/n plotted against regression values of elevation-X plot for streams in the Harir Anticline. The highest regression is achieved for $m/n = 0.41$.

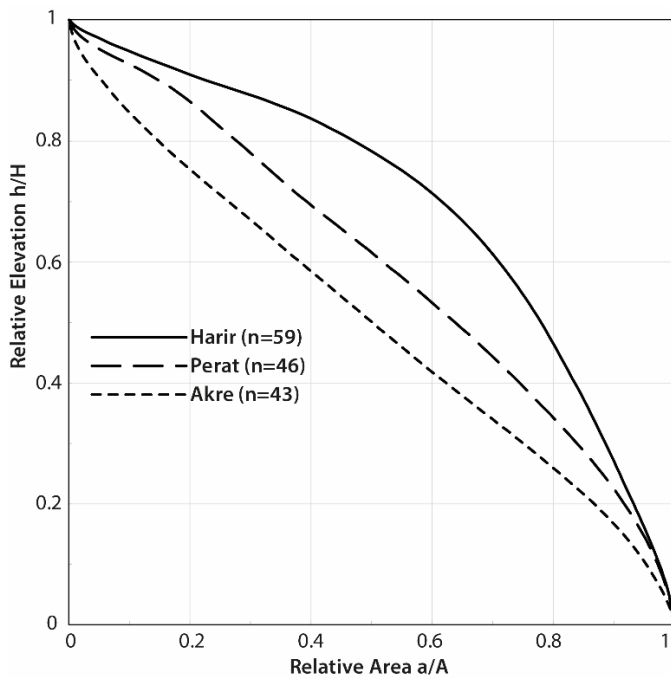
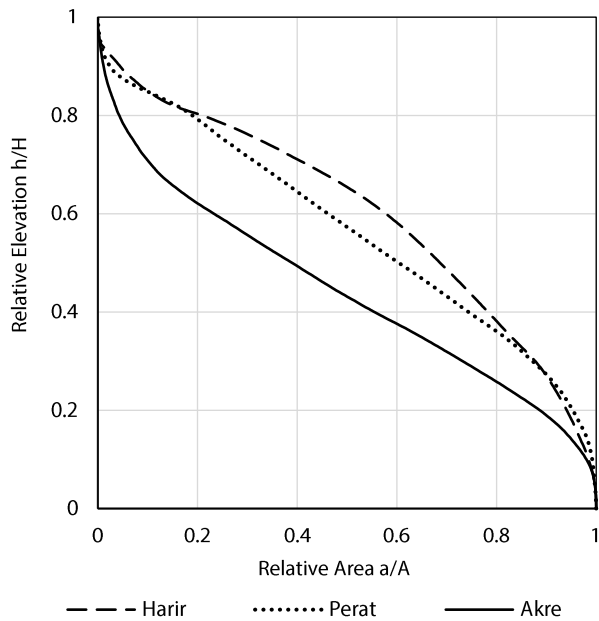


Figure 76: Present-day **Hypsometric** **hypso**metric curves of the studied anticlines. **The curves are calculated as a total weighted mean for drainage basins within each anticline.** We only use those parts where Upper Cretaceous carbonate rocks crop out and we exclude wind gaps, water gaps, and the plunging tips of anticlines. **n is the number of basins used in calculation of the hypsometric curve for each anticline.**

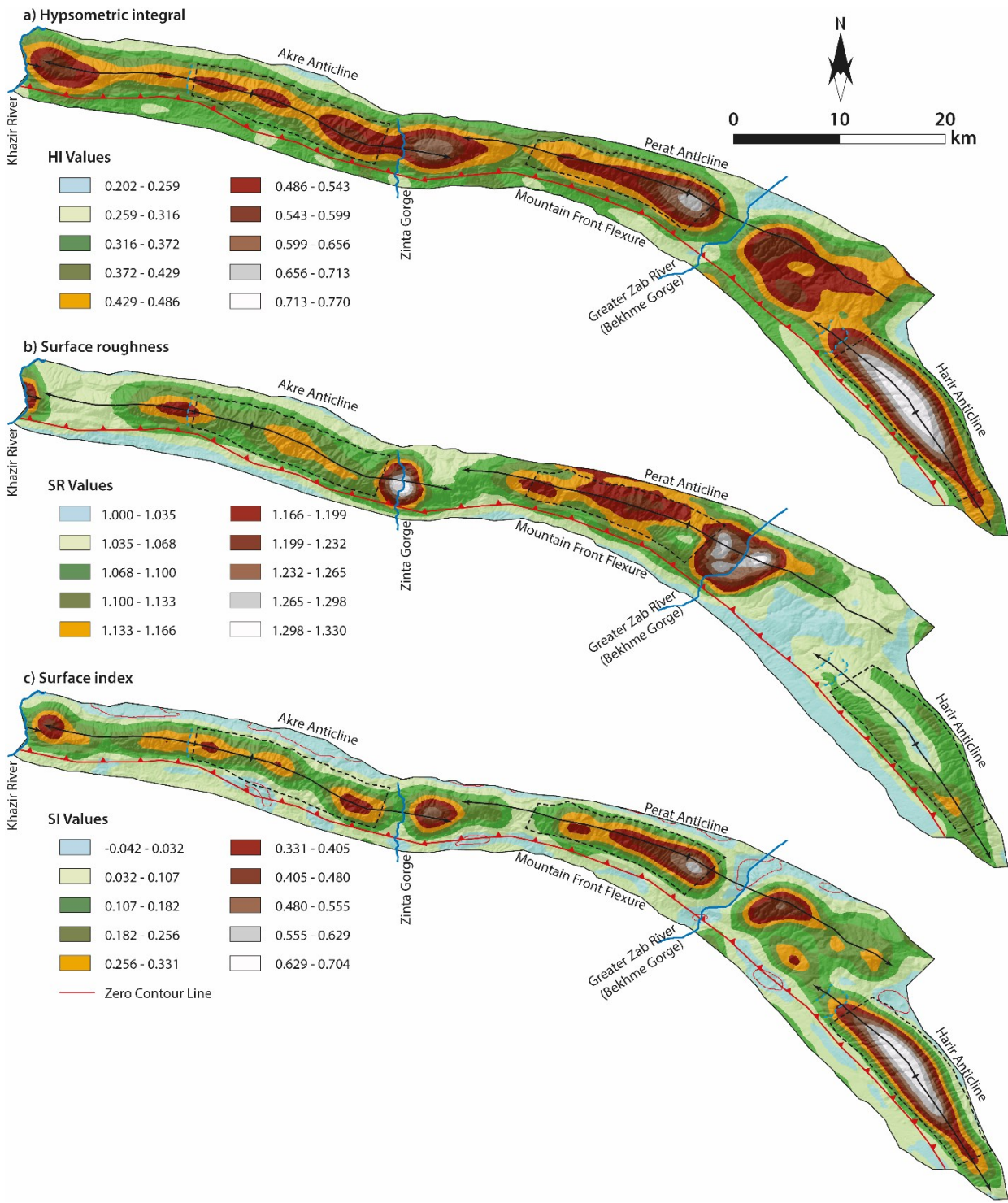
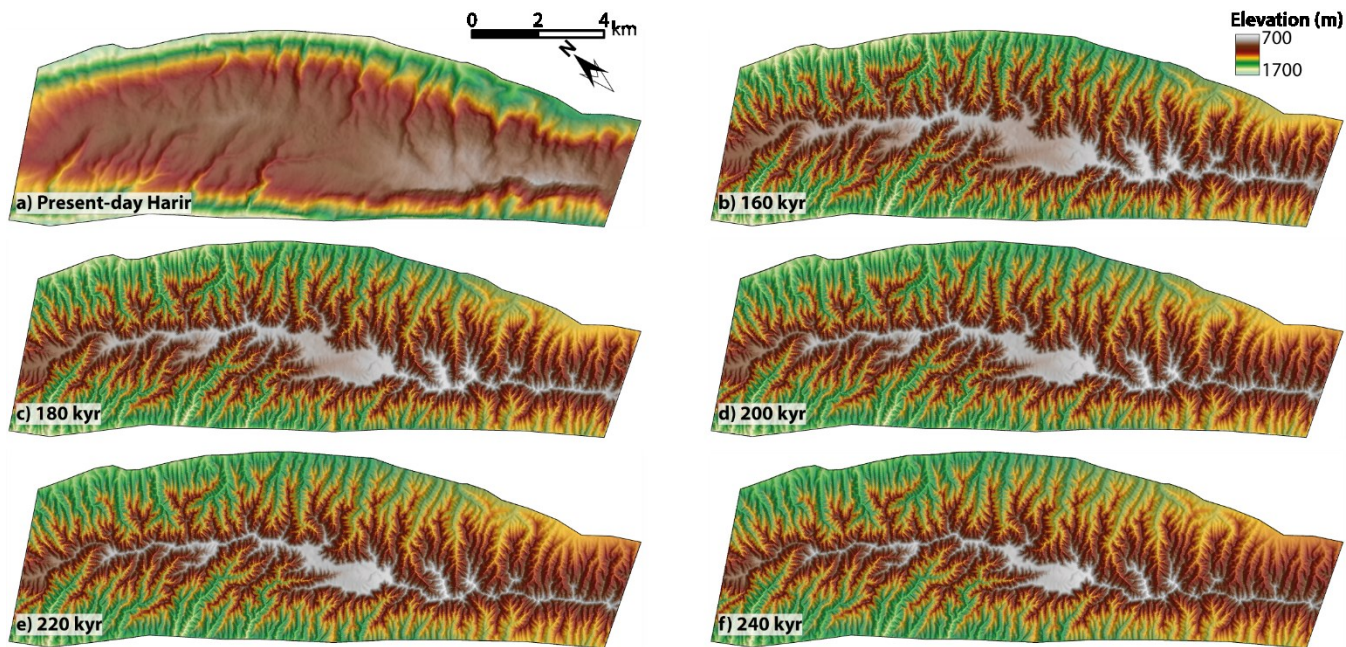


Figure 87: Surface index maps for the three anticlines calculated from 100 x 100 pixel cells (3 x 3 km) and moving windows; a) hypsometric integral, b) surface roughness, and c) surface index.



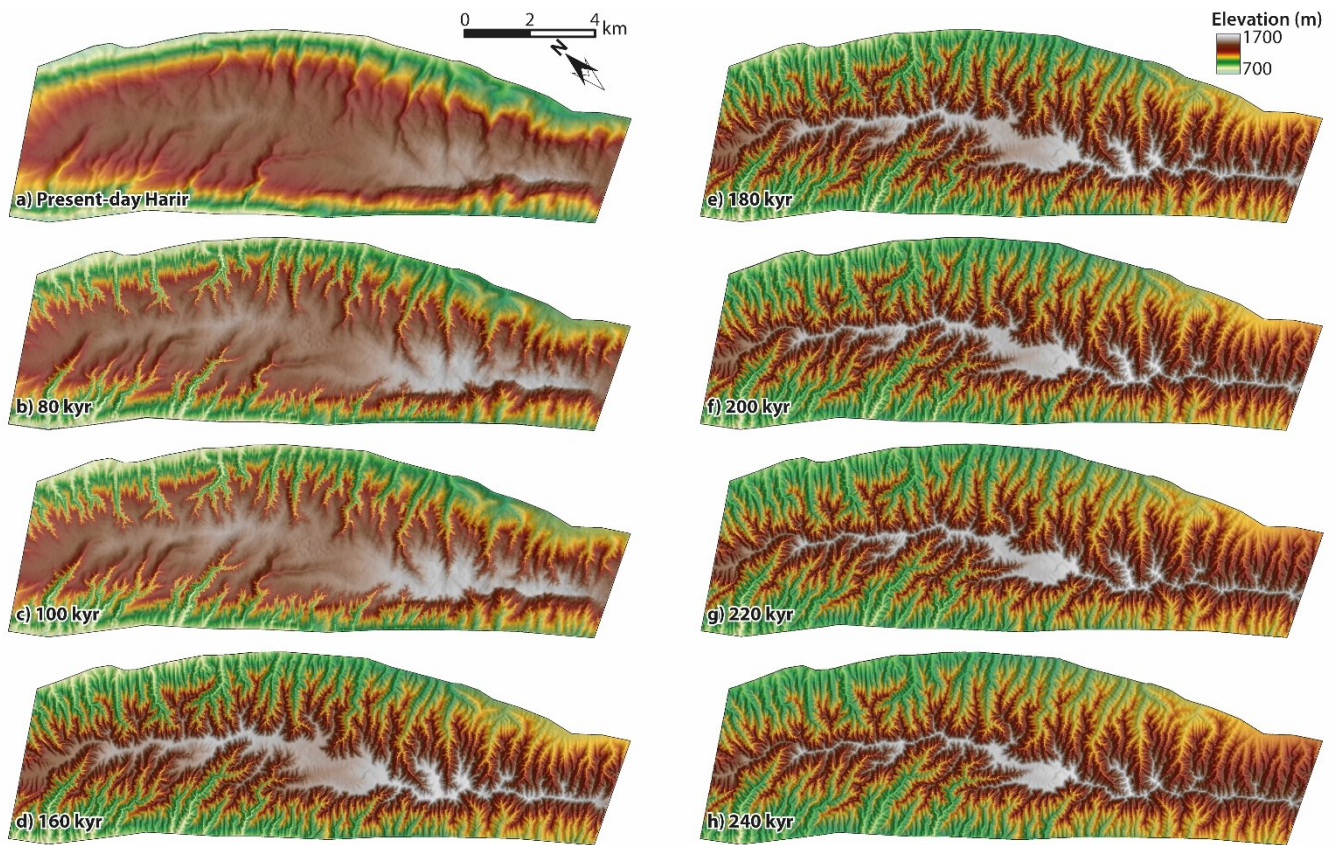


Figure 93: The input landscape (a), which is the present-day Harir topography, and the evolved landscape through time; b) 160-80 kyr, c) 180-100 kyr, d) 200-160 kyr, e) 220-180 kyr, and f) 240-200 kyr, g) 220 kyr, and h) 240 kyr.

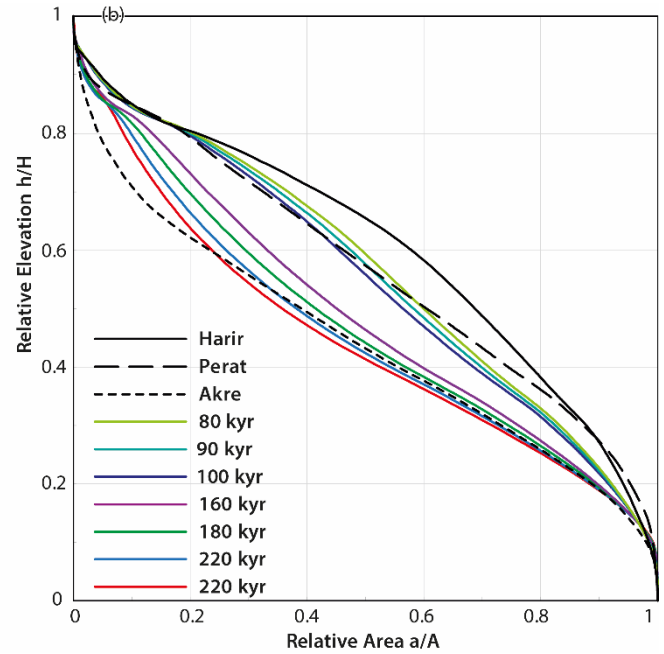
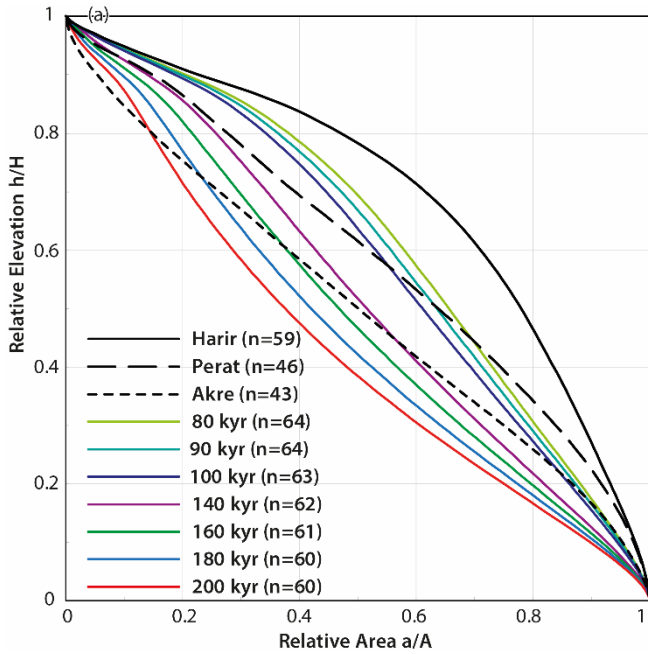
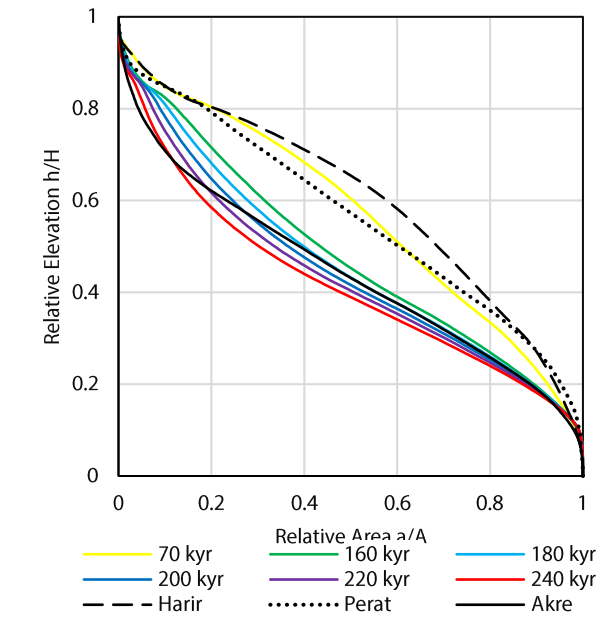


Figure 109: Hypsometric curves of the studied anticlines and those of the evolved Harir landscape from the model for ~~six~~ **six** different time spans. **a)** The curves were calculated using the total weighted mean for drainage basin within each anticline, indicating that the evolved landscapes after 100 and 160 are the closest ones to the present-day Perat and Akre anticlines, respectively. **n** is the number of basins used in calculation of the hypsometric curve for each time; **b)** the curves were calculated for the entire anticline, indicating that the evolved landscapes after 80 and 200 are the closest ones to the present-day Perat and Akre anticlines, respectively.

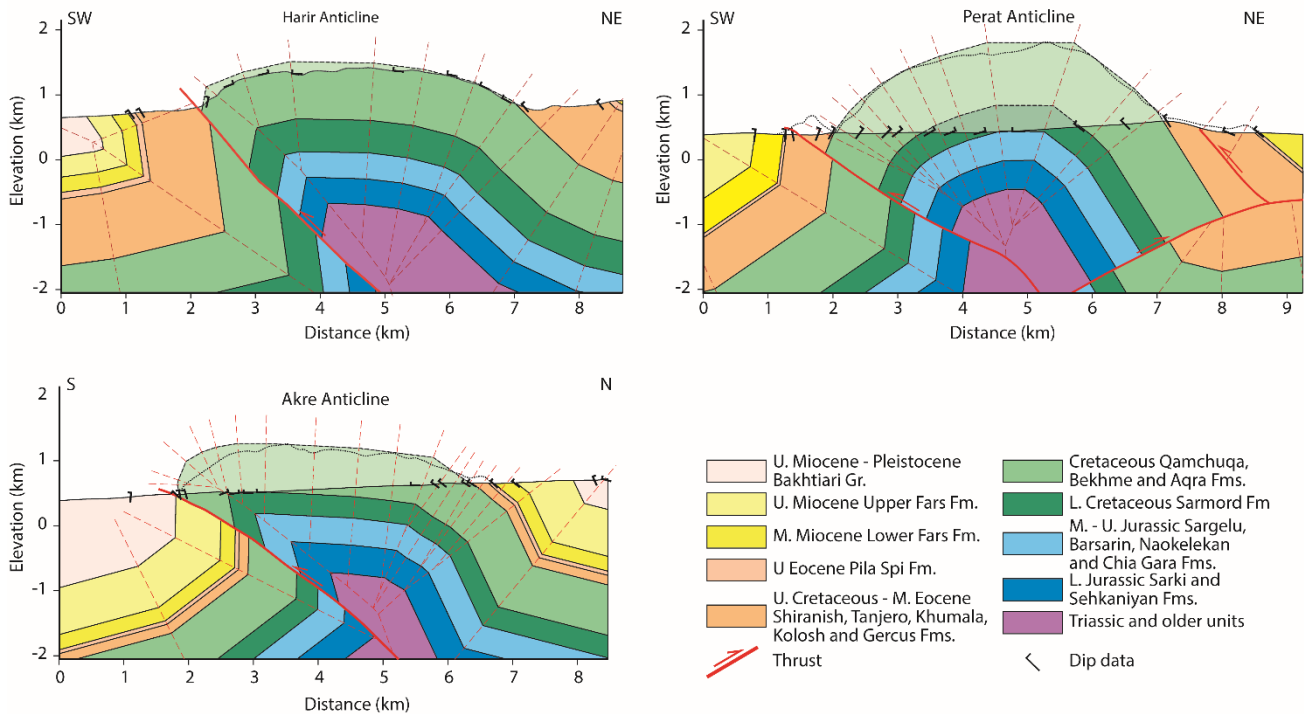


Figure 10: Structural cross-section across the three studied anticlines; a) Harir section (modified after Svan, 2014), b) Perat section constructed from field data and thrusts inferred from a seismic line by Csontos et al. (2012), c) Akre section constructed from field data (see Figure 2 and 4 for the locations).

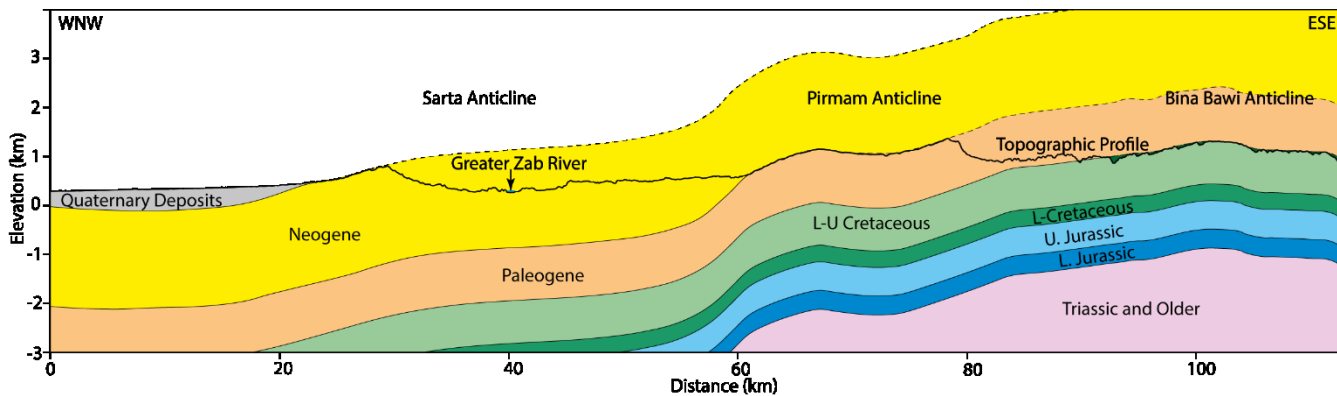


Figure 11: Topographic profile along the axis of Bina Bawi, Pirman, and Sarta Anticlines (see Figure 2 for location), showing the distinctive successive stages of uplift/erosion due to folding within the Zagros Fold-Thrust Belt in KRI.

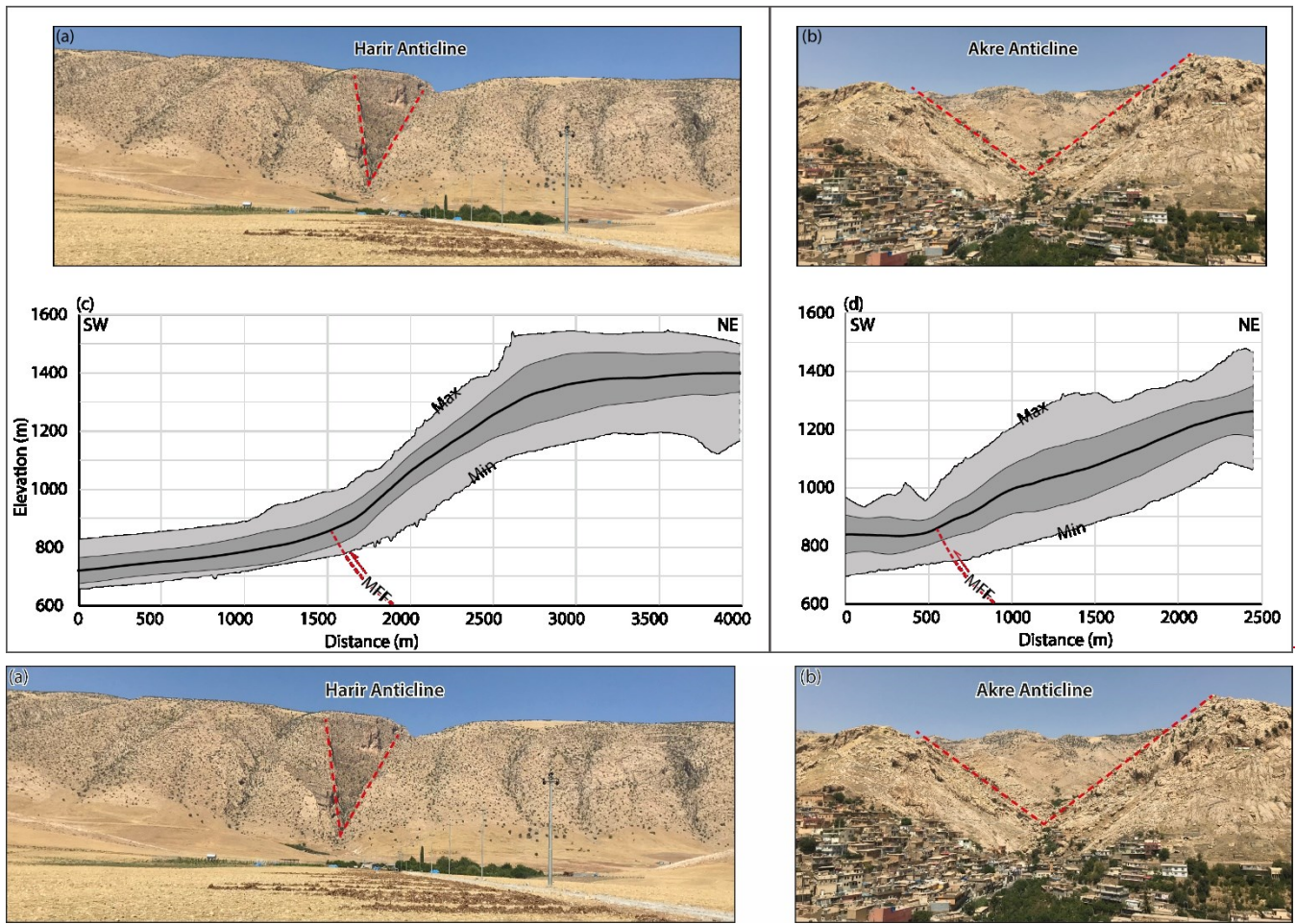


Figure 12.11: Different shape of valleys in the Harir (a) and Akre Anticlines (b); see Figures 2 and 5.4 for the locations, and swath topographic profiles across the southern limb of Harir (c) and Akre (d) Anticlines. Right side of the topographic profiles mark the locations where the Pila Spi Fm crops out in the anticlines' crest. MFF: Mountain Front Flexure.

5

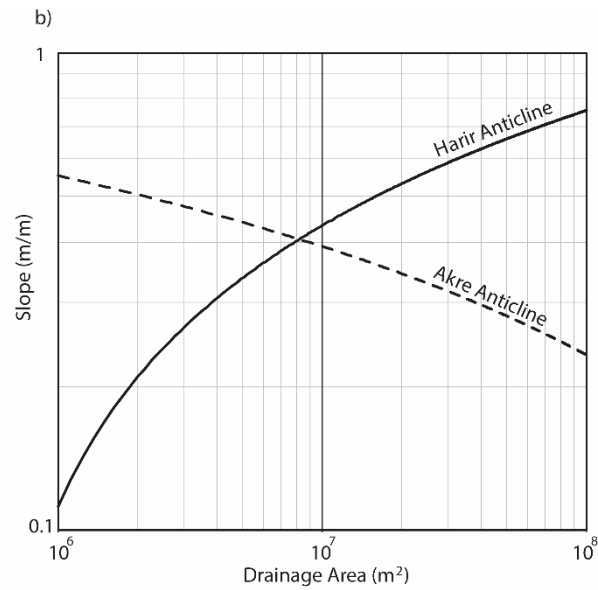
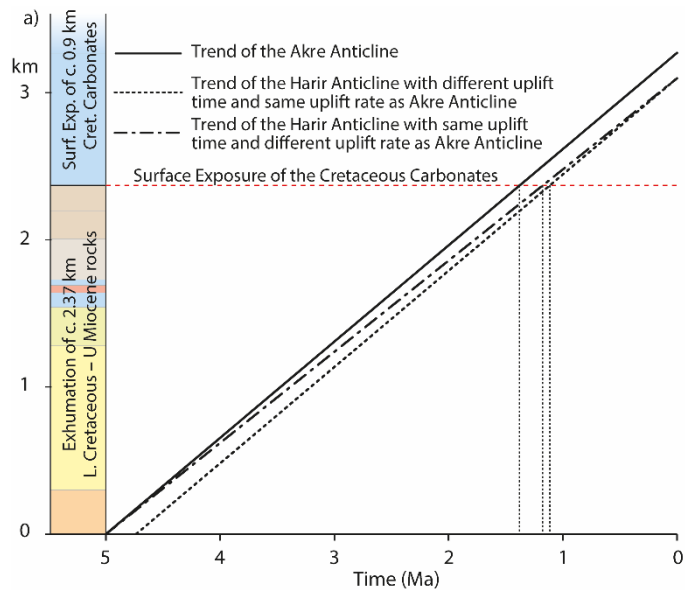
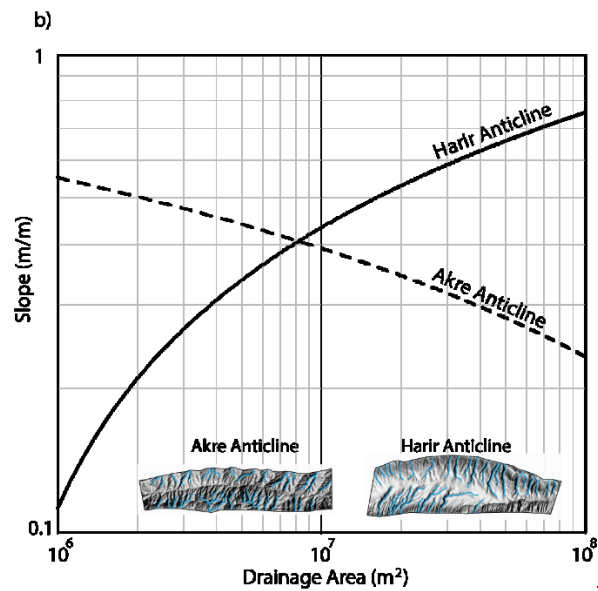
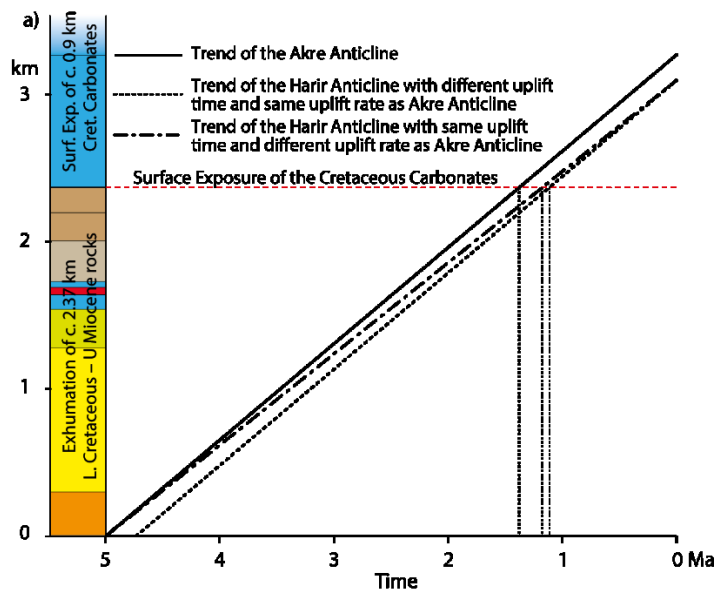


Figure 13.12: a) Diagram showing the exposure time of the Upper Cretaceous carbonates in Akre and Harir Anticlines. Two different scenarios are plotted for Harir: Having a slower uplift rate than Akre, or onset of uplift later than Akre. b) Channel slope-drainage area plots of streams in both Akre and Harir Anticlines.

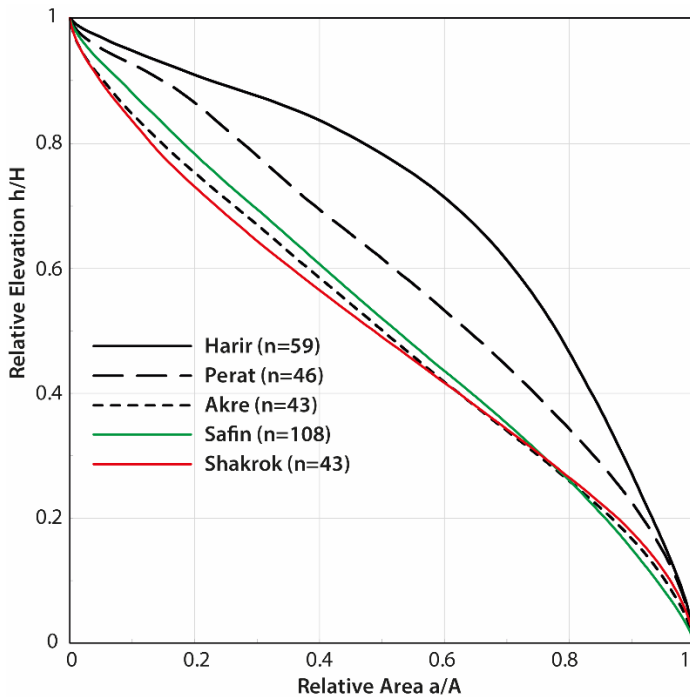
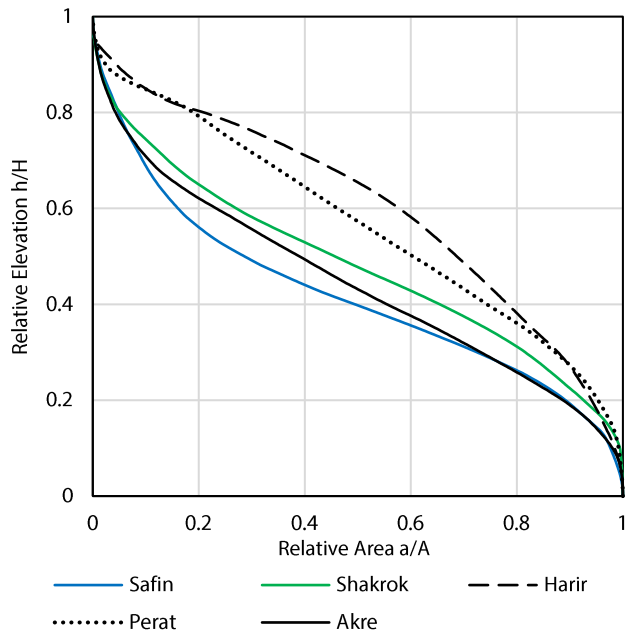
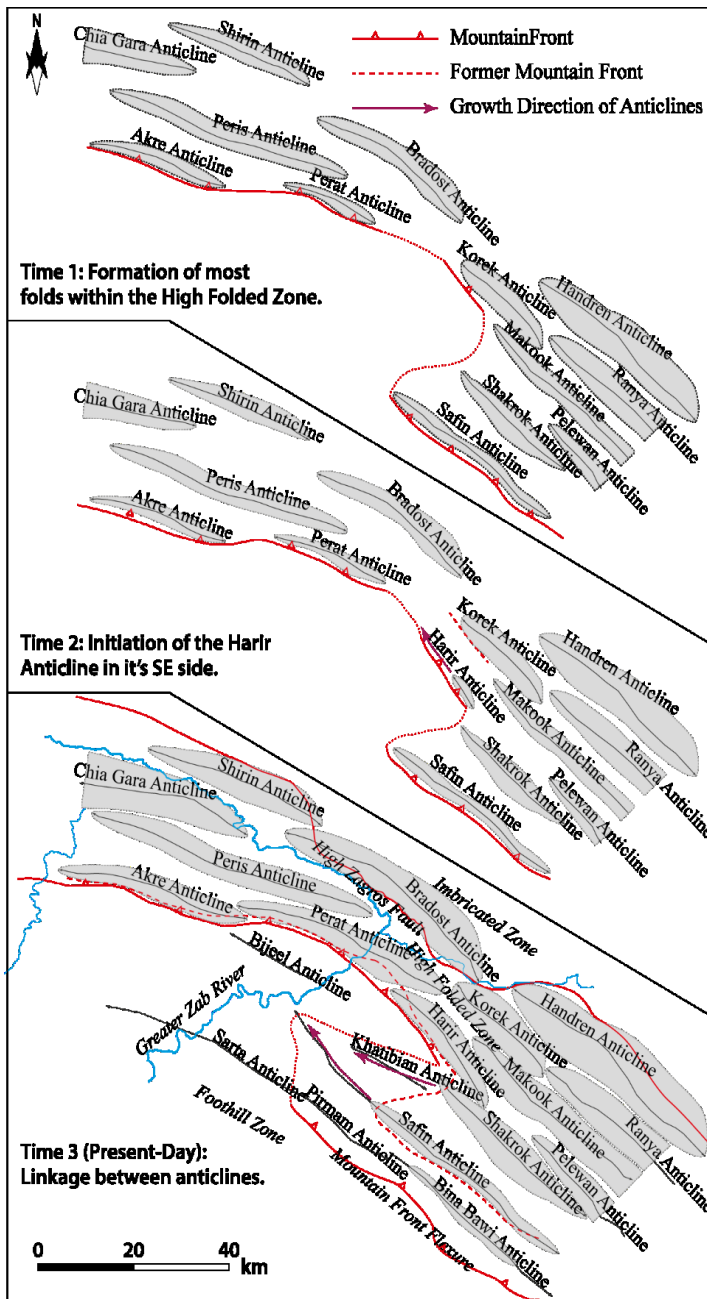


Figure 1413: Total weighted mean H hypsometric curves for drainage basin within the studied anticlines as compared to those of the Shakrok and Safin anticlines, which show that, ~~the~~ Harir's curve is more convex than that of both Shakrok and Safin. n is the number of basins used in calculation of the hypsometric curve for each anticline.



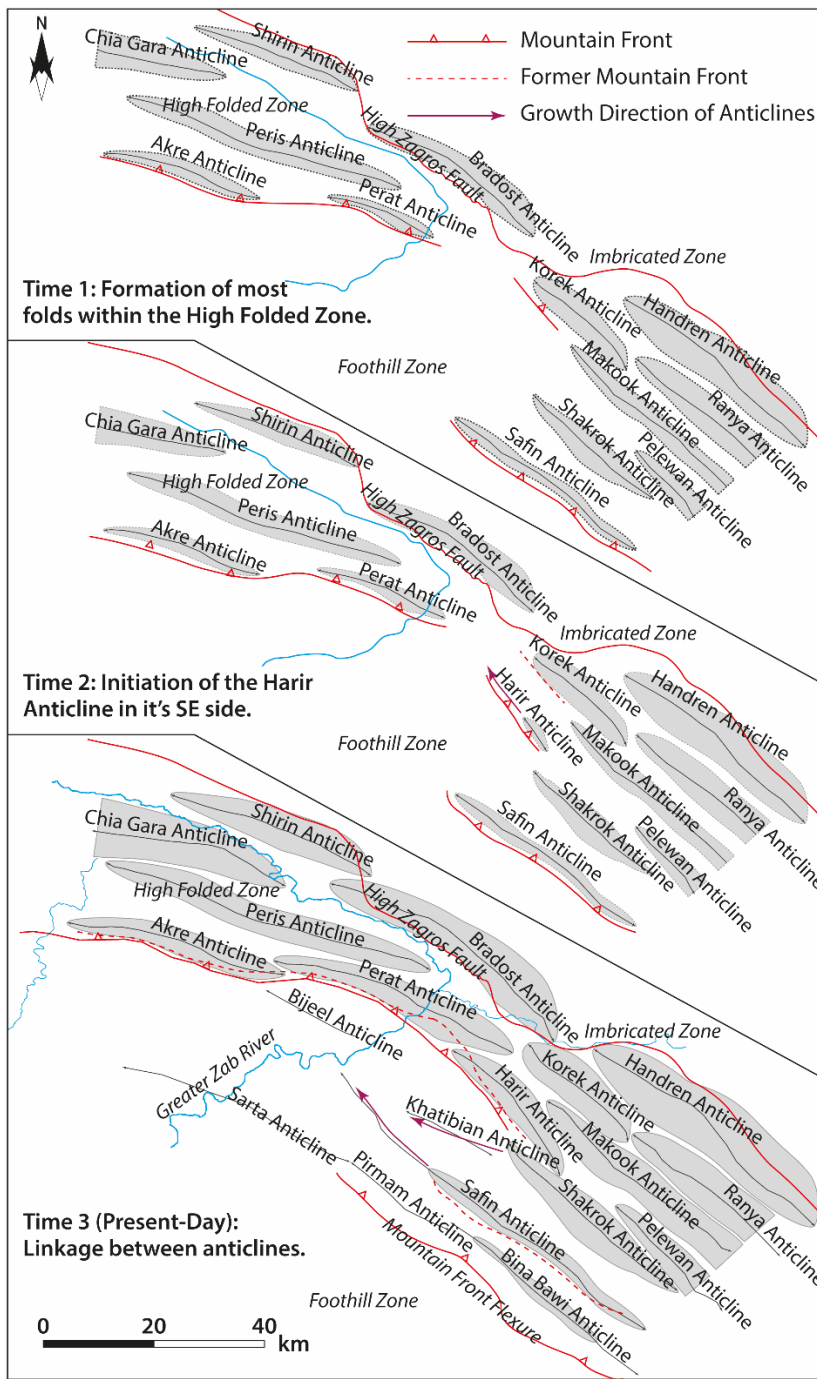


Figure 15: Simplified history of the formation of anticlines during the propagation of the deformation front over time in the study area. The Harir anticline is likely the latest to have formed within the High Folded Zone in its SE end. It occupies the position of a relay structure during the linkage of two adjacent, but overlapping segments of the deformation front. [The anticlines were outlined based on the exposure of Cretaceous carbonates.](#)

5

Response to the Anonymous Referee #1's Interactive comment on **“Relative Timing of Uplift along the Zagros Mountain Front Flexure Constrained by Geomorphic Indices and Landscape Modelling, Kurdistan Region of Iraq”**

by Zebari et al. The responses are given in *“Italic”* font style.

Anonymous Referee #1

Received and published: 27 December 2018

The authors of this manuscript try to use geomorphic indices and results of landscape modelling to constrain the relative timing of uplift of three anticlines. In general, the topic is interesting, and it will be a substantial contribution to the journal. Nevertheless, the revisions including the methodology and discussion, as well as the rearrangements of sections are still needed before publication. Major comments and suggestions are listed below.

1. Introduction: the authors should clearly state the importance of this study. Why the detailed spatial and temporal distribution of deformation ... is not yet well understood? Due to the lack of subsurface data, and/or this region is inaccessible for field surveys?

Authors: It is not well understood due to the lack of comprehensive studies, insufficient surface and subsurface data, as well as access problems because of geopolitical conflicts. The clarification is given in new version of the manuscript (Section 1, Page2, Lines 6-7).

2. Section 3.1.1: with aim of assessing landscape maturity along thrust-related anticlines, hypsometric curves and integrals have often been used for (sub-) drainage basins. The methodology differs from the three incomplete hypsometric curves displayed in Fig. 7. Actually, the authors did not extract drainage basins even if the stream channels of the Harir anticline have been shown in Fig. 6a.

Authors: The hypsometric curves are recalculated again as total weighted mean of hypsometric curves for all drainage basins that have an area of more than 0.25 km² within each anticline. This recalculation is given in the new version of the manuscript (Section 3.1.1, Page 6, Lines 7-10). Additionally, the hypsometric integral is calculated, and the cluster of the high and low values was mapped following the method of Pérez-Peña et al. (2009; Supplementary material S19). The results are similar in aspect of defining clusters of high and low HI values. This comparison proves that our method is equally applicable and valid. We added this information to the manuscript (Section 3.2, Page 7, Lines 20-26; Section 4.1, Page 11, Lines 12-18).

3. Section 3.1.5 Digital elevation models: this section does not belong to the 3.1 geomorphic indices.

Authors: Resolved by renumbering the sections (Section 3.2, Page 7, Lines 10-28).

4. Section 5.1: the authors just described the rock erodibility. They should be included in geological setting, instead of discussion part. Here, the authors stated, “the stratigraphic column in the area consists of rocks with different erodibility” (page 11, line 29), and also mentioned in the conclusion “Due to the similarity in the lithology, structural setting and climate” (page 15, line 23-24). They should clearly state whether the difference exists or not.

Authors: We removed this section. Information on rock erodibility is now included in the section describing the geological setting. In Section 5.1 (page 11, line 29), we mean that there is vertical variation in the rock erodibility in the stratigraphic columns. We have resistant Cretaceous and Paleogene interval of carbonate rocks and less resistant Upper Cretaceous-Tertiary intervals of clastic rocks. In the conclusion section (page 15, line 23-24), we refer to the lateral extent of these stratigraphic units

along the three anticlines, which is similar. We made the distinction between vertical variations in the rock erodibility and the lateral similarity in the exposed rock units clear in the new version of the manuscript to prevent confusion.

Reference:

Pérez-Peña, J. V., Azañón, J. M., Booth-Rea, G., Azor, A., and Delgado, J.: Differentiating geology and tectonics using a spatial autocorrelation technique for the hypsometric integral, J. Geophys. Res., 114(F02018), <https://doi:10.1029/2008JF001092>, 2009.

Response to the Anonymous Referee #2's Interactive comment on **“Relative Timing of Uplift along the Zagros Mountain Front Flexure Constrained by Geomorphic Indices and Landscape Modelling, Kurdistan Region of Iraq”**

by Zebari et al. The responses are given in “Italic” font style.

Anonymous Referee #2

Received and published: 8 February 2019

Comments to the manuscript entitled “Relative Timing of Uplift along the Zagros Mountain Front Flexure Constrained by Geomorphic Indices and Landscape Modelling, Kurdistan Region of Iraq” by Zebari et al. (doi:10.5194/se-2018-124).

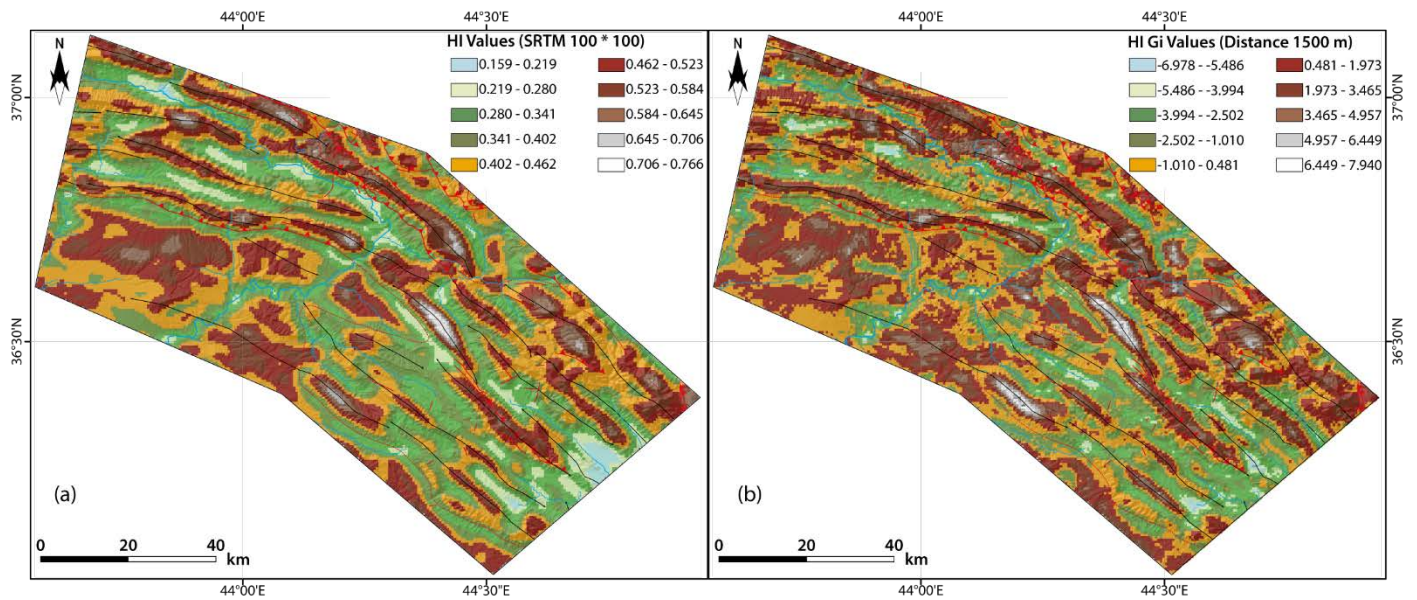
The authors of this manuscript try to constrain the relative timing of uplift of three anticlinal folds of the Iraqi Zagros Mts., combining the results of landscape evolution models and geomorphic indices. The topic fits the ones of the journal and the manuscript has the potential to be interesting for the international scientific community. Nonetheless, some general comments and minor specific ones are listed below, suggesting that some important revisions are needed before publication.

General comments:

1) Considering the deformation style of the Folded Zone of the Zagros Mts. chain, the assumption of constant rock uplift seems too simplistic. Doesn't the evidence of NW-ward propagation of the Harir Anticline (used by the authors for supporting the scenario of independent and diachronist uplift in different fold segments) affect the assumption of homogeneous and constant uplift rate in each structure? In this frame, the hypsometric analysis performed for the entire anticlinal ridges seems to have no sense, while I would suggest using an approach to the hypsometric analysis such as the one proposed by Pérez-Peña et al. (2009).

Authors: We built our model to estimate the time it will take the present day Harir Anticline to reach the maturity level of the Akre Anticline under the assumption of constant climate and uplift rate. Then, we assume if the climate and uplift were the same in the past, the Akre Anticline has started to uplift before Harir Anticline in that estimated time. For this reason and for the sake of simplicity we used a constant uplift rate in the model.

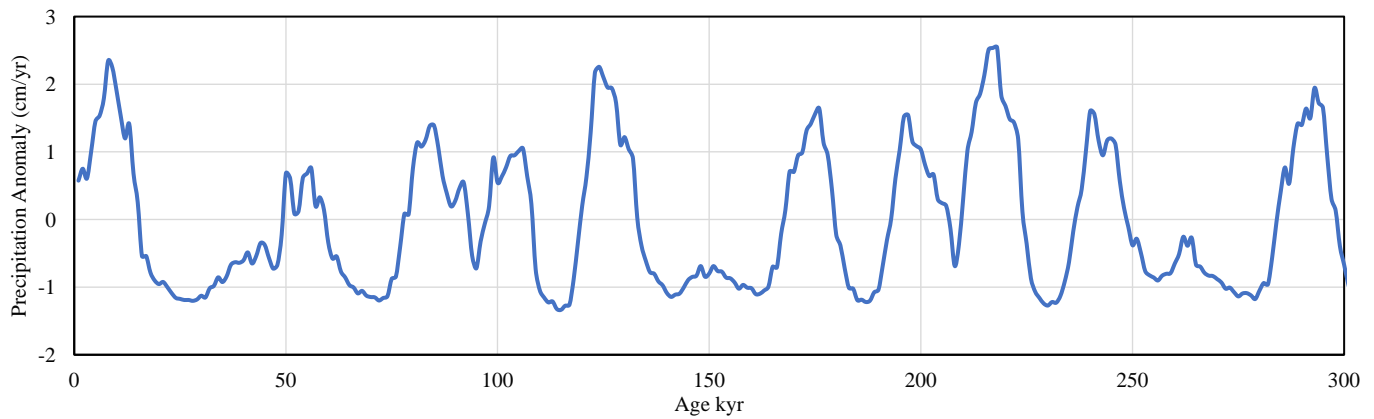
We do not use absolute values of the geomorphic indices in our analysis, but we try to distinguish areas with relatively high values from those with relatively low values. Therefore, we think there is no need for applying the approach proposed by Pérez-Peña et al. (2009), because both the approach of Pérez-Peña et al. (2009) and our approach give similar results when it comes to defining areas with high and low (hypsometric integral, HI) values. Pérez-Peña et al. (2009) calculated HI for the given area with specific grid sizes (500m, 1km and 2km) and then calculated Moran's I index for each case to detect autocorrelation patterns in the data distributions. They conducted hot spot analyses by using the Getis-Ord G_i^ analysis within a specified distance (5km) to map the clusters of high and low HI values. In our approach, we calculated HI (and other indices) for each pixel by including the surrounding data of a specified distance based on the size of the used moving window. This means the results already have a relation with the surrounding cell without using Moran's I index and Getis-Ord G_i^* analysis. In the example given here (see the Figure below), first, we calculated HI from SRTM (30m resolution) by using a moving window of 3*3 km and resample it to a 500m grid, then we used the approach by Pérez-Peña et al. (2009) for the same SRTM data with a grid of 500m and conducted Moran's I index and Getis-Ord G_i^* analysis for the cluster using 1.5 km distance. The results are similar in aspect of defining clusters of high and low HI values. We added this information to the manuscript (Section 3.2, Page 7, Lines 20-26; Section 4.1, Page 11, Lines 12-18).*



*a) HI calculated from the SRTM (30m) 100 * 100 cell (3*3 km) moving window and resampled to 500 m cells; b) Getis-Ord statistic estimation with 1.5 km distance for the HI that was calculated from the SRTM (30m) and with a 500 m grid following the method described by Pérez-Peña et al. (2009).*

2) Also the use of the only equations for fluvial erosion and diffusion processes for landscape evolution modelling may be too simplistic. Besides the justifications provided by the authors in section 5.2, it sounds not realistic that sedimentation on the slopes of anticlines can be neglected over the time-span of landscape evolution modelling (105 years), as well as the assumption of constant erosion rates (and climate!).

Authors: The use of equations for fluvial erosion and diffusion processes only and neglecting the sedimentation in the model is explained in section 3.2. In such a landscape with steep slopes, the detachment-limited erosion due to the fluvial system tends to be the dominant process. Even if there is some fluvial sedimentation, it will be too small to affect the landscape. In addition, no notable sites of fluvial deposition were found on the anticline and its flanks from the field investigation and from satellite imagery. We add this information in the new version of the manuscript to clarify the reason for neglecting slope deposition (Section 3.3, Page 8, Lines 5-9). In the model, the applied parameters were constant, while the erosion rate varies with the instant upstream drainage area and instant slope following the stream power incision law. The climate was kept constant for the sake of simplicity. The average of modeled paleo-precipitation anomalies for at least the last 300 kyr in the Eastern Mediterranean was close to zero as seen from the record of Lake Van in Turkey, some 200 km NNW of our study area (see the Figure below). This is described in the new manuscript (Section 3.3, Page 9, Lines 22-24) Furthermore, considering the dimensions of the area, the changes in climate, if any, would have been constant over the entire study area, hence, affecting the three anticlines in the same way.



Precipitation anomalies for Lake Van, Turkey, for the last 300 ka (data were obtained from Mona Stockhecke by personal communication; Stockhecke et al., 2016).

3) The authors justify the choice of the present topography of the Harir Anticline as LEM input asserting that in this structure the evolved drainage network overprinted the pre-existing one. Looking at Fig. 6 it seems that the drainage has a pattern similar to the one described by Ramsey et al. (2008; Basin Research (2008) 20, 23–48, doi: 10.1111/j.1365-2117.2007.00342.x) as evidence of lateral propagation of folds in the Zagros. This implies a diachronic fingerprint in the drainage network which could void the sense of performing the hypsometric analysis for the entire anticlinal ridges.

Authors: In order to resolve this problem and in order to overcome the limitations of performing the hypsometric analysis for the entire anticlinal ridges, we recalculated the hypsometric curves as total weighted mean of hypsometric curves for all drainage basins that have an area of more than 0.25 km² within each anticline. The manuscript was modified accordingly (Section 3.1.1, Page 6, Lines 7-9; Figs. 6, 9. And 13).

4) Some of the units stratigraphically above the Cretaceous limestones outcropping on the anticlines' crest are transitional to continental (i.e. the Bakhtiari Fm.), thus likely being affected by lateral variability of thickness. What about the effects on the uplift rate calculation based on thickness? Furthermore, this uplift rate was calculated based on the thickness and elevation of units on the anticline crest, but (again) is it correct to extend such a rate to the entire folds given their lateral growth?

Authors: Since we have calculated the uplift rates based on the exhumed and exposed thickness since the onset of the MFF at 5 Ma, the variation in thickness of the units overlying the Cretaceous carbonates will affect the used uplift rate in the model. This thickness varies in between these three anticlines and even along strike within one anticline. The thickness of the units overlying the Cretaceous carbonates in the area ranges from ~ 2.0 km to maximum of 2.7 km. The uplift rates calculated based on these thicknesses will be in between 0.0007 to 0.0008 mm/yr. This range is not significant to noteworthy effect on the result of our model. We used the thicknesses found in well Bijeel-1, which is in a central part with respect to the three anticlines, to calculate the uplift rate. There will be variation also along a single anticline and we tried to overcome this by neglecting the two ends of anticlines in our analysis, and here our scope is to make a comparison in between the three anticlines omitting changes along a single anticline. We have clarified this in the new version of the manuscript (Section 4.3, Page 12, Lines 25-30).

5) There are several repetitions over the manuscript (see “specific comments”).

Authors: We reviewed the manuscript and tried to remove the repetitions wherever they existed.

6) Some original data (geological cross sections of Fig. 4) are referred to in the geological setting, while should be better described in the results.

Authors: Fig. 4 is now moved to the result section and is described there (Section 4.3 Page 12, Lines 17-30; Fig 10).

7) In some cases, the interpretations seem not supported by data. For example, the fit between some of the hypsometric curves obtained with LEM and the ones computed for the three analyzed anticlines is not evident in Fig. 10 and the “minimum RMS” invoked by the authors to demonstrate the fit is not quantified. On the other hand, authors provide a quite specific timing for the inferred “delay” in the deformation sequence of the three folds which is based on this “fit” and use it to support the diachronic scenario of fold development. In my opinion such a constrain is weak, if based on the hypsometric analysis. Other doubt interpretations are listed in the specific comments.

Authors: We don't find a better way of comparing the evolved landscape with that of the more mature anticlines in term of maturity rather than using hypsometric curves and other indices. Here, we used minimum RMS to find the closest curve statistically. Also, we have recalculated the hypsometric curves for output as the weighted mean of hypsometric curves for basins with area larger than 0.25 km² within each anticlinal ridge weighted by the basin area within that anticline, and we have compared to that of the relatively more mature anticline. The specific time that we come calculate is the run time of the model that matches bests with the mature anticline. And with such model it is also difficult to assign a specific tolerance with \pm and assign a margin of error. We provide the updated calculations in the new version of the manuscript (Fig 9).

8) Section 5.1 doesn't sound necessary.

Authors: We removed this section.

9) In the Discussion new data are presented (i.e. Fig. 13), but it is not explained how they have been obtained, in particular the calculation of the slope/area. Is it obtained using just the drainage network or the whole topography?

Authors: The data were obtained from the drainage network extracted from SRTM DEMs, so the slope is the stream slope at any specific point and the area is the upstream drainage area from that point. We added a short note in the methods about it in the new version (Section 3.2, Page 7, Lines 27-28).

10) In the Conclusions authors refer to the three analyzed anticlines as “active folds”, while in section 5.2 they state that the youngest unit affected by folding is the Mio-Pliocene Bakhtiari Fm.

Authors: The Upper Bakhtiari Fm is also the youngest stratigraphic unit in the area. We point to this as the start for folding and consequent uplift and calculate the exhumed and exposed thickness of older strata in the area. When the Pliocene units are folded, it means that the folding should have been active in Pleistocene-Holocene (Section 5.1, Page 13, Lines 21-24).

Specific comments and technical corrections

-TITLE: I would suggest to change the title into: “Relative Timing of Uplift along the Zagros Mountain Front Flexure (Kurdistan Region of Iraq): Constrains by Geomorphic Indices and Landscape Evolution Modelling”

Authors: Done.

- ABSTRACT:

PAGE 1, LINE 13: maybe “fold and thrust belt” and not “fault and thrust belt”

Authors: Done.

- INTRODUCTION:

PAGE 2, LINES 16-17: Why “The timing of this activity is expected to differ along-strike”? Any reference or explanation?

Authors: In the literature, different times have been assigned to the onset of uplift in different part of the Zagros. This is explained in the next sentence in the manuscript by stating the activity period in the Iranian part of the MFF, referring to the corresponding citation (Section 1, Page 2, Lines 16-23).

- GEOLOGICAL SETTING:

PAGE 4, LINE 31: change “river terraces” into “terraced alluvium”.

Authors: Here we mean aggregational river terraces that presents in varies elevated layers along the side of major rivers in the area. These sediments have been mapped and described under the term of “reviver terraces” (Jassim and Goff, 2006; Sissakian, 1997).

PAGE 5, LINES 18-19: I suggest not to refer to new data in the geological setting. Fig.4 should be described (if made with newly surveyed data) in the Results.

Authors: We have moved this to the result section (Section 4.3, Page 12, Lines 17-30).

- DATA AND METHODS:

PAGE 5, LINE 26: the hypsometric curve is not an “index”

Authors: Separated.

PAGE 5, LINE 27-29: the definition/meaning of the geomorphic tools is vague and in some cases, not correct (i.e. “The hypsometric curve and the hypsometric integral highlight raised and flat surfaces”).

Authors: Edited.

PAGE 6, LINES 3-4: in general, the convex vs. concave shape of the hypsometric curve not necessarily reflects the “maturity” of a landscape (in terms of its absolute age) but can also depend on the type and rates of earth surface processes which dominate the landscape evolution (e.g. linear incision vs. hillslope diffusion processes).

Authors: Rephrased.

PAGE 6, LINES 10-11: again, the meaning of HI is not clearly defined. Please, rephrase.

Authors: Redefined.

PAGE 7, LINE 1: change the order of terms into “Nh, NHI and NSR”

Authors: Done.

PAGE 7, LINE 5: Digital Elevation Models (3.1.5.) are not Geomorphic Indices. This section should become 3.2

Authors: Solved (Section 3.2, Page 7, Lines 10-28).

PAGE 7, LINE 22: soil creep is mentioned as second main process inputed in LEM. Maybe the authors should refer more generally to hillslope diffusion processes.

Authors: Done.

PAGE 7, LINE 23-24: see general comment 2): it sounds strange that over the time-span of the modelling the sedimentation on slopes can be neglected.

Authors: Here we mean sedimentation from the fluvial system. We clarified this meaning in the manuscript (see our response to the general comment 2 above).

PAGE 8, LINE 8: again, the authors refer to “soil creep” (see comment above).

Authors: Replaced.

PAGE 8, LINES 17-18: see general comment 3).

Authors: This may be the case for the majority of anticlines in the Zagros Belt; initiating from a segment, growing laterally, and then linking in the plunging end. This is addressed in the new version by recalculating the hypsometric curves as total weighted mean of hypsometric curves (see our answer to general comment 3).

PAGE 8, LINE 30: authors refer to “time steps” before defining them.

Authors: We redefined time step as follows: “In this approach, we ascribed values for m/n ranging from zero to one, and X was calculated for each time from Eq. 7”.

PAGE 9, LINE 13: “ $K_d = 0.001 \text{ m}^2\text{yr}^{-1}$ ”: why exactly this value?

Authors: Diffusivity coefficient varies with the thickness of soil (regolith) and since the soil is rare and very thin when it occurs, we assigned a low coefficient as explained by (Fernandes and Dietrich, 1997).

- RESULTS:

PAGE 10, LINE 6: “HI values are maximum at the Greater Zab River”: maybe authors mean that HI values are minimum?

Authors: Typo; edited.

PAGE 10, LINE 6-12: This part seems not necessary and the authors should pay attention to the meaning of HI when calculated for square areas and not for single basins. In this case HI measures how rapidly elevation changes and not strictly the amount of incision.

Authors: We rephrased the paragraph.

PAGE 10, LINE 13-18: results concerning roughness analysis are quite obvious...is it really necessary?

Authors: We rephrased and reduced this section.

PAGE 10, LINE 26-34: this part should be moved to the methodological section.

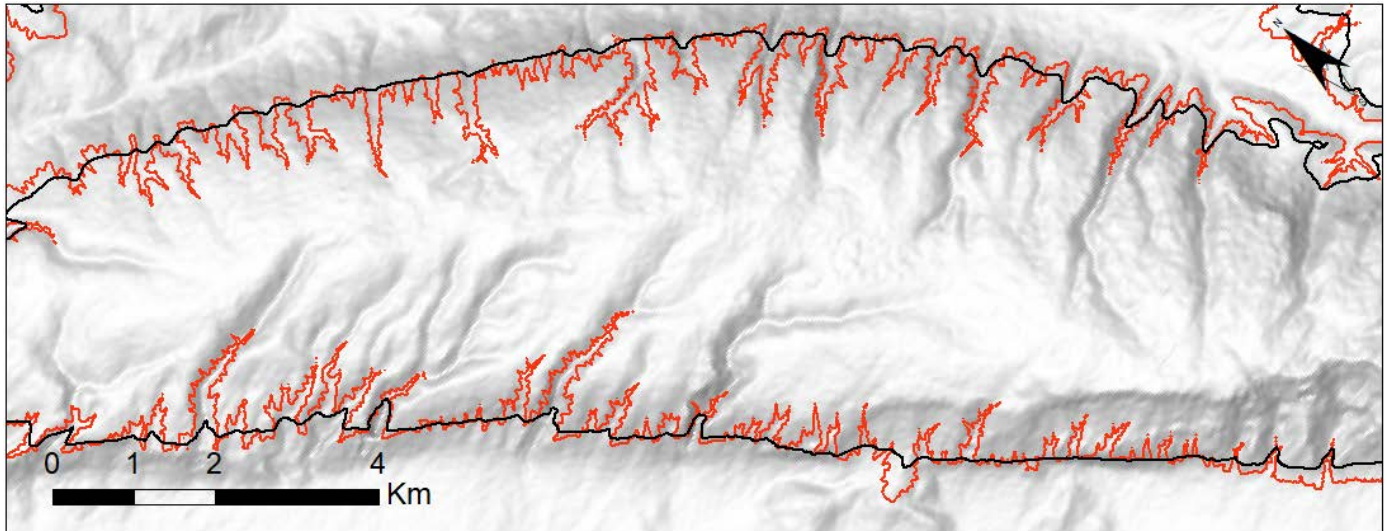
Authors: It has been rephrased to match the results and unnecessary parts have been removed.

PAGE 11, LINES 11-12: authors state that “In the landscape modelling, various simulations with different parameters and time spans were performed”, nonetheless they do not provide details on the simulation (neither in the supplementary material). How did they select the best outputs?

Authors: The results are added in the supplementary material and referred to in the manuscript.

PAGE 11, LINES 13-14: authors state that “The evolving drainage system overprints the pre-existing one in the input and gradually becomes more deeply incised from the anticline flanks curving toward its core (Fig. 9)”. This is not evident in Fig. 9, according to what already explained in the general comment 3).

Authors: We think it is clear how the erosion is carving deeply toward the anticline core as it can be noticed from the contour map. Here, we show the 1000-contour line to show that (see the Figure below).



Black is the 1000-contour line from the input and red is the 1000-counter line from the output after 100 kyr.

PAGE 11, LINES 15: change “plain” into “flat”.

Authors: Done.

PAGE 11, LINES 20-22: see general comment 7)

Authors: We addressed this by recalculating the hypsometric curves for output as the weighted mean of hypsometric curves for basins with area larger than 0.25 km² within each anticlinal ridge weighted by the basin area within that anticline, and we have calculated HI for the output and compared to that of the relatively more mature anticline (see our answer to the general comment 7).

- DISCUSSION:

Is section 5.1 necessary?

Authors: The section is removed.

PAGE 12, LINES 14-15: what the authors mean with “The maturity level along these anticlines therefore represents the level when these carbonates cropped out in their latest stage”?

Authors: The section is removed.

PAGE 12, LINES 17-19: authors state that “A landscape survives when its uplift is not completely counterbalanced by erosion (Andreani and Gloaguen, 2016; Burbank and Anderson, 2012; Pérez-Peña et al., 2015)”: it does not sound. . . maybe authors refer to relict landscapes?

Authors: Yes, we mean that. We made this clear in the new version of manuscript to avoid confusion.

PAGE 12, LINES 21-22: the sentence “The locations dissected by rivers show high surface roughness” seems obvious and not necessary.

Authors: Removed.

PAGE 12, LINES 29-31: “The same effect is visible in swath topographic profiles (Figs. 12c and 12d): in Harir Anticline, there is a clear topographic step with a higher slope angle, while in Akre Anticline the slope is gentler and more linear”: to outline this evidence swath profiles are not necessary. . .if they can provide further evidence, the latter should be discussed.

Authors: We removed these swath profiles.

PAGES 12-13: “This can be interpreted with one of these premises: either both anticlines started to uplift successively (first Akre, then Perat, and finally Harir), or all of them started at the same time but with different uplift and exhumation rates (Akre the fastest, Harir the slowest)”. This concept is repeated too many times over the manuscript. Furthermore, to justify the different geomorphic stage of the three folds with different uplift rates, shouldn’t the latter be “fastest” in Harir and “slowest” in Akre??

Authors: Due to high erodibility of the Upper Cretaceous – Lower Eocene succession in the area, it is flattened to the local base level by erosion wherever it crops out and does not make a notable topography. The indices measured for these anticlinal ridges, which are made of the Cretaceous carbonates, express the erosion action since the exposure of the carbonates. Based on these indices the Akre is relatively more mature than Harir, so the carbonate rocks must have been exposed to the erosion for a longer time than in Harir. Therefore, Akre’s carbonates were at the surface before Harir’s carbonate; either through an earlier onset of uplift or by a faster uplift rate, hence faster exposure to erosion.

PAGE 13, LINE 13: How much does the assumption of constant rock uplift affect the results obtained? Since it is a “strong” assumption you should give an estimation of that.

Authors: Since there are only data about the uplift rates in the area averaged over the last 5 Ma and for simplicity of the model, we had no option rather than applying a constant uplift rate. To know the effects of constant (linear) uplift on the result, we need to apply nonlinear uplift rates and compare the results. Using any nonlinear uplift rates will be arbitrary. The uplift rate used in our model was estimated from the exhumed and/or exposed thickness from the onset of the MFF.

PAGE 13, LINE 15-26: This part of the discussion is not so clear. E.g. how did the authors perform the slope/area \sim analysis?

Authors: The slope/area curve was obtained as an average trendline for the streams in each anticline. The slope is for specific points at defined distance along the stream; where area is the upstream watershed area at each point. It is now better explained in the manuscript (Section 3.2, Page 7, Lines 27-28; Section, 5.1 Pages 13-14, Lines 34 and 1-4).

Some statements seem wrong: e.g. “In the Akre Anticline, this relationship [slope/area] is negative (Fig. 13b), which means that the streams have a concave shape and the segments with steeper slopes have migrated toward the core of the anticline. This implies that tectonic activity in the Harir Anticline is younger than in the Akre Anticline. Therefore, the premise of having Harir Anticline starting its uplift later than Akre Anticline is most likely”. Why a higher uplift rate in the Harir couldn’t have caused the same effect?

Authors: We mean that the Harir Anticline was not exposed to erosion for a longer time, so the streams have not had as much time to carve deep in to the anticline as at Akre. Considering a unique onset, if Harir had a higher uplift rate, it would be exposed to erosion earlier than Akre, hence experienced more maturity, but it did not. Considering different onsets, even with a higher uplift rate, Harir should have been exposed to erosion later than Akre to have less maturity as it does.

“Since the Upper Cretaceous carbonates in Harir Anticline were exposed later than in Akre Anticline, a landscape evolution model is a viable approach to estimate the exposure time difference. Here the model is built for the first premise of different onsets of uplift. Even if the second premise of different uplift rates is correct, the estimated time difference of the carbonate exposure will only be 28% less than that for the first scenario. As described in section 4.2, the calculated uplift time difference

between Akre and Harir anticline is 200 ± 20 kyr, and if the second scenario is correct, the time difference of the carbonate exposure would be 144 ± 14.4 kyr” This sentences are confused and the interpretation is not clear and a bit circular (choice of scenario based on modelling, based on constant uplift rates. . .).

Authors: Since the first premise is better evidenced from the present-day morphology of both anticlines, we do not need to add an additional assumption based on the second scenario, so we have removed this part from the manuscript to avoid confusion.

PAGE 13, LINE 27-34: see general comment 2).

Authors: We addressed this in new version of the manuscript as explained in our answer to general comment 2 above.

PAGE 14, LINE 8: The variations in stratigraphic thickness in between the anticlines is constrained by field data? And how does this variability affect the calculations of uplift rates?

Authors: Since we have calculated the uplift rates based on the exhumed and exposed thickness since the onset of the MFF at 5 Ma, the variation in thickness of the units overlying the Cretaceous carbonates will affect the used uplift rate in the model. This thickness varies in between the three anticlines and even along strike within one anticline. The thickness of the units overlying the Cretaceous carbonates in the area ranges from ~ 2.0 km to maximum of 2.7 km. The uplift rates calculated based on these thicknesses will be in between 0.0007 to 0.0008 m/yr. This range is not noteworthy to effect on the result of our model. For this we used thickness in the well Bijeel-1, which is in a central part with respect to the three anticlines, to calculate the uplift rate. There will be variation also along a single anticline, we tried to overcome this by neglecting the two ends of anticlines in our analysis, and here our scope is to make a comparison in between the three anticlines omitting changes along a single anticline. We made this more clear in the new version of the manuscript (Section 4.3, Page 12, Lines 17-30).

PAGE 14, LINE 13-26: Is this part really necessary and functional?

Authors: This paragraph is added in order to explain the tectonic framework of further propagation of deformation in the SE side of the Greater Zab River and presence of another anticline to the south and southeast of Harir Anticline. And to explain the fold relay and to make sure that the uplift was not continuous from the NW to SW but rather in separated segments that propagated NW-ward until folds had linkage with each other.

- CONCLUSIONS: See general comment 10

Authors: The answer is provided under general comment 10 above.

FIGURES:

FIG.1: i) I suggest to change “transform fault” into “strike-slip fault” in legend; ii) I suggest to add a legend for the different colors in transparency (e.g. the rose one corresponds to 2 zones. . .); check the use (or not) of parenthesis in the naming of zones;

Authors: i) Done, ii) the colors in transparency characterize different morpho-tectonic zones of the Region. The names of these zones are given on the map, hence there is no need for a legend. The names within the parenthesis are equivalent names of these zones in the Iranian Zagros in the literature. This is made clear in the manuscript.

FIG.2: i) I suggest to draw the border between different units in map; ii) check the numbering of the figures recalled in the sketch (they do not correspond to the figure recalled)

Authors: i) Done, ii) Done.

FIG.4: move and comment it in the Results.

Authors: Done.

FIG.5: symbols for wind gap and limit of Cretaceous limestone outcrop are not visible in figure Fig 6.

Authors: We have updated and improved all figures in the manuscript.

FIG.6: Symbols for the strike-slip component of displacement are missing

Authors: There are no strike-slip faults within the Fig. 6.

FIG.7: i) I suggest to prepare a new figure after having used the approach by Pérez-Peña et al (2009) to the hypsometric analysis.

Authors: Same response as in the general comment 1; a new figure was added to the supplementary material, covering the entire study area.

FIGs.8, 9, 10: to be revised according to the comments on the analytical procedures.

Authors: These Figures were revised, accordingly.

Reference:

Jassim, S. Z. and Goff, J. C.: Geology of Iraq, Dolin, Prague and Moravian Museum, Brno, Czech Rep., 2006.

Pe´rez-Peña, J. V., Azañón, J. M., Booth-Rea, G., Azor, A., and Delgado, J.: Differentiating geology and tectonics using a spatial autocorrelation technique for the hypsometric integral, J. Geophys. Res., 114(F02018), <https://doi.org/10.1029/2008JF001092>, 2009.

Sissakian, V. K.: Geological Map of Arbeel and Mahabad Quadrangles Sheets NJ-38- 14 and NJ-38-15, Scale 1:250.000, 1997.

Stockhecke, M., Timmermann, A., Kipfer, R., Haug, G., Kwiecien, O., Friedrich, T., Menviel, L., Litt, T., Pickarski, N., Anselmetti, F. S.: Millennial to orbital-scale variations of drought intensity in the eastern Mediterranean, Quaternary Science Reviews, 133, 77–95. <https://doi.org/10.1016/j.quascirev.2015.12.016>, 2016.

Relative Timing of Uplift along the Zagros Mountain Front Flexure (Kurdistan Region of Iraq): Constrained by Geomorphic Indices and Landscape Evolution Modelling

Mjahid Zebari^{1,2}, Christoph Grützner¹, Payman Navabpour¹, Kamil Ustaszewski¹

5 ¹Institute of Geological Sciences, Friedrich-Schiller-University Jena, Jena, 07749, Germany

²Geology Department, Salahaddin University-Erbil, Erbil, 44002, Kurdistan Region of Iraq

Correspondence to: Mjahid Zebari (mjahid.zebari@uni-jena.de)

Abstract. The Mountain Front Flexure marks a dominant topographic step in the frontal part of the Zagros Fold-Thrust Belt. It is characterized by numerous active anticlines atop of a basement fault. So far, little is known about the relative activity of the anticlines, about their evolution, and about how crustal deformation migrates over time. We assessed the relative landscape maturity of three along-strike anticlines (from SE to NW: Harir, Perat, and Akre) located on the hanging wall of the Mountain Front Flexure in the Kurdistan Region of Iraq to identify the most active structures and to get insights into the evolution of the fold-thrust belt. Landscape maturity was evaluated using geomorphic indices such as hypsometric curves, hypsometric integral, surface roughness, and surface index. Subsequently, numerical landscape evolution models were run to estimate the relative time difference between the onset of growth of the anticlines, using the present-day topography of the Harir Anticline as a base model. A stream power equation was used to introduce fluvial erosion, and a hillslope diffusion equation was applied to account for colluvial sediment transport. For different time steps of model evolution, we calculated the geomorphic indices generated from the base model. While Akre Anticline shows deeply incised valleys and advanced erosion, Harir and Perat anticlines have relatively smoother surfaces and are supposedly younger than the Akre Anticline. The landscape maturity level decreases from NW to SE. A comparison of the geomorphic indices of the model output to those of the present-day Akre Anticline topography revealed that it would take the Harir Anticline about 80-100 kyr and 160-200 kyr to reach the maturity level of the Perat and Akre anticlines, respectively, assuming erosion under constant conditions and constant rock uplift rates along the three anticlines. Since the factors controlling geomorphology (lithology, structural setting and climate) are similar for all three anticlines, and under the assumption of constant growth and erosion conditions, we infer that uplift of the Akre Anticline started 160-200 kyr before that of the Harir Anticline, with the Perat Anticline showing an intermediate age. A NW-ward propagation of the Harir Anticline itself implies that the uplift has been independent within different segments. Our method of estimating the relative age difference can be applied to many other anticlines in the Mountain Front Flexure region to construct a model of temporal evolution of this belt.

1 Introduction

The Zagros Fold-Thrust Belt is an active orogen that resulted from the collision between the Arabian and Eurasian plates and contains the deformed portions of the NE part of the former Arabian passive margin (Fig. 1; Berberian, 1995; Mouthereau et al., 2012). Many aspects of the structural configuration and the evolution of the Zagros Fold-Thrust Belt are by now satisfactorily constrained, but the detailed spatial and temporal distribution of deformation across the belt is not yet well understood. This concerns especially the NW part of the belt in the Kurdistan Region of Iraq (KRI) due to a lack of comprehensive studies and for geopolitical reasons that make access to the field challenging. The style, timing, and relative activity of front thrusts, deformation propagation, and along-strike variations have not been sufficiently studied. It is not well-known which structures are currently the most active ones either.

One of the morphologically most conspicuous structural elements of the Zagros Fold-Thrust Belt is the Mountain Front Flexure (MFF), which separates the High Folded Zone and the Foothill Zone (known in Iran as the Zagros Simply Folded Belt and Zagros Foredeep, respectively; Figs. 1 and 2; Berberian, 1995; Jassim and Goff, 2006; McQuarrie, 2004; Mouthereau et al., 2012; Vergés et al., 2011). In most parts of the Zagros, the MFF marks a pronounced topographic step, separating folds with high amplitudes, narrow wavelengths, and higher topography in the High Folded Zone from folds with relatively low amplitudes, long wavelengths, and lower topography in the Foothill Zone (Fig. 2). The MFF is characterized by numerous active anticlines atop of fault strands emerging from a basement fault. It was suggested that the onset of the MFF activity in the NW Zagros was about 5 ± 1 Ma based on low temperature thermochronology (Koshnaw et al., 2017). The timing of this activity is expected to differ along-strike the belt and, hence, the initiation of uplift of the anticlines on the hanging wall of the MFF is the key to understand this temporal and spatial evolution. In the neighbouring Iranian part, the MFF was a relatively long-lived structure active from 8.1 to 7.2 Ma to about the Pliocene-Pleistocene boundary. After that, only the southwesternmost anticline remained active in front of the MFF. This was inferred from progressive unconformities and magnetostratigraphy (Hessami et al., 2001, 2006; Homke et al., 2004).

In active orogens, the main factor that contributes to building up topography is ongoing convergence (e.g. Bishop, 2007; Burbank and Anderson, 2012; Whittaker, 2012). Recent advancements in the availability of high-resolution digital elevation models (DEMs) and GIS software allowed to quantitatively analyse the landscape (Bishop, 2007; Tarolli, 2014). Tectonic geomorphology approaches and landscape maturity studies have been used extensively and proven to be efficient in studying the relative tectonic activity of different areas in contractional settings (Cheng et al., 2012; Mahmood and Gloaguen, 2012; Ramsey et al., 2008; Regard et al., 2009). Nevertheless, the NW part of the Zagros lacks modern studies on tectonic geomorphology - with few exceptions. Bretis et al. (2011) detected sets of wind gaps (i.e. segments of river valleys abandoned due to lateral and vertical fold growth) in the High Folded Belt, NE of the MFF, suggesting that larger folds grew by linkage of smaller, shorter folds. Zebari and Burberry (2015) performed detailed analyses of various geomorphic indices for numerous anticlines in the High Folded Zone, concluding that the combination of clearly asymmetric drainage patterns and the mountain front sinuosity index (Bull, 2007; Keller et al., 1999) is a valuable tool for identifying putatively active

fault-related folds. Obaid and Allen (2017) studied the landscape maturity of various anticlines within the Zagros Foothill Zone and constrained the order of deformation of these anticlines by proposing an out-of-sequence propagation of underlying faults into the foreland. They proposed that the Zagros Deformation Front was among the earliest faults that have been reactivated within the Foothill Zone.

5 In an active orogen such as the Zagros, a better understanding of the temporal and spatial distribution of deformation due to ongoing tectonics can be achieved with landscape modelling. In the last two decades, numerical models have been extensively used to study landscape evolution (Chen et al., 2014; Tucker and Hancock, 2010) and several software packages were specifically developed for this purpose (e.g. Hancock and Willgoose, 2002; Hobley et al., 2017; Refice et al., 2012; Salles and Hardiman, 2016; Tucker et al., 2001). Most of these models include algorithms for bedrock fluvial incision and
10 hillslope creep as input parameters. Several studies have constrained the landscape evolution with the involvement of the corresponding tectonics and structures elsewhere (Collignon et al., 2016; Cowie et al., 2006; Miller et al., 2007; Refice et al., 2012).

In this study, we assessed variations in the landscape maturity of three anticlines (from SE to NW, the Harir, Perat and Akre anticlines) located on the hanging wall of the MFF by quantitatively analysing landscape indices (hypsometric curve, 15 hypsometric integral, surface roughness, and surface index) in order to distinguish more mature segments from less mature ones, and to reconstruct the relative variation of uplift time and/or rate along these anticlines. We then computed the difference in the onset of uplift between more mature anticlines and less mature ones using a landscape evolution model. The present-day topography of the least mature anticline served as an input model for computing the time that it takes this anticline to reach the same state as the most mature one. Also, three structural cross-sections were constructed across the
20 three anticlines to delineate their structural style and to link it with their landscape maturity.

2 Geological Setting

The Zagros Fold-Thrust Belt is the result of the collision between the Arabian and Eurasian plates (Fig. 1; Berberian, 1995; Mouthereau et al., 2012). Continental collision started in the Early Miocene following the progressive subduction of Neo-Tethyan oceanic lithosphere underneath Eurasia (Agard et al., 2011; Csontos et al., 2012; Koshnaw et al., 2017; Mouthereau
25 et al., 2012). The Zagros Fold-Thrust Belt extends for about 2000 km from the Strait of Hormuz in southern Iran to the KRI and further into SE Turkey. Since the onset of collision, the deformation front has propagated 250-350 km southwestward, involving the northeastern margin of the Mesopotamian foreland basin and the Persian Gulf into a largely NW-SE-trending foreland fold-thrust belt (Mouthereau, 2011; Mouthereau et al., 2007). The shortening across different sectors of the Zagros Fold-Thrust Belt is estimated to range between 10% and 32% (Blanc et al., 2003; McQuarrie, 2004; Molinaro et al., 2005;
30 Mouthereau et al., 2007; Vergés et al., 2011). GPS-derived horizontal velocities between Arabia and Eurasia show present-day convergence rates between 19 and 23 mm/yr (McClusky et al., 2003). It is suggested that deformation partitioning occurs between the external and internal portions of the Iranian part of the Zagros Fold-Thrust Belt. While the internal

Zagros Fold-Thrust Belt currently accommodates 3-4 mm/yr of right-lateral displacement along the Main Recent Fault (Fig. 1; Reilinger et al., 2006; Vernant et al., 2004), the external part accommodates 7-10 mm/yr of shortening by thrusting and folding (Hessami et al., 2006; Vernant et al., 2004), 2-4 mm/yr of which is taken up by the MFF in the Fars Arc (Oveisi et al., 2009). However, no such estimates are available for the Iraqi segment of the Zagros Mountains. It is hence not known how much of the total Arabia-Eurasia plate convergence is being accommodated across the Iraqi part of the Zagros Fold-Thrust Belt.

The NW segment of the Zagros Fold-Thrust Belt in the KRI is subdivided into several NE-trending morphotectonic zones. These zones from NE to SW are: (i) Zagros Suture, (ii) Imbricated Zone, (iii) High Folded Zone and (iv) Foothill Zone (Figs. 1 and 2; Jassim and Goff, 2006). These zones are bounded by major faults in the area. The faults include Main Zagros Thrust separating the Zagros Suture from the Imbricated Zone, High Zagros Fault that separates the Imbricate Zone from the High Folded Zone, and the Mountain Front Flexure that separates the High Folded Zone from the Foothill Zone (Figs. 1 and 2; Berberian, 1995; Jassim and Goff, 2006).

The deformed sedimentary succession is composed of 8 - 12 km thick Paleozoic to Cenozoic strata that rest on the Precambrian crystalline basement (Aqrabi et al., 2010; Jassim and Goff, 2006). The thick sedimentary cover consists of various competent and incompetent rock successions separated by detachment horizons. The infra-Cambrian Hormuz salt, which acts as a basal detachment in much of the Southern and Central Zagros Mountains in Iran, pinches out towards northwest (Hinsch and Bretis, 2015; Kent, 2010). Other intermediate detachment horizons influence the structural style of Central Zagros in Iran (e.g., Sherhati et al., 2006; Sepehr et al., 2006), but their behaviour is uncertain in NW Zagros due to limitations in outcrops and insufficient seismic profiles southwest of the Main Zagros Thrust. Some proposed detachment levels include Ordovician and Silurian shales (Aqrabi et al., 2010), Triassic-Jurassic anhydrites (Aqrabi et al., 2010; Hinsch and Bretis, 2015; Zebari, 2013; Zebari and Burberry, 2015), and Lower Miocene anhydrite (Aqrabi et al., 2010; Csontos et al., 2012; Jassim and Goff, 2006; Kent, 2010; Zebari and Burberry, 2015).

The exposed geological units within the High Folded Zone are limited to c. 5 km thick Upper Triassic to Recent rocks (Fig. 2; Jassim and Goff, 2006; Law et al., 2014). Most anticlines are made up of Cretaceous carbonate rocks, while Upper Triassic-Lower Cretaceous strata are only exposed in the core of some anticlines. The Tertiary clastic rocks are preserved within the adjacent synclines. Within the studied structures, the Upper Jurassic-Lower Cretaceous Chia Gara and Lower Cretaceous Sarmord formations only crop out in Bekhme and Zinta gorges and consist of medium to thick bedded marly limestone, dolomitic limestone, and shale (Figs. 2 and 3). The Lower Cretaceous succession of Qamchuqa and Upper Cretaceous Bekhme and Aqra formations consist of thick bedded and massive reef limestone, dolomitic limestone, and dolomite. These units are generally rigid and resistant to erosion. Thus, they build the raised cores of anticlines. The Upper Cretaceous-Tertiary succession consists primarily of clastic rocks, which are mostly denuded, and alternating Upper Paleocene and Upper Eocene limestone of Khurmala and Pila Spi formations, respectively. They form a ridge surrounding the anticlines (Figs. 2 and 3). Unconsolidated Quaternary sediments in the study area consist of slope deposits, residual soil, alluvial fan deposits, and river terraces.

There is no agreement concerning the overall structural style of the NW Zagros in KRI. Several authors (Al-Qayim et al., 2012; Ameen, 1991; Fouad, 2014; Jassim and Goff, 2006; Numan, 1997) suggested that the Iraqi part of the Zagros Fold-Thrust Belt reveals a combination of both thin- and thick-skinned deformation. Partly relying on reflection seismic data, it was also suggested that contraction has been localized on inherited passive-margin normal faults in the basement, which were inverted during the late stage of deformation since c. 5 Ma (Abdulnaby et al., 2014; Burberry, 2015; Koshnaw et al., 2017). The structural relief across the MFF (Fig. 2) is likely linked to blind thrusts in the basement (Al-Qayim et al., 2012; Ameen, 1991, 1992; Fouad, 2014; Koshnaw et al., 2017; Numan, 1997). The same linkage between structural relief and a regional basement blind thrust is also documented in the Iranian Zagros (Blanc et al., 2003; Emami et al., 2010; Leturmy et al., 2010; Sherkati et al., 2006). Alternatively, Hinsch and Bretis (2015) argued that the structural relief in the hanging wall of the MFF is related to an underlying duplex structure that is linked to a stepped detachment horizon rooting in a Lower Paleozoic detachment in the internal parts of the orogen. The relief has been attributed to the accumulation of the Hormuz salt in the Iranian Zagros (McQuarrie, 2004). Even though the MFF is believed to be a major blind thrust in the basement (Berberian, 1995), it is usually mapped along the southwestern limb of the last high anticline where the Pila Spi limestones or the Bekhme and Aqra limestones crop out (Fouad, 2014; Jassim and Goff, 2006; Numan, 1997). Given that landforms in the vicinity of the MFF indicate ongoing tectonic deformation, we suspect that these blind faults might be active at present. Unfortunately, however, instrumental seismicity in the entire region is too diffusely distributed to be attributed to any particular faults (Jassim and Goff, 2006).

Structurally, this segment of Zagros Fold-Thrust Belt is dominated by NW-SE trending fault-related folds, the trend of folds changes to nearly E-W to the west of the Greater Zab River (Fig 2). The folds are usually S-verging and the related faults emerge to the surface within both Imbricated Zone and High Folded Zone, while they remain blind within the Foothill Zone (Fouad, 2014; Hinsch and Bretis, 2015).

3 Data and Methods

We calculated and analysed landscape indices from DEMs for the studied anticlines and built a landscape evolution model that simulates progressive uplift and erosion of the landscape. We also constructed structural cross-section across these anticlines based on literature data and our own field observations.

3.1 Geomorphic Indices

The present-day relief in the study area resulted from a competition between rock uplift triggered by horizontal contraction and erosion destroying it. Parameters controlling these competing processes are the rate of tectonic accretion, rock erodibility and climate (Bishop, 2007; Burbank and Anderson, 2012).

In order to quantitatively analyse the landscape for the Harir, Perat and Akre anticlines (Figs. 2 and 4), we calculated hypsometric curves and determined three geomorphic indices: (i) hypsometric integral, (ii) surface roughness, and (iii)

5 surface index. These are considered proxies for the relative maturity of a particular landscape. The hypsometric curve and integral refer to the distribution of surface area of a landscape with respect to the elevation (Strahler, 1952). The surface roughness value is mainly sensitive to incision (Andreani et al., 2014; Andreani and Gloaguen, 2016; Pike and Wilson, 1971); the surface index is a measure for the amount of erosion. When referring to the results obtained by using this set of geomorphic indices, we colloquially refer to them as “landscape maturity” parameters.

3.1.1 Hypsometric Curve

10 The hypsometric curve for a basin is the frequency distribution of elevation of the watershed area below a given height (Strahler, 1952). Convex-shaped hypsometric curves represent relatively youthful stages of the basin, s-shaped and concave curves refer to more mature and old stages (Strahler, 1952). Hypsometric curves are usually calculated for a specific drainage basin. In this study, we calculated the weighted mean of the hypsometric curves for basins with areas > 0.25 km² within each anticlinal ridge, weighted by the basin area within the anticline. We restricted our analyses to those basins where Upper Cretaceous carbonates are exposed (Fig. 4). This allowed us to make realistic comparisons between the three anticlines, neglecting the differences in rock erodibility that arise when varying lithologies are included. Wind gaps and water gaps as well as the plunging crests of the anticlines were also excluded from the calculation.

15 3.1.2 Hypsometric Integral

The hypsometric integral (HI) is the ratio of area under the hypsometric curve (Strahler, 1952). It is used to highlight the erosional stage of a landscape with high values corresponding to less mature landscapes and low values indicating advanced stages of erosion. The hypsometric integral is computed for a certain area by the following equation (Pike and Wilson, 1971):

$$20 \quad HI = \frac{h_{mean} - h_{min}}{h_{max} - h_{min}}, \quad (1)$$

where h_{mean} , h_{min} and h_{max} are the mean, minimum and maximum elevations [m] of the examined area.

3.1.3 Surface Roughness

25 The surface roughness (SR) measures how much an area deviates from being totally flat. It differentiates flat planar surfaces with values close to 1 from irregular surfaces with higher values. It increases with the increase in incision by streams. The surface roughness is calculated using the following equation (Grohmann, 2004; [Hobson, 1972](#)):

$$SR = \frac{TS}{FS}, \quad (2)$$

where TS and FS are the areas [m²] of the actual topographic surface and the corresponding projection of that surface onto a planar surface, respectively.

3.1.4 Surface Index

The surface index (SI; Andreani et al., 2014) combines elevations, hypsometric integral and surface roughness to map simultaneously preserved and eroded portions of an elevated landscape. It is calculated using equation 3 (Andreani and Gloaguen, 2016):

$$5 \quad SI = (N_{HI} * N_h) - N_{SR} , \quad (3)$$

where N_{HI} , N_h and N_{SR} are the normalized hypsometric integral, elevations, and surface roughness values, respectively. Elevated and poorly incised landscapes with high hypsometric integral and low surface roughness show positive surface index values. Highly dissected landscapes with a high surface roughness yield negative surface index values. This means that the surface index is also sensitive to elevation.

10 3.2 Digital Elevation Models

The geomorphic indices for this study were calculated from the 12 m resolution TanDEM-X DEM (Krieger et al., 2007) obtained from the German Aerospace Center (DLR) and the 30 m resolution SRTM1 DEM (NASA JPL, 2013); these two inputs were used since different DEM inputs give slightly different geomorphic results (Andreani et al., 2014; Koukouvelas et al., 2018; Obaid and Allen, 2017). Geomorphic indices were calculated using both the TanDEM-X and the SRTM1 data.

15 However, the TanDEM-X data revealed numerous artefacts and voids, which made calculations unstable and results unreliable (also see the comparison in the supplementary material). All results of the geomorphic indices and subsequent calculations presented in the following sections were calculated from a 100 * 100 cell (3 * 3 km) moving window on the 30 m resolution SRTM1 data. A larger moving window makes the obtained measurements smoother and vice versa. The size of the moving window must be chosen based on the scale of the target; here we targeted anticlines with wavelengths varying
20 from 5 to 8 km. A 3 km moving window covered almost an entire limb of an anticline. We also tested the method proposed by Pérez-Peña et al. (2009) in order to account for the neighbouring cells in the calculation of the geomorphic indices. Rather than using a moving window, this approach uses a spatial autocorrelation of neighbouring cells and maps clusters of high and low values of indices using Moran's I statistic (Moran, 1950) and G_i^* statistics (Ord and Getis, 1995). We have tested the same method here by calculating the HI for a 500 * 500 m grid of the SRTM data. We applied a hot spot analysis using
25 G_i^* statistics with a distance of 1.5 km to define neighbour cells. Then, we resampled the HI map calculated from a 100 * 100 cell (3 * 3 km) moving window to 500 * 500 m grid from SRTM data. The calculations were performed using the focal and zonal toolsets in ESRI ArcGIS 10.4 software. In addition, the SRTM DEMs with 30 m resolution were used to extract topographic profiles, drainage networks, watersheds, stream slopes, and upstream drainage areas wherever required.

3.3 Modelling Landscape Evolution

We built a landscape evolution model to quantify the time difference in between the maturity level of the [Akre](#) [more mature](#) and [Harir](#) [less mature](#) anticlines by comparing the geomorphic indices of the evolved landscape with those of both anticlines based upon the open-source Landlab toolkit (Hobley et al., 2017; <http://landlab.github.io>).

- 5 We used two components in our model: one simulating erosion due to fluvial action and another simulating sediment transport along slopes due to hillslope diffusion processes. Chen et al. (2014) showed that consideration of only these two components is sufficient for many landscapes but cannot model fluvial sedimentation. However, from field observations and from satellite imagery, we know that no significant fluvial sedimentation takes place on the slopes of the analysed anticlines. On slopes of anticline flanks, the detachment-limited erosion due to the fluvial system tends to be the dominant process
- 10 (Howard, 1994). To detect changes in the landscape due to fluvial erosion through time, we applied the commonly accepted idea that the rate of stream incision is directly proportional to the hydraulic shear stress of a stream (Braun and Willett, 2013). Consequently, we used the stream power incision law (Sklar and Dietrich, 1998; Whipple and Tucker, 1999):

$$\frac{\partial z}{\partial t} = KA^m S^n, \quad (4)$$

- where $\partial z/\partial t$ is the erosion rate [myr^{-1}]; K is an erodibility coefficient [$\text{yr}^{-1}\text{m}^{(1-2m)}$] that encompasses the influence of climate, lithology, and sediment transport processes; A is the upstream drainage area [m^2] and is typically taken as a proxy for discharge (Wobus et al., 2006); $S = \partial z/\partial x$ is the local channel slope [m/m]; z is the elevation [m]; and m and n are the area and slope exponents, respectively. The stream power incision law (Eq. 4) is derived since the upstream drainage area A scales with channel discharge and channel width. The magnitude of the sediment flux in the channel is assumed to equal unity in the standard detachment-limited stream power model (Perron, 2017; Whipple, 2002). In the model, an incision
- 20 threshold (C) was included, below which no incision occurs (Hobley et al., 2017).

To account for the provision of sediment due to hillslope diffusion processes from slopes outside the river system, we used the hillslope diffusion equation (Culling, 1963; Tucker and Bras, 1998):

$$\frac{\partial z}{\partial t} = K_d \nabla^2 z, \quad (5)$$

- where K_d is the diffusivity coefficient [m^2yr^{-1}], z is the elevation [m], and ∇^2 is the Laplace operator, i.e. the divergence of the gradient.
- 25

Finally, the overall evolution of the landscape in different time steps was calculated as the uplift rate subtracted by the changes due to both fluvial erosion and the hillslope diffusion (Temme et al., 2017):

$$Y \frac{\partial z}{\partial t} = U - KA^m S^n - K_d \nabla^2 z, \quad (6)$$

where U is the uplift rate [myr^{-1}].

A DEM raster grid of the present-day [less mature anticline \(Harir-Anticline\)](#) and the surrounding basins (Fig. 5a) served as model input. The advantage of using Harir Anticline was that the evolved drainage network overprinted the pre-existing one. The boundary conditions were set as closed on all sides except in pre-existing outlets in the input grid. The basins surrounding Harir Anticline were also included in the input grid to minimize the effect of the boundary conditions on the Harir Anticline itself. In the input raster grid, a flow route of each cell was connected with neighbouring cells both diagonally and orthogonally. This means that each cell had the possibility to be linked with eight surrounding cells across its sides and corners (Hobley et al., 2017; Tucker et al., 2016).

Concerning the parameter used in the model, the value of m/n , n , and K were found following the methodology described by Harel et al. (2016), Mudd et al. (2014), and Perron and Royden (2013), and by comparison with data from Harel et al. (2016). The value of m/n was found by plotting the elevation against X (elevation- X plot) for streams in the input grid (Fig. 5a), where X is found following the equation described by (Perron and Royden, 2013):

$$X = \int_{x_b}^x \left(\frac{A_0}{A(x)} \right)^{m/n} dx, \quad (7)$$

where A_0 is the reference drainage area [m^2] of 166160 m^2 and x is the horizontal upstream distance [m]. In this approach, we ascribed values for m/n range from zero to one, and X was calculated for each time from Eq. 7. The value of m/n with maximum regression (R^2) value in the elevation- X plot was taken as the best-fitting value, which was 0.41 in our case for the present-day Harir Anticline's drainages (Fig. 5b). This value of m/n is located within the theoretically predicted values of m/n , which ranges from 0.3 to 0.7, based on the stream power incision model (Kwang and Parker, 2017; Temme et al., 2017; Whipple and Tucker, 1999).

In the model, $n = 1.7$ and $K = 3.0E-6 \text{ yr}^{-1}m^{-0.4}$ were used; these values were estimated as mean of K and n in Harel et al. (2016) for those areas that are comparable with our study area in aspect of lithology, climate, and precipitation. The value of m was 0.7. We used an incision threshold of $C = 1.0E-5 \text{ myr}^{-1}$, which is widely adopted for erosion of an upland landscape (Hobley et al., 2017). A present-day annual mean precipitation of c. 0.7 myr^{-1} was used through the time due to the lack of nearby paleoclimate data with good quality. The average of the modelled precipitation anomaly data for Lake Van in SE Turkey (200 km to the NNW of the studied anticlines) is close to zero (Stockhecke et al. 2016; [supplementary material](#)). The current elevation of the Bekhme and Aqra formations in the crest of Harir Anticline is about 1500 m above sea level. Above that, 2070 m of Upper Cretaceous-Miocene units (Law et al., 2014) and 300 m of Upper Miocene Lower Bakhtiari were exhumed before exposure of the Bekhme and Aqra formations. If we consider that the Lower Bakhtiari have been deposited close to sea level before onset of the MFF c. 5 Ma, there would be 3872 m of rock uplift at a rate of $\sim 0.0007 \text{ myr}^{-1}$, which was used in the model. [This rate of vertical uplift is reasonable for the area and it matches with the vertical uplift in Kurdistan that has been presented by Tozer et al. \(2019\)](#). Since soil (regolith) is rare and very thin when present on the slopes, a low diffusivity coefficient of $K_d = 0.001 \text{ m}^2\text{yr}^{-1}$ was used (Fernandes and Dietrich, 1997).

There are minor variations in lithology between the three anticlines (they consist of a thick pile of dominantly Cretaceous carbonate) and no variation in climate can be expected on such a relatively local scale. Therefore, no significant variances are expected in the used parameters. Lastly, the parameters were calibrated by comparing the nature of the evolved landscape to other anticlines within the High Folded Zone that are cored by Cretaceous carbonates and more mature than the Harir Anticline to evaluate how realistic the evolved landscape is.

4 Results

4.1 Landscape Maturity

The three studied anticlines are composed of the raised Cretaceous carbonates in their crests, whereas the Tertiary clastic rocks have been denuded, but conserved in the adjacent synclines. The three anticlines are dissected by rivers that form water gaps across them. Bekhme and Zinta gorges cut the Perat and Akre anticlines, respectively. We also observed wind gaps, such as those in the NW end of Harir Anticline (Zebari and Burberry, 2015). Therefore, neither the location of these water and wind gaps nor the plunging tips of anticlines have been considered in interpreting the geomorphic indices as proxies for relative landscape maturity.

The anticlines reach up to c. 1500 m asl. The minimum altitude is c. 700 in the adjacent synclines and c. 400 m in the Greater Zab river course. The hypsometric curves for the three anticlines are presented in Fig. 6. Harir Anticline's curve is more convex, and its shape is close to the youthful stage of Strahler's diagram (Ohmori, 1993; Strahler, 1952) with 78% of the area above the mean elevation, while Akre Anticline is less convex and close to a mature stage with only 50% of the area above the mean elevation. Perat Anticline's values are located in between and closer to the Harir Anticline curve with 64% of its area above the mean elevation.

The three calculated geomorphic indices (HI, SR, and SI) seem to be substantially influenced by the local structure, and wind and water gaps (Fig. 7). Hypsometric integral values vary between 0.2 and 0.77, with lower values in the adjacent synclines and higher values in the crest of the anticlines. The HI values decrease toward the plunging ends of the anticlines and at gorges, e.g. Perat Anticline's HI values are minimum at the Greater Zab River. In general, Harir Anticline shows higher values than the other two anticlines. Harir Anticline has a broad crest and has been incised by narrow valleys. This makes the mean elevation within the moving window in the calculation close to the maximum elevation and, thus, causes higher values of the hypsometric integral. Perat Anticline shows high values of HI on its crest to the west of Bekhme Gorge. Among the three anticlines, Akre Anticline shows the lowest values of HI in its central part, which is due to presence of more incised and wider valleys. Elevation drops rapidly from the hinge of the anticline toward the limbs, which causes the mean elevation within the window to fall.

The surface roughness values range between 1 and 1.33 in the area. The lowest values of the SR are also present in the adjacent synclines and in the plunging tips of the anticlines. The highest values are associated with the location of water gaps. These are areas where rivers deeply incised at both Bekhme and Zinta gorges. Harir Anticline has lowest surface

roughness values. Perat Anticline shows the highest value of SR especially in its northern limb. Akre Anticline has moderate SR values in its central segment and western side where a wind gap is present.

The results of the surface index range between -0.04 to 0.70 in the three anticlines studied. Few locations show negative values. These are associated partly with adjacent synclines and with Bekhme Gorge. Apart from these locations, the area shows positive surface indices. Harir Anticline exhibits higher values on its broad crest. Perat Anticline shows moderate values of SI on its crest to the west and east of Bekhme Gorge. For Akre Anticline, SI values are lower than in both Harir and Perat anticlines, with highest values on its crest east of Zinta Gorge. These high values of SI highlight the flat areas with high elevation and high hypsometric integral. The surface index values also highlight the Pila Spi and Khurmala limestone ridges encircling the anticlines with values close to zero.

In our calculation, the results of geomorphic indices change with changing the size of the moving window and the resolution of the input data (see supplementary material). This was also detected by Andreani et al. (2014) and Obaid and Allen (2017). Andreani et al. (2014) found that the DEM resolution does not affect the hypsometric integral, but it affects the surface roughness, while the size of the moving window affects both hypsometric integral and surface roughness. The results become smoother with an increasing size of the moving window. Here, we found that it is reasonable to use a 100 * 100 cell (3 * 3 km) moving window, which covers approximately one limb of the anticline with 6-7 km width. It therefore highlights the desirable signal. The cluster map for the HI Gi* statistics was calculated following the approach by Pérez-Peña et al. (2009) for the 500 * 500 m grid. We obtained results similar to the HI map calculated from a 100 * 100 cell (3 * 3 km) moving window and resampled to 500 * 500 m grid in terms of highlighting the cluster of high and low HI values (Fig. S19 a and b in supplementary material). This comparison proves that our method is equally applicable and valid. We therefore ran all analyses based on the 100 * 100 cell moving window as described above.

According to the hypsometric curves and the geomorphic indices, we found that there is a measurable difference in landscape maturity between the three anticlines. We classified our anticlines as relatively mature (Akre Anticline), moderately mature (Perat Anticline), and less mature (Harir Anticline). The difference in the maturity level must be due to a difference in one or more of the factors tectonics, climate, or rock erodibility. No variation in the climate is expected for the scale of the studied area, therefore its impact on the landscape maturity can be neglected. The three anticlines show essentially the same lithology (Figs. 2 and 3), i.e. similar lateral rock type and erodibility. Thus, the only factors that may vary along the anticlines are uplift rate or onset time of the uplift. This can be interpreted with one of the following scenarios: either the anticlines started to uplift in the order 1) Akre, 2) Perat and 3) Harir from west to east, or all of them started at the same time but with different rates. In the latter case, the uplift rate would have been highest at Akre and lowest at Harir, exposing Akre to erosion earlier than Harir.

4.2 Landscape Evolution Model

The aged landscape from the model run (Figs. 8 and 9) is the result of fluvial erosion and hillslope diffusion on the one hand, and uplift due to folding on the other hand. In the landscape modelling, various simulations with different parameters and

time spans were performed (supplementary material S24-S27). Harir Anticline was used as an input model and the landscape evolution model was run for a time span of 10 kyr up to 100 kyr and then it was run for a time span of 20 kyr. The evolving drainage system overprints the pre-existing one in the input and gradually becomes more deeply incised from the anticline flanks carving toward its core (Fig. 8). Harir Anticline is a box-shaped anticline with a wide and flat crest area. With ongoing incision towards the core of the anticline, this plain crest narrowed gradually and finally became a sharp ridge that divided the drainage basins of the SW flank from those of the NE.

We compared the hypsometric curves of the model outputs to the present-day curves of the anticlines. The hypsometric curves were calculated first as total weighted mean for basins within the anticline and later calculated for the entire anticlinal ridges (Fig. 9). Statistically (with minimum RMS), the hypsometric curve of Harir Anticline was closest to the present-day Perat Anticline after 100 kyr and 80 kyr of erosion when using total weighted mean and entire anticlinal ridge, respectively, in calculation of the hypsometric curves. The output curve after 160 kyr and 200 kyr matched best with present-day Akre Anticline, when using total weighted mean and entire anticlinal ridge, respectively, in calculation of the hypsometric curves. We conclude that it will take Harir Anticline roughly about 80 to 100 kyr to reach the maturity level of Perat Anticline and about 160 to 200 kyr to reach the level of Akre Anticline based on our model and comparison of the hypsometric curves if the uplift rates of the three anticlines were the same. The other possibility is that the anticlines started to grow at the same time but with different uplift rates. In this case, it is not possible to find the difference in uplift rates via our landscape modelling. Since the factors that control geomorphology (lithology, structural setting, and climate) were similar for all three anticlines, and under the assumption of constant growth and erosional conditions, we infer that uplift of Akre and Perat anticlines started respectively 160-200 kyr and 80-100 kyr before Harir started to grow if their uplift rates were the same.

4.3 Geometry of the Studied Anticlines

The structural cross-sections for the three anticlines (Fig. 10) constructed from field data and literature (Syam, 2014) shows that the anticlines are box-shaped with broad crests. They are asymmetrical verging toward the SW with a nearly vertical or overturned forelimb. The three anticlines are thrust-related, in accordance with published studies of the area (Csontos et al. 2012), and have a thrust in their forelimb. Perat Anticline additionally exhibits a back thrust in its NE limb. The shortening across the three anticlines was calculated using line-length balancing. We found 26%, 28% and 29% shortening for Harir, Perat and Akre anticlines, respectively, and conclude that there is no significant variation. A difference in the fold amplitude between the three anticlines can be discerned in the cross-sections. The amplitude of Perat Anticline is higher than that of both Harir and Akre anticlines. Another difference concerns the thickness of the Upper Cretaceous - Middle Eocene clastic succession, which dwindles toward the Akre Anticline. The whole Miocene succession, however, is the thickest in the Akre Anticline. Both the Upper Cretaceous - Middle Eocene and Miocene successions consist of highly erodible clastic rocks, and the thicker Miocene succession in the Akre Anticline counterbalances the thinner Upper Cretaceous - Middle Eocene succession. Therefore, it is not expected that these variations in the structural geometry and stratigraphic thickness have a great impact on the variation of the landscape maturity in the three anticlines and the landscape model.

5 Discussion

5.1 Landscape Maturity and Modelling

Any relative change in the base level induced by tectonics or climate leads to the change of erosion rates. A relict landscape survives when its uplift is not completely counterbalanced by erosion (Andreani and Gloaguen, 2016; Burbank and Anderson, 2012; Pérez-Peña et al., 2015). The relative relict landscape and its distribution on these three anticlines atop the MFF reveal clues about underlying tectonics since there is no significant variation in climate and lithology.

Within the three studied anticlines, the geomorphic indices effectively highlighted their incision. The surface index which combines both hypsometric integral and surface roughness, sets apart relict landscapes of positive and high values from transient landscapes of negative values that are preferentially incised (Andreani et al., 2014). There is a notable relative deviation in areas where anticlines are crossed by rivers e.g. Bekhme and Zinta gorges, which show a high surface roughness. Also, variations in surface index are found in comparable areas in the three anticlines. Focussing on the crest of the anticlines, we observe that Harir Anticline shows higher values than the two others. The lowest values are found in Akre Anticline. Harir has low incision at elevated surfaces while Akre has more incised uneven landscape, because erosion has worked deeper into the core of the anticline. This can also be inferred from the valley shapes. We observe a tight V-shape valleys in the flanks of Harir and a open V-shape valleys in Akre (Figs. 11a and 11b). We relate this difference to the tectonic uplift and to the effects of longer erosion acting on Akre. The observation can be interpreted with one of the following two premises: either the anticlines started to uplift successively (first Akre, then Perat, and finally Harir), or all of them started at the same time but with different uplift and exhumation rates (Akre the fastest, Harir the slowest). In other words, the Cretaceous carbonates in Harir Anticline were exposed to the erosion later than in Akre Anticline and, consequently, incised less.

The current landscape of these anticlines exposes Cretaceous carbonates of the Qamchuqa, Bekhme and Aqra formations, which became exposed to erosion only after unroofing of the entire Palaeogene - Neogene succession. The Upper Miocene-Pliocene Bakhtiari Group, which is the youngest stratigraphic unit in the area, is affected by folding, as observed from growth strata (Csontos et al., 2012). This has also been observed in the Upper Bakhtiari (Pliocene-Pleistocene) close to the MFF (Koshnaw et al., 2017). In between Bekhme and Aqra and the Upper Bakhtiari formations, 2.37 km of the Upper Cretaceous - Miocene clastic rocks interbedded with thin units of limestone (Law et al., 2014) have been exhumed due to successive rock uplift in the crest of the studied anticlines, triggered by shortening and erosion. They are only preserved in the adjacent synclines. The Cretaceous carbonates themselves have been exposed in the crests of Akre, Perat, and Harir anticlines for c. 0.9 km above the level of the other exhumed units. Based on the thickness, the amount of the exposed Cretaceous carbonate makes c. 28 % of the total exhumed and exposed thickness in the crest of the anticlines. Therefore, with both scenarios (different uplift time or different uplift rate) and with assumption of constant (linear) rock uplift rate through time, the Cretaceous carbonate in Harir Anticline was exposed to erosion later than in the Akre Anticline (Fig. 12a).

The steeper valley flanks in Harir Anticline compared to those of Akre also support higher uplift rates of the Harir Anticline. Furthermore, the relationship between stream slope and upstream drainage area at any given point of streams in the Harir Anticline is positive (Fig. 12b). This means that the streams have a convex shape and the streams' segments with steeper slopes are still located in the flanks of the anticline. In the Akre Anticline, this relationship is negative (Fig. 12b), which means that the streams have a concave shape and the segments with steeper slopes have migrated toward the core of the anticline. This implies that tectonic activity in the Harir Anticline is younger than in the Akre Anticline: in other words, the Harir Anticline was exposed to erosion later than the Akre Anticline. Therefore, the premise of having Harir Anticline starting its uplift later than Akre Anticline is most likely. This is our preferred scenario in the model for the successive tectonic evolution of the study area presented below.

The geomorphic indices have been widely used to assess the landscape maturity and, subsequently, active tectonics (Andreani and Gloaguen, 2016; Mahmood and Gloaguen, 2012; Pérez-Peña et al., 2009). The challenging aspect of landscape maturity modelling is to obtain an absolute quantification of tectonics and the relevant time spans. The same holds true with using a landscape evolution model to estimate the relative time difference between two landscapes, because it is difficult to compare two landscapes in terms of maturity by absolute means. The results of the landscape modelling approach yielded a numerically derived estimate on the relative age difference between the studied anticlines but without absolute growth ages.

In the model, various parameters and two well-known landscape evolution equations for the fluvial erosion and hillslope diffusion were used, but in general it is impossible to mimic nature perfectly. The relative time difference of landscape evolution of these anticlines was estimated from the model assuming that the climate has not changed much during the evolution of the landscape since there was not much variation in the precipitation based on the modelled data (Stockhecke et al. 2016) and for the sake of simplicity, ~~admitting~~ admitting that climatic change has a significant impact on the landscape. In addition, neither rock fall nor karstification were included in the model for simplicity. Field observations suggest that karstification does not have a significant impact on the landscape. Overall, the evolved landscape from the model seems to be plausible in comparison with the other anticlines that surround Harir Anticline, and the landscape models are more mature with respect to the developed topography and to the overall drainage patterns.

5.2 Structural Style and Regional Tectonics

An orogenic bend is depicted in the area where the trend of structures changes across the Greater Zab River from NW-SE at the eastern side of the river to nearly E-W at its western side. The course of the Greater Zab River is suggested to overlie a NE-trending transversal basement fault with right-lateral displacement (Ameen, 1992; Burberry, 2015; Jassim and Goff, 2006; Omar, 2005) evidenced by an offset of the High Folded Zone propagation foreland-ward. At the eastern side of the river the deformation has propagated for about 25 km further than on its western side (Figs. 1 and 2). The origin of this fault reaches back to the Late Proterozoic tectonic history of the Arabian Plate. This fault has been reactivated later in subsequent tectonic events (Ameen, 1992; Aqrabi et al., 2010; Burberry, 2015; Jassim and Goff, 2006). This can also be noticed in the

thickness of the sedimentary cover, which is thinner to the west of the Greater Zab River (Ameen, 1992; Zebari and Burberry, 2015). This change in thickness is attributed to a series of uplift events and erosional/non-depositional gaps during the Mesozoic (Ameen, 1992; Aqrabi et al., 2010). Further propagation of the deformation (Mountain Front) in the eastern side of the Greater Zab River may be due to the existence of a thicker sedimentary cover there than on the western side,

5 which in turn may have influenced the foreland-ward propagation of deformation (Marshak and Wilkerson, 1992). The deference in propagation of deformation may also be due to the convergence being accommodated differently across the curved fold-thrust belt (Csonotos et al., 2012) ~~from~~; ~~which present NW-SE trending structures i~~n the eastern side of the Greater Zab River river where the convergence is accommodated across NW-SE trending structures through belt-normal slip and right-lateral strike-slip ~~across the eastern NW-SE trending this part components, and while E-W trending structures in the~~
10 western side of the river where the convergence is accommodated only by a belt-normal slip across E-W trending structures the western E-W trending segment (it (Csonotos et al., 2012; Reilinger et al., 2006).

Zebari and Burberry (2015) found that anticlines to the east of the Greater Zab River (Harir, Shakrok and Safin anticlines) demonstrate pronounced NW-ward propagation based on their geomorphic criteria, and the start point of the NW-ward propagation of the Harir Anticline is close to its SE end. This implies that progressing uplift in the hanging wall of the MFF
15 was not gradually continuing from the Akre Anticline towards the Perat Anticline and further SE-ward to the Harir Anticline. The uplift progress is probably rather partitioned into segments along the belt. In addition, other anticlines to the south (Safin Anticline) and to the southwest (Shakrok Anticline) of Harir Anticline are more mature than Harir Anticline itself, based on their hypsometric curves (Fig. 13) and geomorphic indices (supplementary material; S1-S18), implying that the foreland-ward propagation of the deformation was also out-of-sequence in this part of the High Folded Zone. This has
20 also been noted in the Foothill Zone based on thermochronological dating (Koshnaw et al., 2017) and landscape maturity (Obaid and Allen, 2017). Thus, the most plausible scenario is that deformation in the Harir segment started sometime after that in Akre segment (160-200 kyr according to our landscape evolution modelling). Harir Anticline uplift would also postdate Perat Anticline uplift (80-100 kyr) to the west and the onset of Safin and Shakrok anticlines to the south and southeast, which are not included in the model (Fig. 14). As discussed by Csonotos et al., (2012), the fold relay corresponds to
25 the change in strain partitioning and rotation of the horizontal stress direction from NE-SW to N-S in Late Pliocene (Navabpour et al., 2008; Navabpour and Barrier, 2012). During the latest stage of the N-S convergence, a right-lateral shear and superposed folding along the NW-SE trending anticlines (Csonotos et al., 2012) can be observed from the relay of the Shakrok, Harir and Perat anticlines (Figs. 2 and 14). Applying this concept requires a comprehensive paleostress analysis investigation especially within these studied anticlines, which is beyond the scope of this paper.

30 **6 Conclusions**

The geomorphic indices used in this study allowed us to quantitatively differentiate between variably degraded landforms in the frontal Zagros Mountain of NE Iraq. This area is characterized by active folding due to ongoing convergence between the

Eurasian and Arabian plates. Three active thrust-related anticlines that are aligned along-strike the MFF were studied in detail. While the Akre Anticline shows deeply incised valleys indicative of advanced erosion, the Harir and Perat anticlines have relatively smooth surfaces and show younger landscape than Akre. We related this difference to the underlying tectonics. This can be interpreted with one of the following concepts: either anticlinal growth started at different times or all
5 of them started to grow at the same time, but with different surface uplift and exhumation rates.

A comparison of the geomorphic indices values of the model output with those of the present-day Akre Anticline topography revealed that it will take Harir Anticline about 160-200 kyr to reach the maturity level of today's Akre Anticline, and about 80-100 kyr to reach the maturity level of the Perat Anticline assuming constant uplift rates along the three anticlines. Due to similarity in the lithology, structural setting and climate along the three anticlines and by assuming constant growth and
10 erosion conditions, we infer that Akre Anticline started to grow 160-200 kyr before Harir Anticline. The onset of growth of Perat Anticline lies in between that of Harir and Akre anticlines. A NW-ward propagation of Harir Anticline itself implies that the uplift has been independent within different segments rather than having been continuous from the NW to the SE. Our method of estimating relative age differences in variously degraded anticlines can be applied to many other anticlines along the MFF and could eventually develop into a model of the temporal evolution of this fold and thrust belt.

15

7 Acknowledgments

The German Academic Exchange Service (DAAD) is acknowledged for providing a scholarship (Research Grants – Doctoral Programmes in Germany, 2016/17; 57214224) to the first author to conduct his PhD research in Germany. The authors express their gratitude to the German Research Foundation (DFG) project no. 393274947 for providing financial
20 research support. The German Aerospace Agency (DLR) and Mr. Thomas Busche in particular are thanked for providing TanDEM-X digital elevation models. We also thank [Bernard Delcaillau and](#) two anonymous peers for their ~~partly~~ very thorough reviews that helped us to further clarify and improve numerous aspects of our work.

References

- Abdulnaby, W., Mahdi, H., Numan, N. M. S. and Al-Shukri, H.: Seismotectonics of the Bitlis–Zagros Fold and Thrust Belt in Northern Iraq and Surrounding Regions from Moment Tensor Analysis, *Pure & Appl. Geophys.*, 171(7), 1237–1250, [https://doi: 10.1007/s00024-013-0688-4](https://doi.org/10.1007/s00024-013-0688-4), 2014.
- 5 Agard, P., Omrani, J., Jolivet, L., Whitechurch, H., Vrielynck, B., Spakman, W., Monié, P., Meyer, B. and Wortel, R.: Zagros orogeny: A subduction-dominated process, *Geol. Mag.*, 148(5–6), 692–725, [https://doi:10.1017/S001675681100046X](https://doi.org/10.1017/S001675681100046X), 2011.
- Al-Qayim, B., Omer, A. and Koyi, H.: Tectonostratigraphic overview of the Zagros Suture Zone, Kurdistan Region, Northeast Iraq, *GeoArabia*, 17(4), 109–156, 2012.
- 10 Alavi, M.: Structures of the Zagros fold-thrust belt in Iran, *Am. J. Sci.*, 307(9), 1064–1095, [https://doi:10.2475/09.2007.02.2007](https://doi.org/10.2475/09.2007.02.2007).
- Ameen, M. S.: Possible forced folding in the Taurus–Zagros Belt of northern Iraq, *Geol. Mag.*, 128(6), 561–584, [https://doi:10.1017/S0016756800019695](https://doi.org/10.1017/S0016756800019695), 1991.
- Ameen, M. S.: Effect of basement tectonics on hydrocarbon generation, migration, and accumulation in Northern Iraq, *Am. Assoc. Pet. Geol. Bull.*, 76(3), 356–370, 1992.
- 15 Andreani, L. and Gloaguen, R.: Geomorphic analysis of transient landscapes in the Sierra Madre de Chiapas and Maya Mountains (northern Central America): Implications for the North American-Caribbean-Cocos plate boundary, *Earth Surf. Dyn.*, 4(1), 71–102, [https://doi:10.5194/esurf-4-71-2016](https://doi.org/10.5194/esurf-4-71-2016), 2016.
- Andreani, L., Stanek, K. P., Gloaguen, R., Krentz, O. and Domínguez-González, L.: DEM-based analysis of interactions between tectonics and landscapes in the Ore Mountains and Eger Rift (East Germany and NW Czech Republic), *Remote Sens.*, 6(9), 7971–8001, [https://doi:10.3390/rs6097971](https://doi.org/10.3390/rs6097971), 2014.
- 20 Aqrabi, A. A. M., Goff, J. C., Horbury, A. D. and Sadooni F. N.: *The Petroleum Geology of Iraq*, Scientific Press, Beaconsfield., 2010.
- Berberian, M.: Master “blind” thrust faults hidden under the Zagros folds: active basement tectonics and surface morphotectonics, *Tectonophysics*, 241(3–4), [https://doi:10.1016/0040-1951\(94\)00185-C](https://doi.org/10.1016/0040-1951(94)00185-C), 1995.
- 25 Bishop, P.: Long-term landscape evolution: linking tectonics and surface processes, *Earth Surf. Process. Landforms*, 32(3), 329–365, <https://doi.org/10.1002/esp.1493>, 2007.
- Blanc, E. J.-P., Allen, M. B., Inger, S. and Hassani, H.: Structural styles in the Zagros Simple Folded Zone, Iran, *J. Geol. Soc. London.*, 160(3), 401–412, [https://doi:10.1144/0016-764902-110](https://doi.org/10.1144/0016-764902-110), 2003.
- 30 Braun, J. and Willett, S. D.: A very efficient O(n), implicit and parallel method to solve the stream power equation governing fluvial incision and landscape evolution, *Geomorphology*, 180–181, 170–179, [https://doi:10.1016/j.geomorph.2012.10.008](https://doi.org/10.1016/j.geomorph.2012.10.008), 2013.

- Bretis, B., Bartl, N. and Grasemann, B.: Lateral fold growth and linkage in the Zagros fold and thrust belt (Kurdistan, NE Iraq), *Basin Res.*, 23(6), 615–630, <https://doi.org/10.1111/j.1365-2117.2011.00506.x>, 2011.
- Bull, W. B.: *Tectonic Geomorphology of Mountains: A New Approach to Paleoseismology*, Wiley-Blackwell, Oxford, 2007.
- Burbank, D. and Anderson, R.: *Tectonic Geomorphology*, 2nd Ed, Wiley-Blackwell, Chichester, UK, 2012.
- 5 Burberry, C. M.: The effect of basement fault reactivation on the Triassic-Recent Geology of Kurdistan, North Iraq, *J. Pet. Geol.*, 38(37–58), 37–58, <https://doi.org/10.1111/jpg.12597>, 2015.
- Chen, A., Darbon, J. Ô. and Morel, J. M.: Landscape evolution models: A review of their fundamental equations, *Geomorphology*, 219, 68–86, <https://doi.org/10.1016/j.geomorph.2014.04.037>, 2014.
- Cheng, K. Y., Hung, J. H., Chang, H. C., Tsai, H. and Sung, Q. C.: Scale independence of basin hypsometry and steady state topography, *Geomorphology*, 171–172, 1–11, <https://doi.org/10.1016/j.geomorph.2012.04.022>, 2012.
- 10 Collignon, M., Yamato, P., Castelltort, S. and Kaus, B. J. P.: Modeling of wind gap formation and development of sedimentary basins during fold growth: application to the Zagros Fold Belt, Iran, *Earth Surf. Process. Landforms*, 41(11), 1521–1535, <https://doi.org/10.1002/esp.3921>, 2016.
- Cowie, P. A., Attal, M., Tucker, G. E., Whittaker, A. C., Naylor, M., Ganas, A. and Roberts, G. P.: Investigating the surface process response to fault interaction and linkage using a numerical modelling approach, *Basin Res.*, 18(3), 231–266, <https://doi.org/10.1111/j.1365-2117.2006.00298.x>, 2006.
- 15 Csontos, L., Sasvári, Á., Pocsai, T., Kósa, L., Salae, A. T. and Ali, A.: Structural evolution of the northwestern Zagros, Kurdistan Region, Iraq: Implications on oil migration, *GeoArabia*, 17(2), 81–116, 2012.
- Culling, W. E. H.: Soil Creep and the Development of Hillside Slopes, *J. Geol.*, 71(2), 127–161, 1963.
- 20 Emre, Ö., Duman, T. Y., Özalp, S., Elmacı, H., Olgun, Ş. and Şaroğlu, F.: *Active Fault Map of Turkey with an Explanatory Text. 1:1,250,000 Scale*, General Directorate of Mineral Research and Exploration, Ankara., 2013.
- Emami, H., Vergés, J., Nalpas, T., Gillespie, P., Sharp, I., Karpuz, R., Blanc, E. P. and Goodarzi, M. G. H.: Structure of the Mountain Front Flexure along the Anaran anticline in the Pusht-e Kuh Arc (NW Zagros, Iran): insights from sand box models, *Geol. Soc. London, Spec. Publ.*, 330(1), 155–178, <https://doi.org/10.1144/SP330.9>, 2010.
- 25 Fernandes, N. F. and Dietrich, W. E.: Hillslope evolution by diffusive processes: The timescale for equilibrium adjustments, *Water Resour. Res.*, 33(6), 1307–1318, <https://doi.org/10.1029/97WR00534>, 1997.
- Fouad, S. F. A.: Western Zagros Fold – Thrust Belt, Part II: The High Folded Zone, *Iraqi Bull. Geol. Min., Special Iss.* (6), 53–71, 2014.
- Grohmann, C. H.: Morphometric analysis in geographic information systems: Applications of free software GRASS and R, *Comput. Geosci.*, 30(9–10), 1055–1067, <https://doi.org/10.1016/j.cageo.2004.08.002>, 2004.
- 30 Hancock, G. R. and Willgoose, G. R.: The use of a landscape simulator in the validation of the Siberia landscape evolution model: Transient landforms, *Earth Surf. Process. Landforms*, 27(12), 1321–1334, <https://doi.org/10.1002/esp.414>, 2002.
- Harel, M. A., Mudd, S. M. and Attal, M.: Global analysis of the stream power law parameters based on worldwide 10Be denudation rates, *Geomorphology*, 268, 184–196, <https://doi.org/10.1016/j.geomorph.2016.05.035>, 2016.

- Hessami, K., Koyi, H. A., Talbot, C. J., Tabashi, H. and Shabanian, E.: Progressive unconformities within an evolving foreland fold-thrust belt, Zagros Mountains, *J. Geol. Soc. London.*, 158(6), 969–981, <https://doi:10.1144/0016-764901-007>, 2001.
- Hessami, K., Nilforoushan, F. and Talbot, C. J.: Active deformation within the Zagros Mountains deduced from GPS measurements, *J. Geol. Soc. London.*, 163(1), 143–148, <https://doi:10.1144/0016-764905-031>, 2006.
- Hinsch, R. and Bretis, B.: A semi-balanced section in the northwestern Zagros region: Constraining the structural architecture of the Mountain Front Flexure in the Kirkuk Embayment, Iraq, *GeoArabia*, 20(4), 41–62, 2015.
- Hobley, D. E. J., Adams, J. M., Siddhartha Nudurupati, S., Hutton, E. W. H., Gasparini, N. M., Istanbuluoglu, E. and Tucker, G. E.: Creative computing with Landlab: An open-source toolkit for building, coupling, and exploring two-dimensional numerical models of Earth-surface dynamics, *Earth Surf. Dyn.*, 5(1), 21–46, <https://doi:10.5194/esurf-5-21-2017>, 2017.
- [Hobson, R. D.: Surface roughness in topography: quantitative approach, in: Spatial analysis in geomorphology, edited by Chorley, R. J., Methuen, London, 225–245, 1972.](#)
- Homke, S., Vergés, J., Garcés, M., Emami, H. and Karpuz, R.: Magnetostratigraphy of Miocene-Pliocene Zagros foreland deposits in the front of the Push-e Kush Arc (Lurestan Province, Iran), *Earth Planet. Sci. Lett.*, 225(3–4), 397–410, <https://doi:10.1016/j.epsl.2004.07.002>, 2004.
- Howard, A. D.: A detachment limited model of drainage basin evolution, *Water Resour. Res.*, 30(7), 2261–2285, <https://doi:10.1029/94WR00757>, 1994.
- Jassim, S. Z. and Goff, J. C.: *Geology of Iraq*, Dolin, Prague and Moravian Museum, Brno, Czech Rep., 2006.
- Keller, E. A., Gurrola, L. and Tierney, T. E.: Geomorphic criteria to determine direction of lateral propagation of reverse faulting and folding, *Geology*, 27(6), 515–518, [https://doi.org/10.1130/0091-7613\(1999\)027<0515:GCTDDO>2.3.CO;2](https://doi.org/10.1130/0091-7613(1999)027<0515:GCTDDO>2.3.CO;2), 1999.
- Kent, W. N.: Structures of the Kirkuk Embayment, northern Iraq: Foreland structures or Structures of the Kirkuk Embayment, northern Iraq: Foreland structures or Zagros Fold Belt structures?, *GeoArabia*, 15(4), 147–157, 2010.
- Koshnaw, R. I., Horton, B. K., Stockli, D. F., Barber, D. E., Tamar-Agha, M. Y. and Kendall, J. J.: Neogene shortening and exhumation of the Zagros fold-thrust belt and foreland basin in the Kurdistan region of northern Iraq, *Tectonophysics*, 694, 332–355, <https://doi:10.1016/j.tecto.2016.11.016>, 2017.
- Koukouvelas, I. K., Zygouri, V., Nikolakopoulos, K. and Verroios, S.: Treatise on the tectonic geomorphology of active faults: The significance of using a universal digital elevation model, *J. Struct. Geol.*, 116(June), 241–252, <https://doi:10.1016/j.jsg.2018.06.007>, 2018.
- Krieger, G., Moreira, A., Fiedler, H., Hajnsek, I., Werner, M., Younis, M., and Zink, M.: TanDEM-X: A satellite formation for high-resolution SAR interferometry, *IEEE Trans. Geosci. Remote Sens.*, 45, 3317–3341, <https://doi:10.1109/TGRS.2007.900693>, 2007.

- Kwang, J. S. and Parker, G.: Landscape evolution models using the stream power incision model show unrealistic behavior when m/n equals 0.5, *Earth Surf. Dyn.*, 5(4), 807–820, <https://doi:10.5194/esurf-5-807-2017>, 2017.
- Leturmy, P., Molinaro, M. and de Lamotte, D. F.: Structure, timing and morphological signature of hidden reverse basement faults in the Fars Arc of the Zagros (Iran), *Geol. Soc. London, Spec. Publ.*, 330(1), 121–138, <https://doi:10.1144/SP330.7>,
5 2010.
- Mahmood, S. A. and Gloaguen, R.: Appraisal of active tectonics in Hindu Kush: Insights from DEM derived geomorphic indices and drainage analysis, *Geosci. Front.*, 3(4), 407–428, <https://doi:10.1016/j.gsf.2011.12.002>, 2012.
- Marshak, S. and Wilkerson, M. S.: Effect of overburden thickness on thrust belt geometry and development, *Tectonics*, 11(3), 560–566, <https://doi:10.1029/92TC00175>, 1992.
- 10 McClusky, S., Reilinger, R., Mahmoud, S., Ben Sari, D. and Tealeb, A.: GPS constraints on Africa (Nubia) and Arabia plate motions, *Geophys. J. Int.*, 155(1), 126–138, <https://doi:10.1046/j.1365-246X.2003.02023.x>, 2003.
- McQuarrie, N.: Crustal scale geometry of the Zagros fold-thrust belt, Iran, *J. Struct. Geol.*, 26(3), 519–535, <https://doi:10.1016/j.jsg.2003.08.009>, 2004.
- Miller, S. R., Slingerland, R. L. and Kirby, E.: Characteristics of steady state fluvial topography above fault-bend folds, *J. Geophys. Res. Earth Surf.*, 112(4), 1–21, <https://doi:10.1029/2007JF000772>, 2007.
15
- Molinaro, M., Leturmy, P., Guezou, J. C., Frizon de Lamotte, D. and Eshraghi, S. A.: The structure and kinematics of the southeastern Zagros fold-thrust belt, Iran: From thin-skinned to thick-skinned tectonics, *Tectonics*, 24(3), 1–19, <https://doi:10.1029/2004TC001633>, 2005.
- Moran, P.P.: Notes on continuous stochastic phenomena, *Biometrika*, 37(1–2), 17–23, <https://doi:10.1093/biomet/37.1-2.17>,
20 1950.
- Mouthereau, F.: Timing of uplift in the Zagros belt/Iranian plateau and accommodation of late Cenozoic Arabia-Eurasia convergence, *Geol. Mag.*, 148(5–6), 726–738, <https://doi:10.1017/S0016756811000306>, 2011.
- Mouthereau, F., Tensi, J., Bellahsen, N., Lacombe, O., De Boisgrollier, T. and Kargar, S.: Tertiary sequence of deformation in a thin-skinned/thick-skinned collision belt: The Zagros Folded Belt (Fars, Iran), *Tectonics*, 26(5),
25 <https://doi:10.1029/2007TC002098>, 2007.
- Mouthereau, F., Lacombe, O. and Vergés, J.: Building the Zagros collisional orogen: Timing, strain distribution and the dynamics of Arabia/Eurasia plate convergence, *Tectonophysics*, 532–535, 27–60, <https://doi:10.1016/j.tecto.2012.01.022>, 2012.
- Mudd, S. M., Attal, M., Milodowski, D. T., Grieve, S. W. D. and Valters, D. A.: A statistical framework to quantify spatial variation in channel gradients using the integral method of channel profile analysis, *J. Geophys. Res. Earth Surf.*, 119(2), 138–152, <https://doi:10.1002/2013JF002981>, 2014.
30
- NASA JPL: NASA Shuttle Radar Topography Mission Global 1 arc second [Data set]. NASA EOSDIS Land Processes DAAC. <http://doi:10.5067/MEaSURES/SRTM/SRTMGL1.003>, 2013.

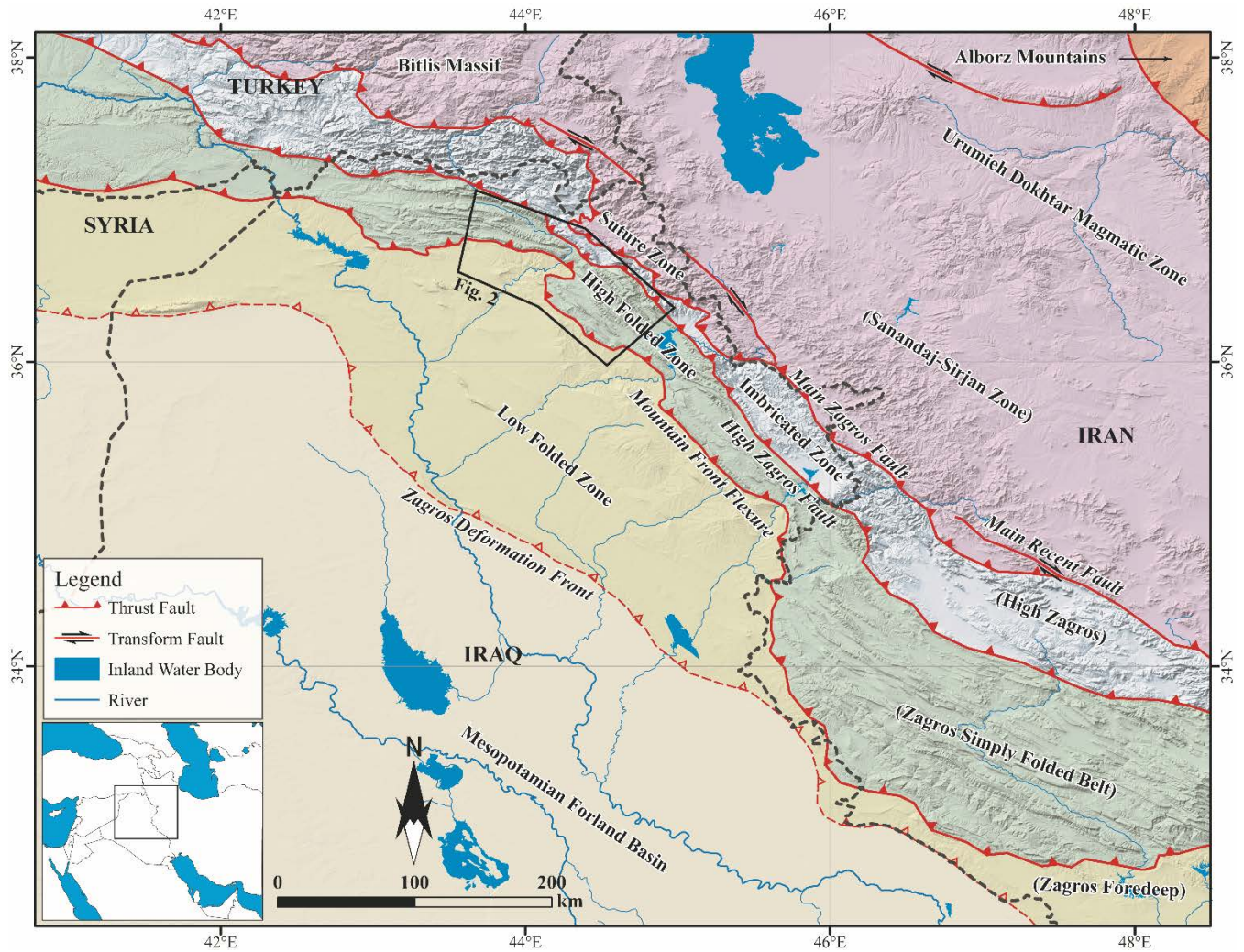
- Navabpour, P., Angelier, J. and Barrier, E.: Stress state reconstruction of oblique collision and evolution of deformation partitioning in W-Zagros (Iran, Kermanshah), *Geophys. J. Int.*, 175(2), 755–782, <https://doi.org/10.1111/j.1365246X.2008.03916.x>, 2008.
- Navabpour, P. and Barrier, E.: Stress states in the Zagros fold-and-thrust belt from passive margin to collisional tectonic setting. In: Gudmundsson, A. & Bergerat, F. (eds) *Crustal Stresses, Fractures, and Fault Zones: The Legacy of Jacques Angelier*. *Tectonophysics*, 581, 76–83, doi: 10.1016/j.tecto.2012.01.011, 2012.
- Numan, N. M. S.: A plate tectonic scenario for the phanerozoic succession in Iraq, *J. Geol. Soc. Iraq*, 30(2), 85–110, 1997.
- Obaid, A. K. and Allen, M. B.: Landscape maturity, fold growth sequence and structural style in the Kirkuk Embayment of the Zagros, northern Iraq, *Tectonophysics*, 717, 27–40, <https://doi.org/10.1016/j.tecto.2017.07.006>, 2017.
- Ohmori, H.: Changes in the hypsometric curve through mountain building resulting from concurrent tectonics and denudation, *Geomorphology*, 8(4), 263–277, [https://doi.org/10.1016/0169-555X\(93\)90023-U](https://doi.org/10.1016/0169-555X(93)90023-U), 1993.
- Ord, J. K., and Getis, A.: *Local Spatial Autocorrelation Statistics, Distributional Issues and Application*, *Geogr. Anal.*, 27(4), 286–306, <https://doi.org/10.1111/j.1538-4632.1995.tb00912.x>, 1995.
- Oveisi, B., Lavé, J., Van Der Beek, P., Carcaillet, J., Benedetti, L. and Aubourg, C.: Thick- and thin-skinned deformation rates in the central Zagros simple folded zone (Iran) indicated by displacement of geomorphic surfaces, *Geophys. J. Int.*, 176(2), 627–654, <https://doi.org/10.1111/j.1365-246X.2008.04002.x>, 2009.
- Pérez-Peña, J. V., Azañón, J. M., Booth-Rea, G., Azor, A., and Delgado, J.: Differentiating geology and tectonics using a spatial autocorrelation technique for the hypsometric integral, *J. Geophys. Res.*, 114(F02018), <https://doi.org/10.1029/2008JF001092>, 2009.
- Pérez-Peña, J. V., Azañón, J. M., Azor, A., Booth-Rea, G., Galve, J. P., Roldán, F. J., Mancilla, F., Giaconia, F., Morales, J. and Al-Awabdeh, M.: Quaternary landscape evolution driven by slab-pull mechanisms in the Granada Basin (Central Betics), *Tectonophysics*, 663, 5–18, <https://doi.org/10.1016/j.tecto.2015.07.035>, 2015.
- Perron, J. T.: Climate and the Pace of Erosional Landscape Evolution, *Annu. Rev. Earth Planet. Sci.*, 45(1), annurev-earth5060614-105405, <https://doi.org/10.1146/annurev-earth-060614-105405>, 2017.
- Perron, J. T. and Royden, L.: An integral approach to bedrock river profile analysis, *Earth Surf. Process. Landforms*, 38(6), 570–576, <https://doi.org/10.1002/esp.3302>, 2013.
- Pike, R. J. and Wilson, S. E.: Elevation-relief ratio, hypsometric integral, and geomorphic area-altitude analysis, *Bull. Geol. Soc. Am.*, 82(4), 1079–1084, [https://doi.org/10.1130/0016-7606\(1971\)82\[1079:ERHIAG\]2.0.CO;2](https://doi.org/10.1130/0016-7606(1971)82[1079:ERHIAG]2.0.CO;2), 1971.
- Ramsey, L. A., Walker, R. T. and Jackson, J.: Fold evolution and drainage development in the Zagros mountains of Fars province, SE Iran, *Basin Res.*, 20(1), 23–48, <https://doi.org/10.1111/j.1365-2117.2007.00342.x>, 2008.
- Refice, A., Giachetta, E. and Capolongo, D.: SIGNUM: A Matlab, TIN-based landscape evolution model, *Comput. Geosci.*, 45, 293–303, <https://doi.org/10.1016/j.cageo.2011.11.013>, 2012.

- Regard, V., Lagnous, R., Espurt, N., Darrozes, J., Baby, P., Roddaz, M., Calderon, Y. and Hermoza, W.: Geomorphic evidence for recent uplift of the Fitzcarrald Arch (Peru): A response to the Nazca Ridge subduction, *Geomorphology*, 107(3–4), 107–117, <https://doi.org/10.1016/j.geomorph.2008.12.003>, 2009.
- Reilinger, R., McClusky, S., Vernant, P., Lawrence, S., Ergintav, S., Cakmak, R., Ozener, H., Kadirov, F., Guliev, I., Stepanyan, R., Nadariya, M., Hahubia, G., Mahmoud, S., Sakr, K., ArRajehi, A., Paradissis, D., Al-Aydrus, A., Prilepin, M., Guseva, T., Evren, E., Dmitrova, A., Filikov, S. V., Gomez, F., Al-Ghazzi, R. and Karam, G.: GPS constraints on continental deformation in the Africa-Arabia-Eurasia continental collision zone and implications for the dynamics of plate interactions, *J. Geophys. Res. Solid Earth*, 111(5), 1–26, <https://doi.org/10.1029/2005JB004051>, 2006.
- Salles, T. and Hardiman, L.: Badlands: An open-source, flexible and parallel framework to study landscape dynamics, *Comput. Geosci.*, 91, 77–89, <https://doi.org/10.1016/j.cageo.2016.03.011>, 2016.
- Sepehr, M., Cosgrove, J. and Moieni, M.: The impact of cover rock rheology on the style of folding in the Zagros fold-thrust belt, *Tectonophysics*, 427(1–4), 265–281, <https://doi.org/10.1016/j.tecto.2006.05.021>, 2006.
- Sherkati, S., Letouzey, J. and De Lamotte, D. F.: Central Zagros fold-thrust belt (Iran): New insights from seismic data, field observation, and sandbox modeling, *Tectonics*, 25(4), 1–27, <https://doi.org/10.1029/2004TC001766>, 2006.
- Sissakian, V. K.: Geological Map of Arbel and Mahabad Quadrangles Sheets NJ-38- 14 and NJ-38-15, Scale 1:250.000, 1997.
- Sklar, L. and Dietrich, W. E.: River Longitudinal Profiles and Bedrock Incision Models: Stream Power and the Influence of Sediment Supply, in *Rivers Over Rock: Fluvial Processes in Bedrock Channels*, edited by K. J. Tinkler and E. E. Wohl, pp. 237–260, American Geophysical Union., 1998. <https://doi.org/10.1029/GM107p0237>, 1998.
- Stockhecke, M., Timmermann, A., Kipfer, R., Haug, G., Kwiecien, O., Friedrich, T., Menviel, L., Litt, T., Pickarski, N., Anselmetti, F. S.: Millennial to orbital-scale variations of drought intensity in the eastern Mediterranean, *Quaternary Science Reviews*, 133, 77–95. <https://doi.org/10.1016/j.quascirev.2015.12.016>, 2016.
- Strahler, A.: Hypsometric (Area-Altitude) Analysis of Erosional Topography, *GSA Bull.*, 63(11), 1117–1142, [https://doi.org/10.1130/0016-7606\(1952\)63\[1117:HAAOET\]2.0.CO;2](https://doi.org/10.1130/0016-7606(1952)63[1117:HAAOET]2.0.CO;2), 1952.
- Syan, S. H. A.: Tectonic Criteria from Shortening Estimation in different geological time and space using Balancing Cross Sections in the Harir and Khatibian Anticlines, Zagros Fold-Thrust Belt, Kurdistan of Iraq, MSc. Thesis, Salahaddin University-Erbil., 2014.
- Tarolli, P.: High-resolution topography for understanding Earth surface processes: Opportunities and challenges, *Geomorphology*, 216, 295–312, <https://doi.org/10.1016/j.geomorph.2014.03.008>, 2014.
- Temme, A. J. A. M., Armitage, J., Attal, M., van Gorp, W., Coulthard, T. J. and Schoorl, J. M.: Developing, choosing and using landscape evolution models to inform field-based landscape reconstruction studies, *Earth Surf. Process. Landforms*, 42(13), 2167–2183, <https://doi.org/10.1002/esp.4162>, 2017.

[Tozer, R., Hertle, M., Petersen, H. I. and Zinck-Joergensen, K.: Quantifying vertical movements in fold and thrust belts: subsidence uplift and erosion in Kurdistan Northern Iraq, Geological Society, London, Special Publications 490 https://doi.org/10.1144/SP490-2019-118, 2019.](https://doi.org/10.1144/SP490-2019-118)

- 5 Tucker, G. E. and Bras, R. L.: Hillslope processes, drainage density, and landscape morphology, *Water Resour. Res.*, 34(10), 2751–2764, <https://doi.org/10.1029/98WR01474>, 1998.
- Tucker, G. E. and Hancock, G. R.: Modelling landscape evolution, *Earth Surf. Process. Landforms*, 35(1), 28–50, <https://doi.org/10.1002/esp.1952>, 2010.
- Tucker, G., Lancaster, S., Gasparini, N., and Bras, R.: The channel hillslope integrated landscape development model (CHILD), in: *Landscape erosion and evolution modeling*, edited by: Harmon, R. S. and Doe III, W. W., 349–388, Kluwer Academic/Plenum Publishers, New York, USA, 2001.
- 10 Tucker, G. E., Hobbey, D. E. J., Hutton, E., Gasparini, N. M., Istanbuluoglu, E., Adams, J. M. and Siddartha Nudurupati, S.: CellLab-CTS 2015: Continuous-time stochastic cellular automaton modeling using Landlab, *Geosci. Model Dev.*, 9(2), 823–839, <https://doi.org/10.5194/gmd-9-823-2016>, 2016.
- Vergés, J., Saura, E., Casciello, E., Fernández, M., Villaseñor, A., Jiménez-Munt, I. and García-Castellanos, D.: Crustal-scale cross-sections across the NW Zagros belt: Implications for the Arabian margin reconstruction, *Geol. Mag.*, 148(5–6), 739–761, <https://doi.org/10.1017/S0016756811000331>, 2011.
- Vernant, P., Nilforoushan, F., Hatzfeld, D., Abbassi, M. R., Vigny, C., Masson, F., Nankali, H., Martinod, J., Ashtiani, A., Bayer, R., Tavakoli, F. and Chéry, J.: Present-day crustal deformation and plate kinematics in the Middle East constrained by GPS measurements in Iran and northern Oman, *Geophys. J. Int.*, 157(1), 381–398, <https://doi.org/10.1111/j.1365246X.2004.02222.x>, 2004.
- 20 Whipple, K. X.: Implications of sediment-flux-dependent river incision models for landscape evolution, *J. Geophys. Res.*, 107(B2), 2039, <https://doi.org/10.1029/2000JB000044>, 2002.
- Whipple, K. X. and Tucker, G. E.: Dynamics of the stream-power river incision model: Implications for height limits of mountain ranges, landscape response timescales, and research needs, *J. Geophys. Res. Solid Earth*, 104(B8), 17661–17674, <https://doi.org/10.1029/1999JB900120>, 1999.
- 25 Whittaker, A. C.: How do landscapes record tectonics and climate? *Lithosphere*, 4(2), 160–164, <https://doi.org/10.1130/RF.L003.1>, 2012.
- Wobus, C., Whipple, K. X., Kirby, E., Snyder, N., Johnson, J., Spyropolou, K., Crosby, B. and Sheehan, D.: Tectonics from topography: procedures, promise, and pitfalls, *Geol. Soc. Am. Spec. Pap.*, 398(04), 55–74, [https://doi.org/10.1130/2006.2398\(04\)](https://doi.org/10.1130/2006.2398(04)), 2006.
- 30 Zebari, M.: *Geometry and Evolution of Fold Structures within the High Folded Zone: Zagros Fold-Thrust Belt, Kurdistan Region-Iraq*, University of Nebraska-Lincoln., 2013.
- Zebari, M. M. and Burberry, C. M.: 4-D evolution of anticlines and implications for hydrocarbon exploration within the Zagros Fold- Thrust Belt, Kurdistan Region, Iraq, *GeoArabia*, 20(1), 161–188, 2015.

Figures



5

Figure 1: Tectonic subdivision of the NW segment of the Zagros Fold-Thrust Belt (modified after Berberian, 1995; Emre et al., 2013; Koshnaw et al., 2017; Zebari and Burberry, 2015). Names within the parentheses are known in the Iranian part of Zagros.

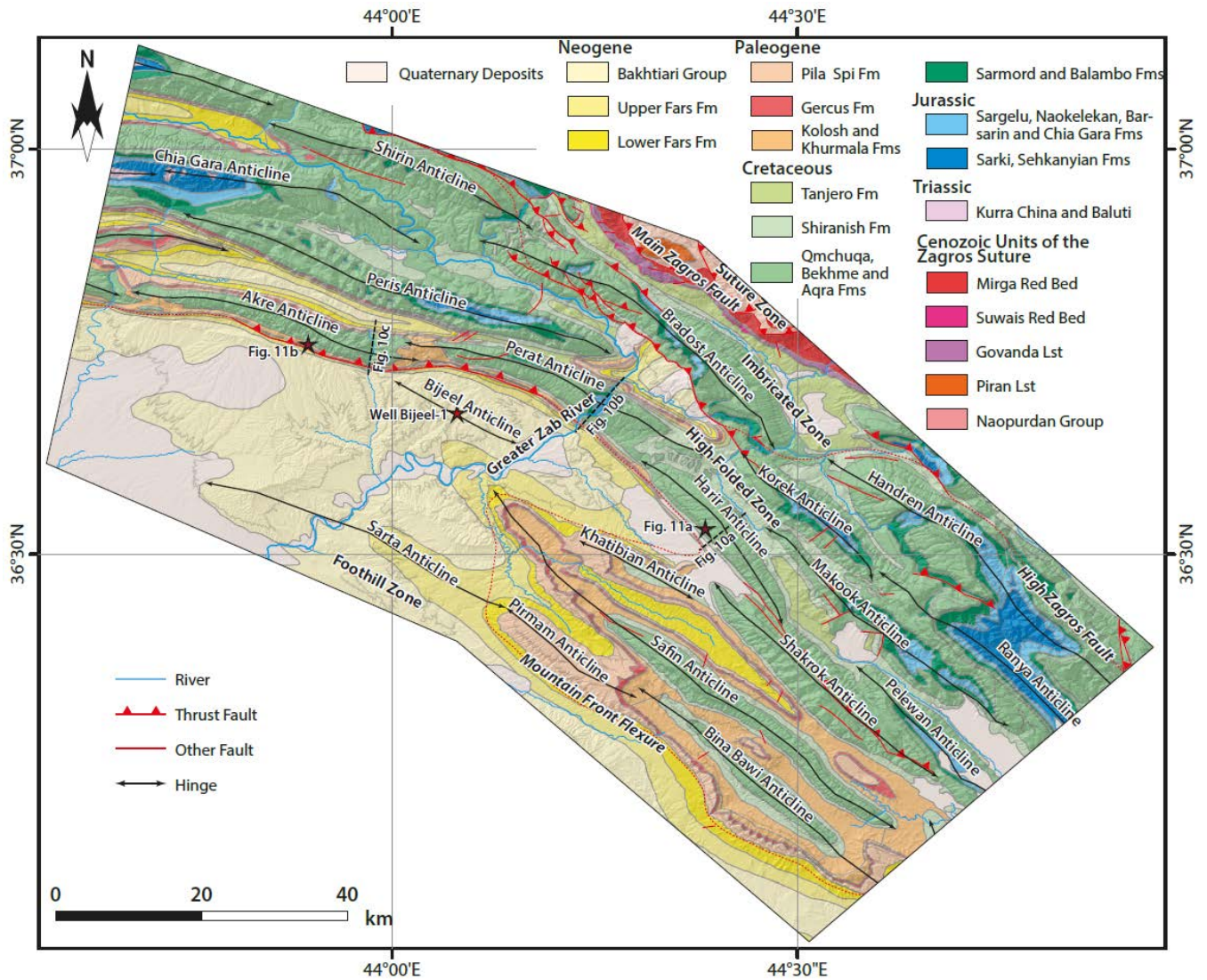


Figure 2: Geological map of the Zagros Belt in KRI showing the location of the three anticlines Harir, Perat, and Akre with respect to the MFF that separates the High Folded Zone from the Foothill Zone (modified after Csontos et al., 2012; Sissakian, 1997; Zebari and Burberry, 2015).

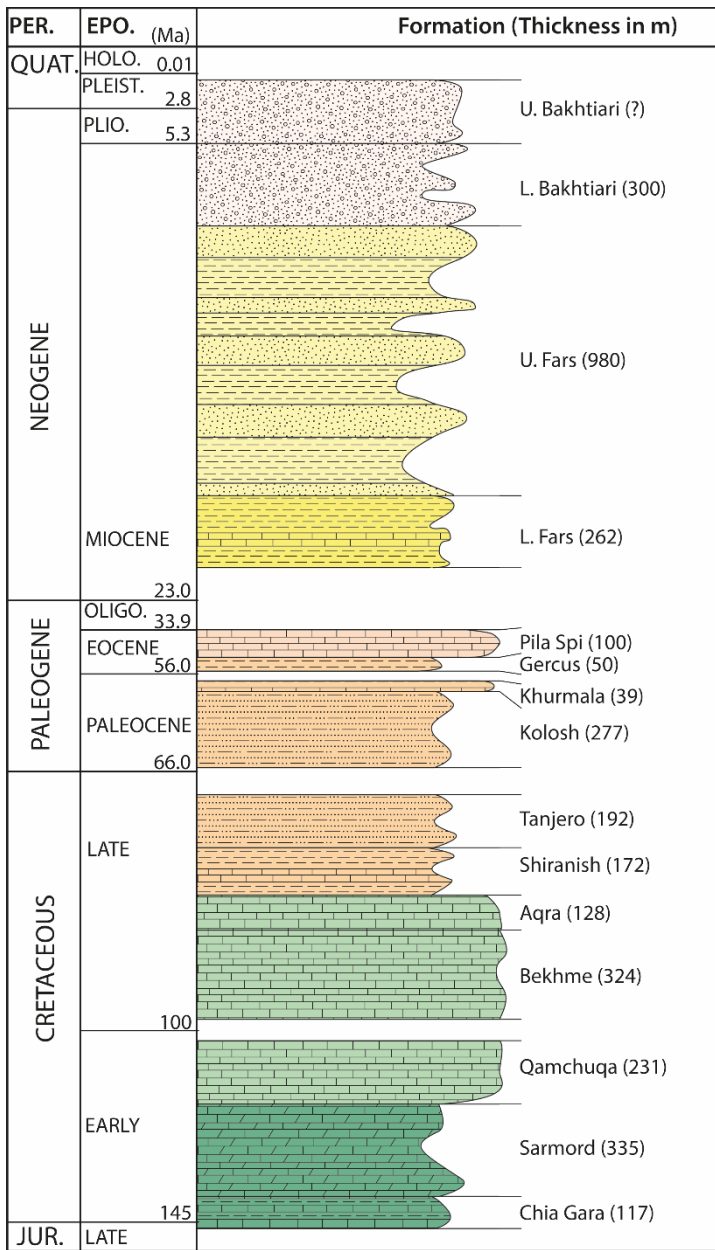


Figure 3: Stratigraphic column of the exposed rock units in the area. Thicknesses are given as in well Bijeel-1 (Fig. 2), which is located 5 km to the south of Perat Anticline (modified after Law et al., 2014). The column is scaled to the stratigraphic thicknesses.

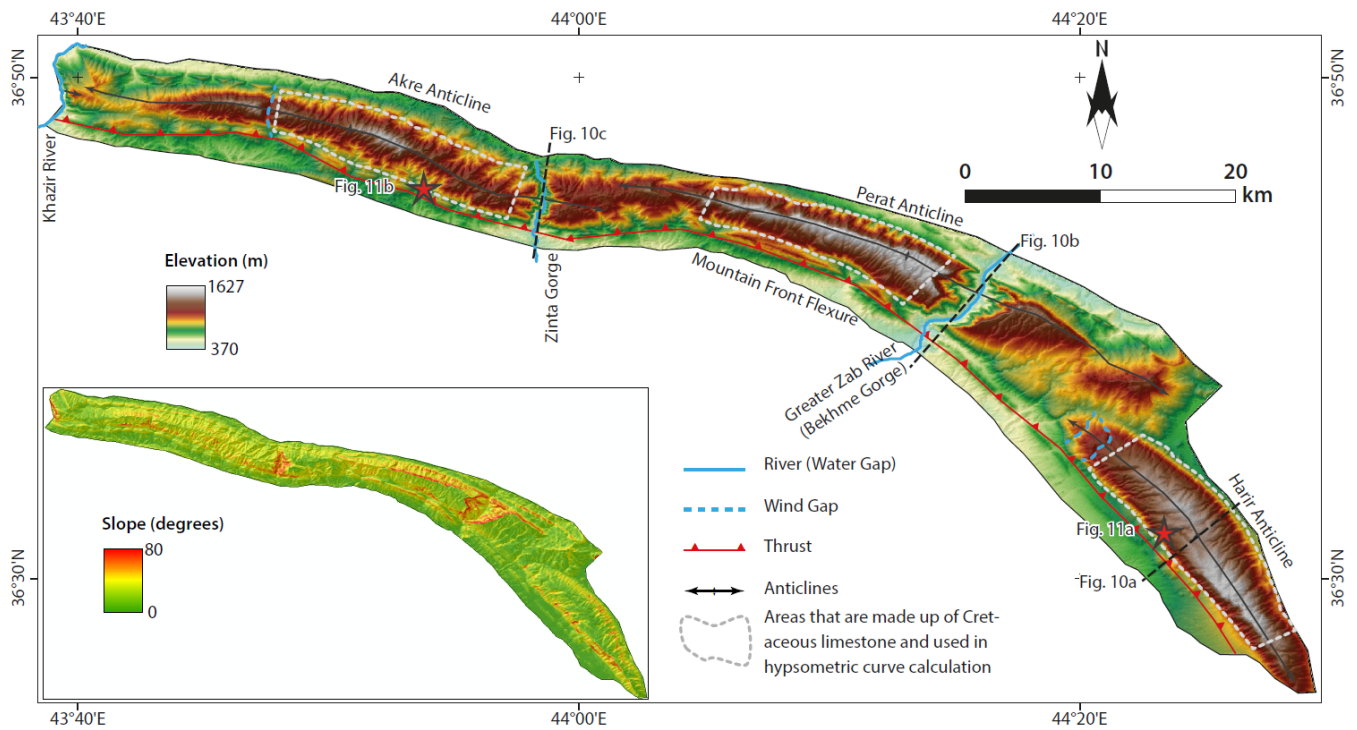


Figure 4: Topography and slope maps of the studied anticlines obtained from 30 m resolution SRTM1 DEM data showing the location of water and wind gaps across these anticlines.

5

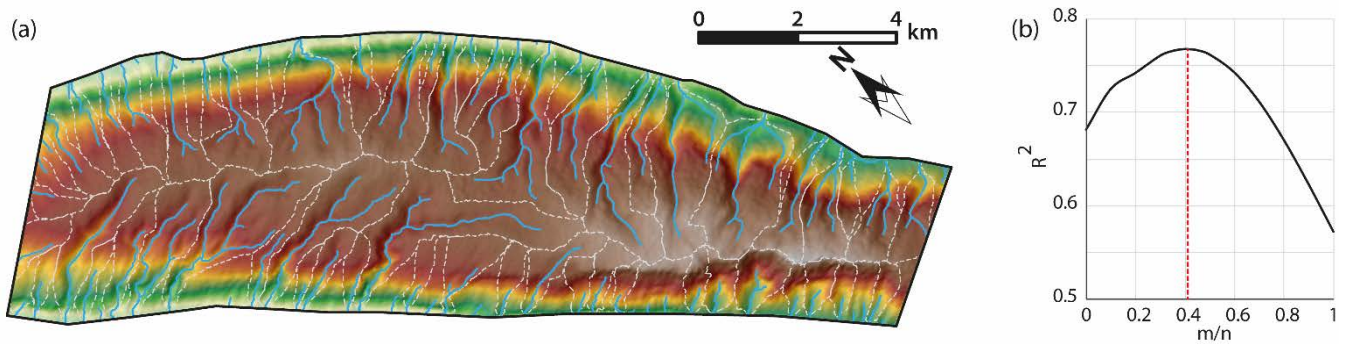


Figure 5: a) DEM grid, drainage network and basins for the present-day Harir Anticline that is used as an input for the model. White lines are basin divides; b) m/n plotted against regression values of elevation-X plot for streams in the Harir Anticline. The highest regression is achieved for $m/n = 0.41$.

10

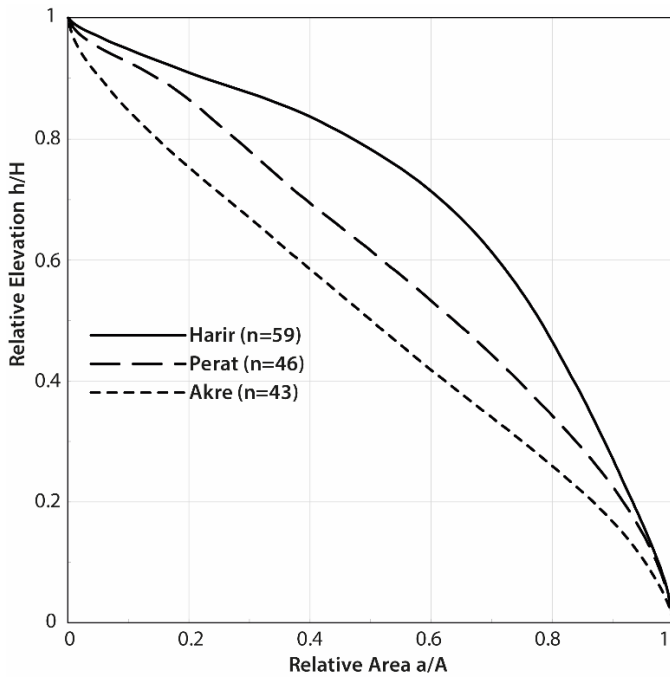


Figure 6: Present-day hypsometric curves of the studied anticlines. The curves are calculated as a total weighted mean for drainage basins within each anticline. We only use those parts where Upper Cretaceous carbonate rocks crop out and we exclude wind gaps, water gaps, and the plunging tips of anticlines. n is the number of basins used in calculation of the hypsometric curve for each anticline.

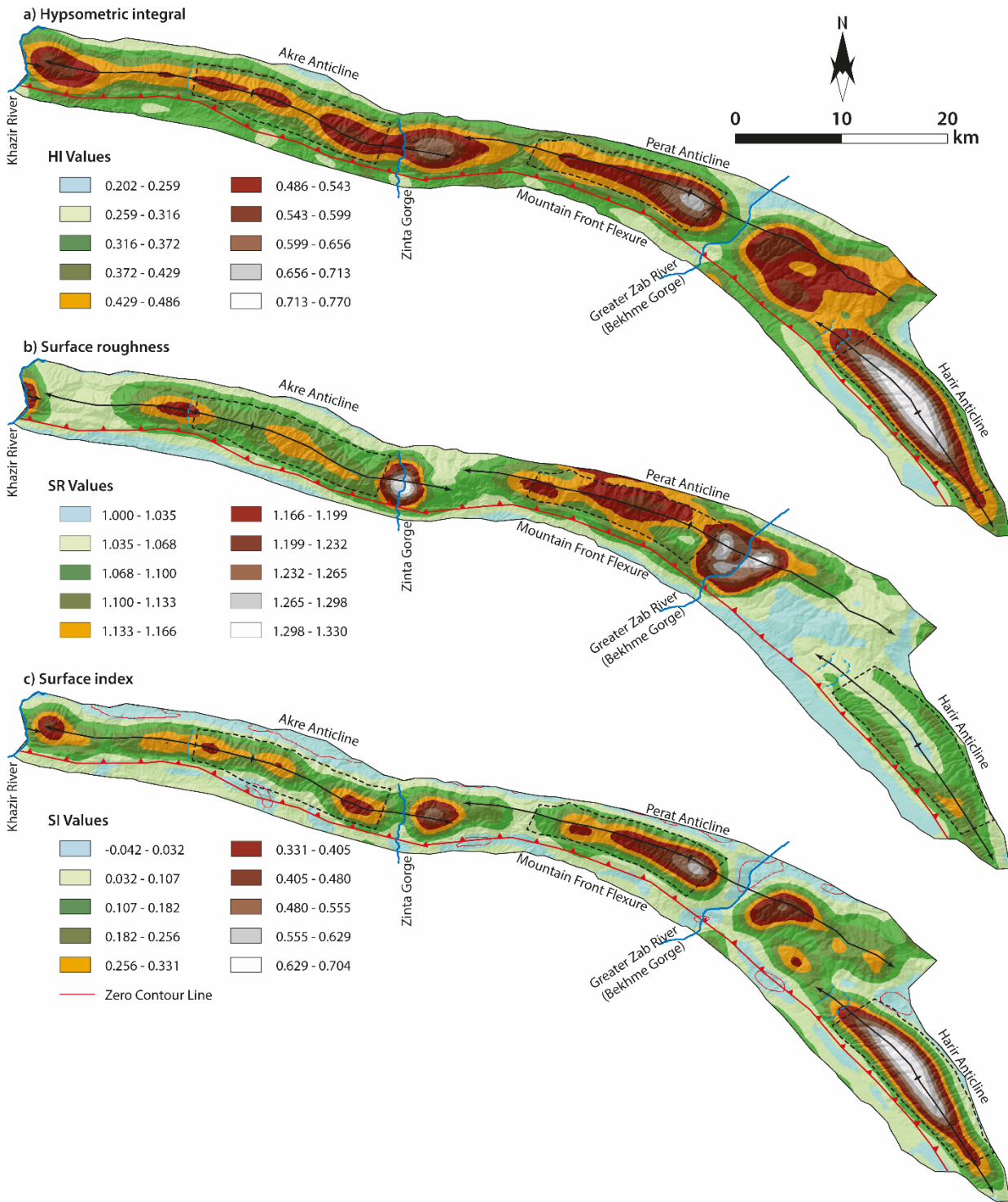


Figure 7: Surface index maps for the three anticlines calculated from 100 * 100 cell (3 * 3 km) and moving windows; a) hypsometric integral, b) surface roughness, and c) surface index.

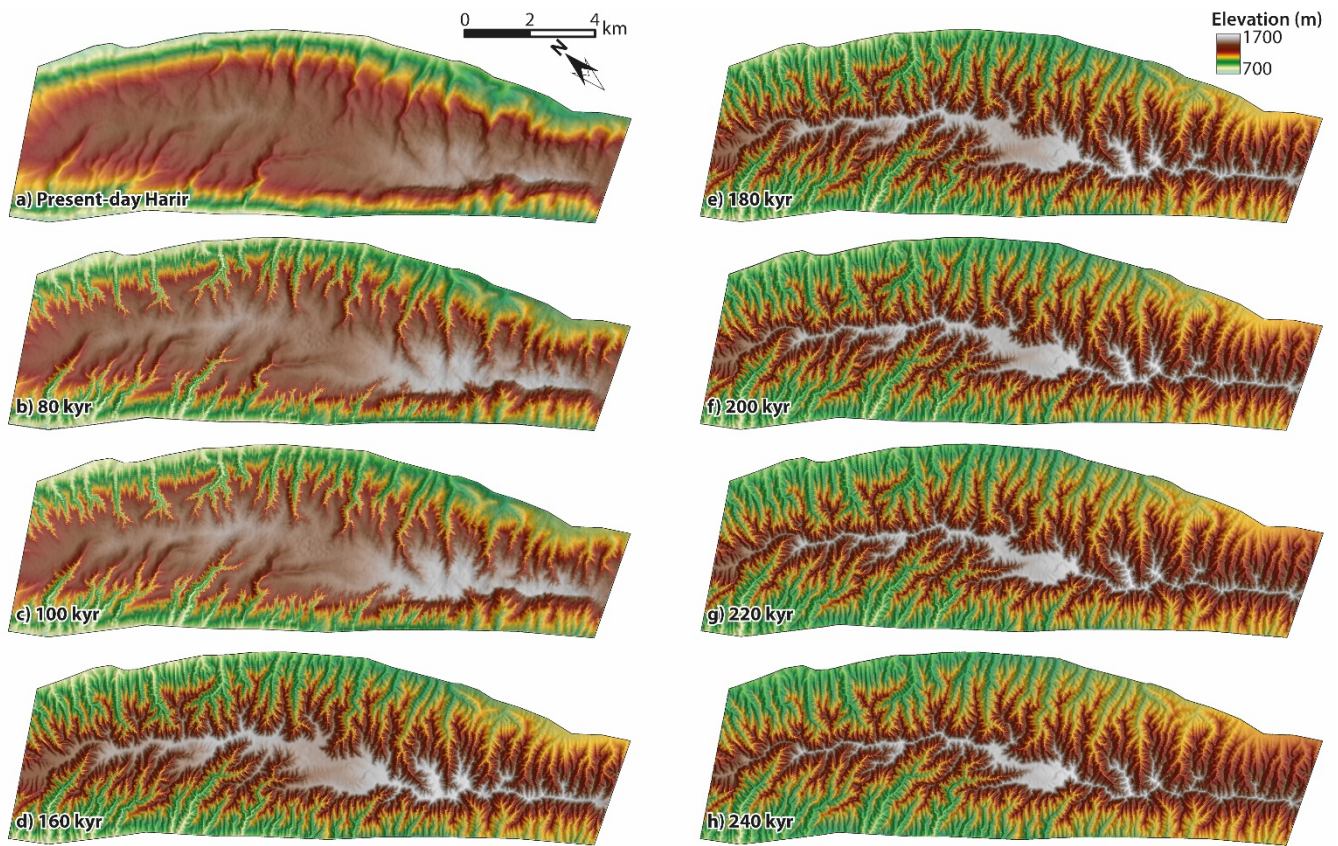
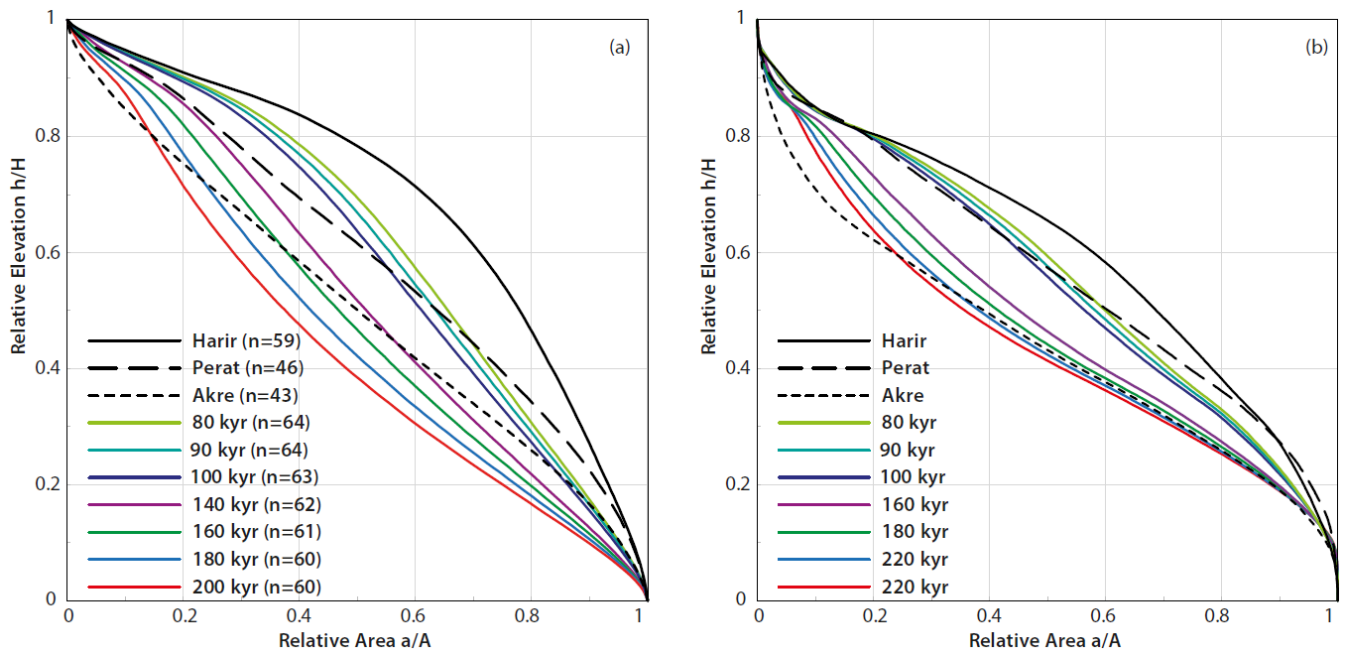


Figure 8: The input landscape (a), which is the present-day Harir topography, and the evolved landscape through time; b) 80 kyr,
 5 c) 100 kyr, d) 160 kyr, e) 180 kyr, f) 200 kyr, g) 220 kyr, and h) 240 kyr.



5 **Figure 9: Hypsometric curves of the studied anticlines and those of the evolved Harir landscape from the model for different time spans. a) The curves were calculated using the total weighted mean for drainage basin within each anticline, indicating that the evolved landscapes after 100 and 160 are the closest ones to the present-day Perat and Akre anticlines, respectively. n is the number of basins used in calculation of the hypsometric curve for each time; b) the curves were calculated for the entire anticline, indicating that the evolved landscapes after 80 and 200 are the closest ones to the present-day Perat and Akre anticlines, respectively.**

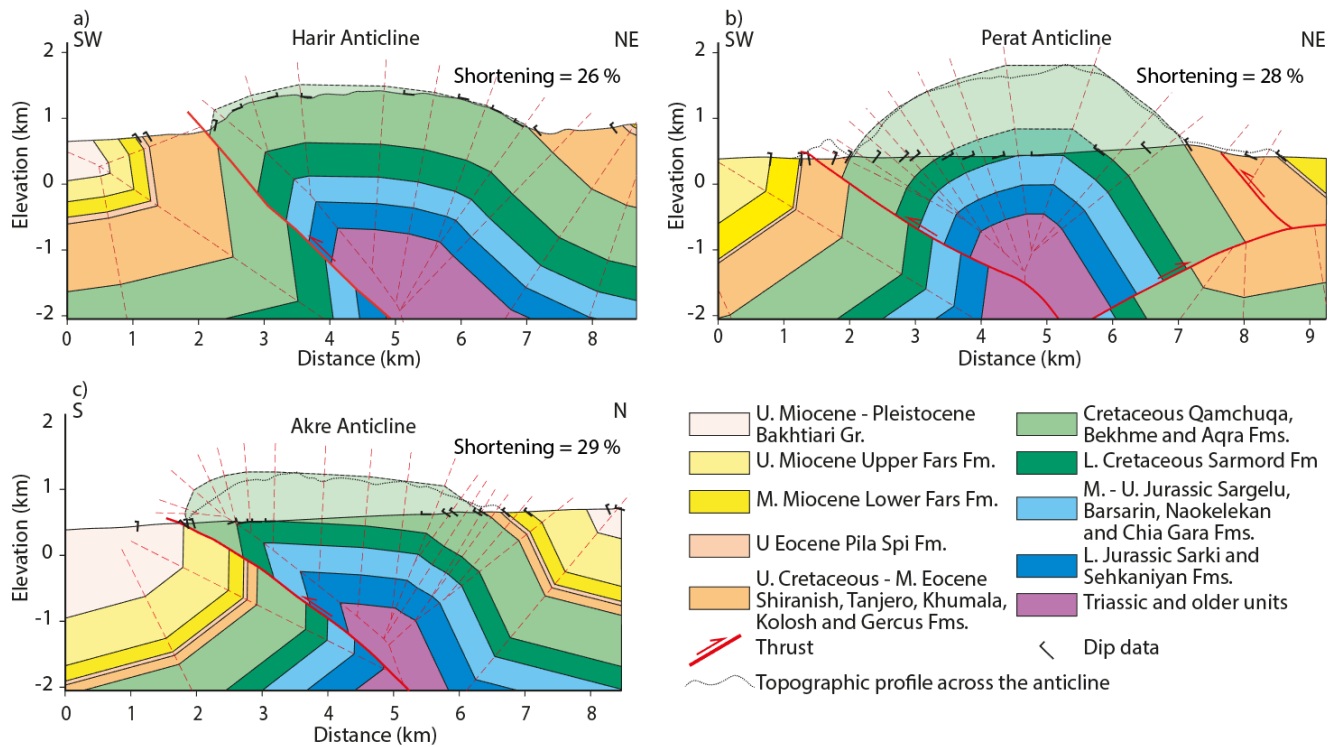


Figure 10: Structural cross-section across the three studied anticlines; a) Harir section (modified after Syan, 2014), b) Perat section constructed from field data and thrusts inferred from a seismic line by Csontos et al. (2012), c) Akre section constructed from field data (see Figure 2 and 4 for the locations). In Akre and Perat anticlines the data were collected along gorges and the topographic profile across the anticline along an adjacent transect to the gorges are delineated by a dotted line. The shortening percentage since Late Miocene is shown on each cross-section.



10 Figure 11: Different shape of valleys in the Harir (a) and Akre anticlines (b). See Figures 2 and 4 for the locations.

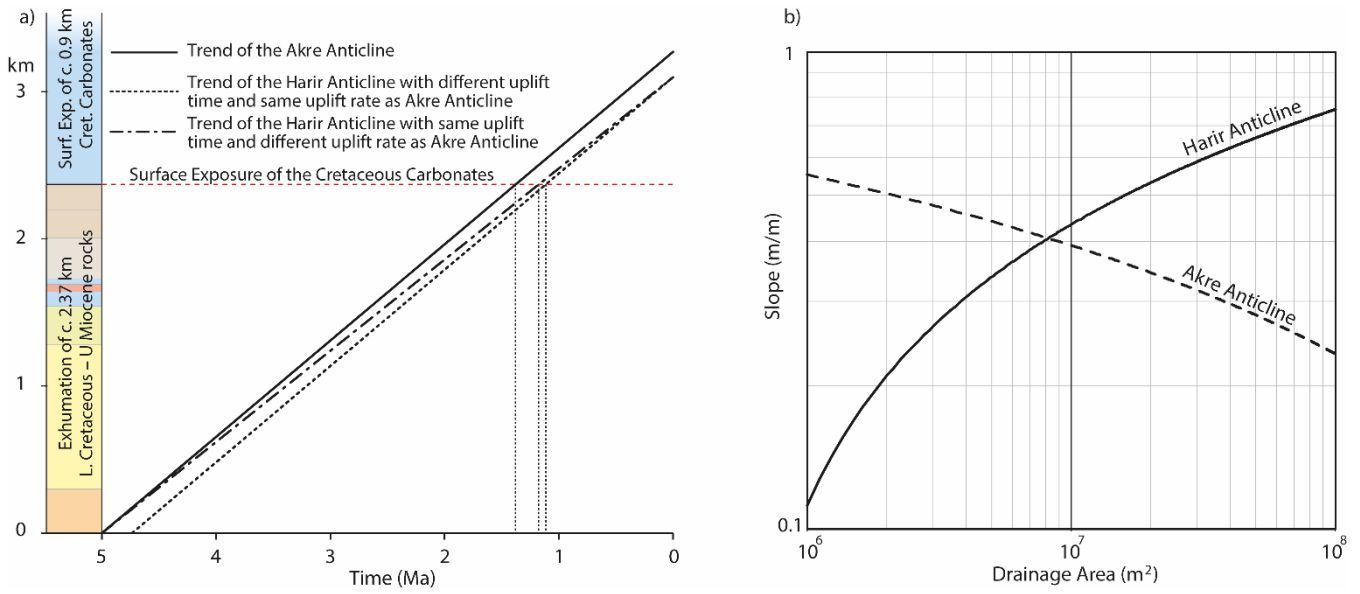


Figure 12: a) Diagram showing the exposure time of the Upper Cretaceous carbonates in Akre and Harir Anticlines. Two different scenarios are plotted for Harir: Having a slower uplift rate than Akre, or onset of uplift later than Akre. b) Channel slope-drainage area plots for streams in both Akre and Harir Anticlines.

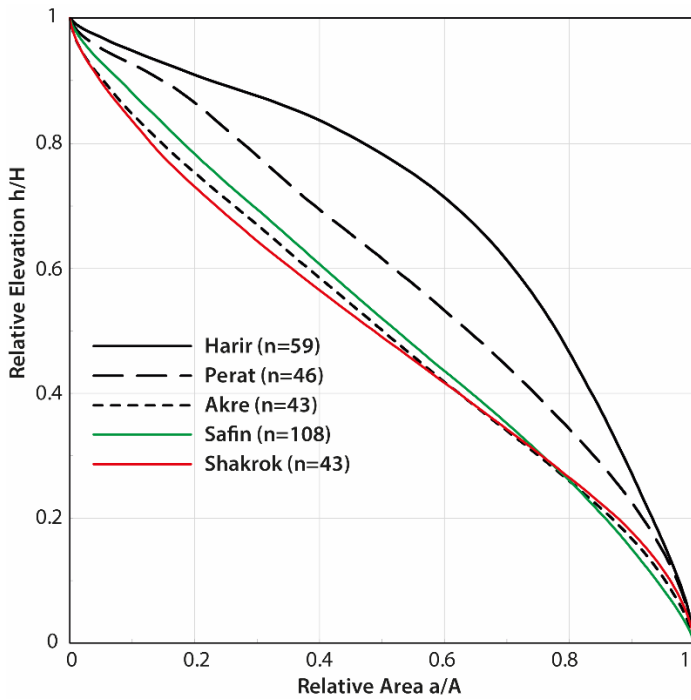


Figure 13: Total weighted mean hypsometric curves for drainage basin within the studied anticlines as compared to those of the Shakrok and Safin anticlines. The Harir's curve is more convex than that of both Shakrok and Safin. n is the number of basins used in calculation of the hypsometric curve for each anticline.

5

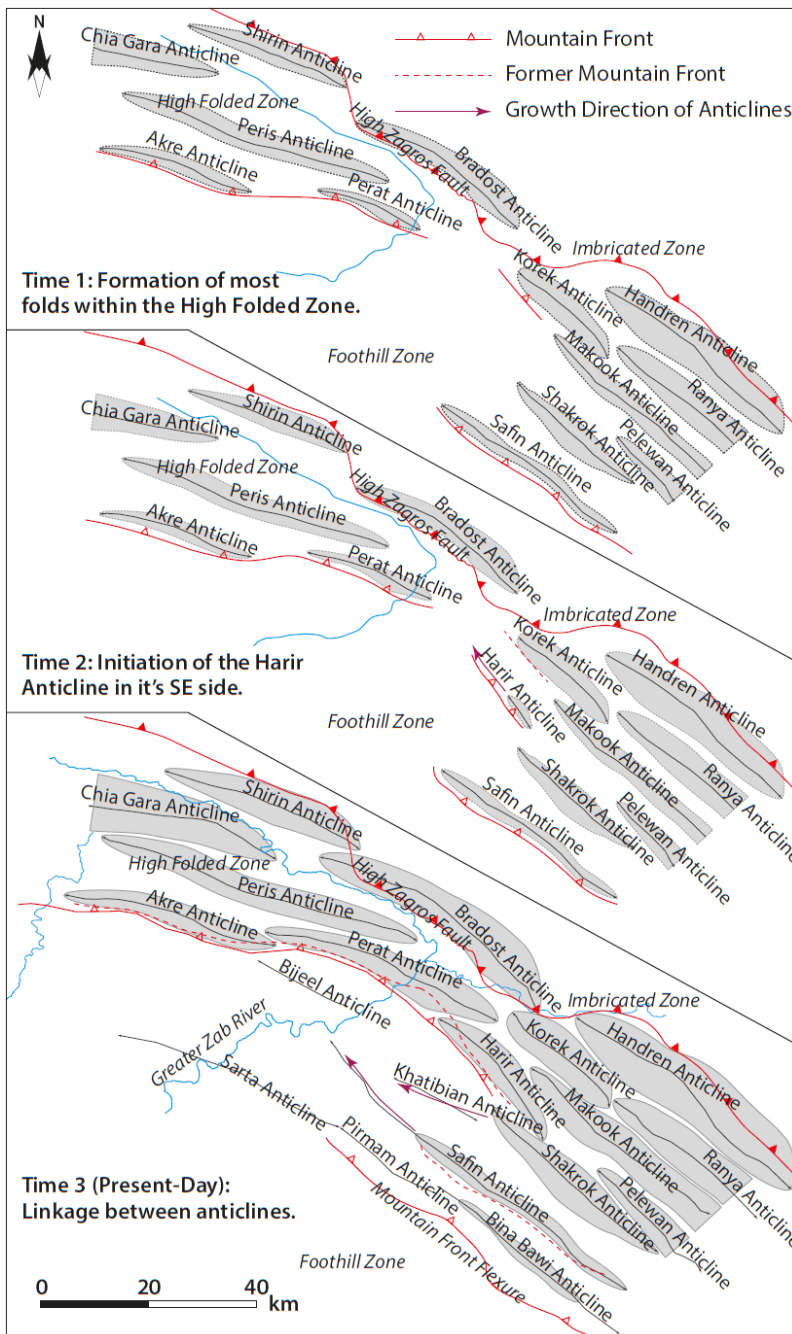


Figure 15: Simplified history of the formation of anticlines during the propagation of the deformation front over time in the study area. The Harir anticline is likely the latest to have formed within the High Folded Zone in its SE end. It occupies the position of a relay structure during the linkage of two adjacent, but overlapping segments of the deformation front. The anticlines were outlined based on the exposure of Cretaceous carbonates.

Response to the Anonymous Referee #1_v2's Interactive comment on **“Relative Timing of Uplift along the Zagros Mountain Front Flexure Constrained by Geomorphic Indices and Landscape Modelling, Kurdistan Region of Iraq”**

by Zebari et al. The responses are given in *“Italic”* font style.

Anonymous Referee #1_v2

Submitted: 27 March 2019

The authors have fully considered my previous suggestions, and the revised manuscript has been greatly improved. Very few comments/suggestions are listed as follows.

1. from page 11, line 30 to page 12, line 7, and lines 23-30, these sentences seem like discussion.

Authors: The mentioned pages and lines above are located within the result section. Here we tried to give information about the presented results and explain where the results of landscape modelling came from.

2. page 32, three separate figures marked by a, b, c are encouraged, similar to the following figures.

Authors: Appreciate it.

3. page 33, two figures are displayed. BTW, how to identify wind and water gaps? DEM-based ridge lines of the anticlines may help to clarify.

Authors: The first one is already removed but it remained there due to tracking changes. The water gaps are identified wherever an anticline is crossed by a stream; whereas, the wind gaps are identified wherever an anticline is crossed by a dry valley (abandoned river). The valley is above the base of the anticline and formed when the anticline uplift was higher than the erosional cut down of the river, therefore the river deviates around the tip of anticline and leave an abandoned valley crossing the anticline. We identified the wind gaps and water gaps on the DEMs and in the field.

4. page 39, check the fig. 9 again. Find better places for annotating the (a) and (b).

Authors: Done.

5. page 44-45, which is figure 14 in revised version. No fig. 15 mentioned in the text.

Authors: The one in page 45 is figure 14. The figure in the page 44 is already removed but it remained there due to tracking changes. This problem is resolved in the last revised version.

Response to the Anonymous Referee #3's Interactive comment on **“Relative Timing of Uplift along the Zagros Mountain Front Flexure Constrained by Geomorphic Indices and Landscape Modelling, Kurdistan Region of Iraq”**

by Zebari et al. The responses are given in *“Italic”* font style.

Referee #3 Bernard Delcaillau

Submitted: 21 March 2019

We appreciate the reviewer for his thoughtful comment on the manuscript. We have considered these comments carefully and we respond to the comments with taking the following points into consideration:

1. The reviewer has commented on the initial version of the manuscript (submitted on 28.11.2018) before the first round of revision, therefore, some of the comments are not relevant to the revised manuscript (submitted on 13.03.2019). Some other comments have already been taken into consideration based on the comments of the first two reviewers.
2. Some of the comments either request for another way of identifying the landscape maturity, which yields similar results to those of our approach, or they are not applicable to our work due to limitation of approaches to overcome these shortages, or they are not necessary based on our observation. We provide clear explanation/reasoning for this type of comments in our responses below.
3. We carefully considered the remaining relevant comments and made relevant changes to the manuscript.

General comments:

1) In my opinion, it would be useful the index Normalized channel steepness index (K_{sn}) which determines the relative gradient of channels. In this work does not appear the slope map also essential.

Authors: We have tested many other indices including normalized channel steepness index (K_{sn}), which is presented in the figure below, stream power index, and stream length-gradient index. All of them show almost the same results in aspect of the relative maturity between the three anticlines. The indices show that Harir is less mature and Akre is more mature. Therefore, we rely on the indices that are already presented in the manuscript. However, a slope map is added to the Figure 4, Page 27.

The normalized channel steepness index (K_{sn}) is calculated as (Wobus et al., 2006):

$$K_{sn} = \frac{S}{A^{-\theta}}$$

Where S is the local channel slope [m/m], A is the upstream drainage area [m^2] and is typically taken as a proxy for discharge, and θ is the channel concavity.

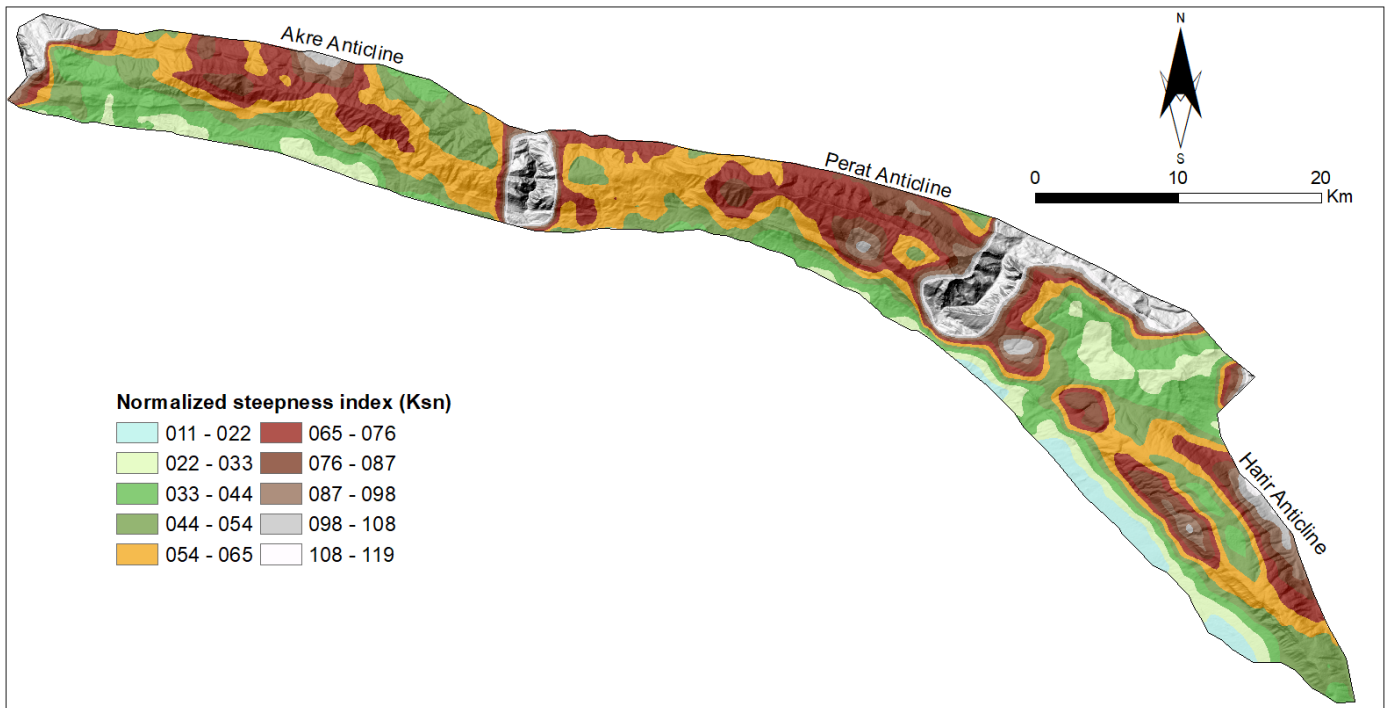


Figure: Normalized steepness index (Ksn) for streams in the studied anticlines. It shows that Ksn is low in the crest and higher in the flank of the Harir Anticline, while it is lower in the flanks and increase toward the crest in both Akre and Perat anticlines. Ksn around main rivers that cross the anticlines was not calculated to exclude their effect in analysis.

2) The concept of maturity of landscape is to be redefined more precisely according to poorly presented criteria in the manuscript.

Authors: In this manuscript we tried to asses relative maturity between the studied anticlines and make a comparison between them using the geomorphic criteria that are widely used in many other similar studies. As we explained in the comment no. 1, we obtained the same results in aspect of relative maturity between the three anticlines from most of the indices that are used for defining the landscape maturity. The relative maturity of the anticlines is clearly explained in the revised version based on the comments by previous reviewers.

3) The use of the only equations for fluvial erosion and diffusion processes for landscape evolution modelling may be too simplistic. Parameters concerning erosion processes are lacking in the modelling of landscape evolution.

Authors: The reason behind using only equations for fluvial erosion and diffusion processes and uplift in the model is explained explicitly in Section 3.3, Page 8, Lines 5-9. Chen et al. (2014) showed that consideration of only these two components is sufficient for many landscapes, but cannot model fluvial sedimentation. From field observations and from satellite imagery, we infer that no significant fluvial sedimentation takes place on the slopes of the analyzed anticlines. On slopes of anticline flanks, the detachment-limited erosion due to the fluvial system tends to be the dominant process (Howard, 1994). To detect changes in the landscape due to fluvial erosion through time, we applied the commonly accepted idea that the rate of stream incision is directly proportional to the hydraulic shear stress of a stream (Braun and Willett, 2013). Consequently, we used the stream power incision law (Sklar and Dietrich, 1998; Whipple and Tucker, 1999). To account for the provision of sediment due to hillslope diffusion processes from slopes outside the river system, we used the hillslope diffusion equation (Culling, 1963; Tucker and Bras, 1998). Finally, the uplift rate is accounted for as well, as it is subtracted by the changes due to both fluvial erosion and hillslope diffusion. Only these two components were used in most of the studies that relate the landscape evolution with

underlying tectonics (e. g. Braun and Sambridge, 1997; Collignon et al., 2016; Cowie et al., 2006; Koons, 1995; Maniatis et al., 2009; Miller et al., 2007; Refice et al., 2012; Yanites et al., 2017; and others). Therefore, we think that applying only these components does not affect the validity of our landscape evolution model. Besides, it makes our study easily comparable with similar studies elsewhere. Since the three anticlines are made up of the same lithology (carbonates), there is no necessity to account for varying lithology and erodibility in our model.

Regarding the parameter used in the model, some of them are obtained directly from the present-day topography of the input, e.g. power-law coefficients m/n . Others were obtained from the literature on areas that are comparable with our study area in the aspects of lithology and precipitation, because there are no in situ denudation data that are necessary for obtaining parameters like the erodibility coefficient K for our model. Actually, if the in situ comprehensive erosional data were available for streams in the flank of these anticlines, there was no need for landscape evolution modeling. We could use them directly to measure the time difference between the maturity (erosion state) of the studied anticlines.

4) The relationship between the hydrographic network and the growth of active anticlines is insufficient. It lacks a more serious morphometric study (for example: geometry of the profiles along the rivers, measurement of recent denudation rates at the outlet of catchment draining basins by the cosmogenic ^{10}Be detrital sediment method).

Authors: Here we do not study the tectonic activity along specific rivers. That is why we used those indices that can quantify the whole study area. We also do not have denudation data; therefore, we used remote sensing data. However, we are well aware that the knowledge of denudation rates along rivers in that area would greatly improve our understanding of the tectonic activity (uplift) of the anticlines there, as correctly suggested by the reviewer. The measurement of denudation rates from cosmogenic ^{10}Be is beyond the scope of this study.

5) Lack of bibliographic references: in the paleoclimatological domain.

Authors: The paleoclimatological data are added in the supplementary materials and are referred in latest version of the manuscript Section 3.3, Page 9, Lines 22-24.

Response to the in-line comments on the manuscript:

Section 1, Page 2, Lines 22-23: Others references

Authors: There are many references on the topic, but here we cited only few of them for keeping it short.

Section 3.1, Page 5, Line 27: This degree...

Authors: We used the terms “proxies” and “relative” here along with using the indices for assessing the landscape maturity. Thereby we already left possibility for some uncertainties.

Section 3.1.3, Page 6, Lines 18: (e.g. Hobson, 1972)

Authors: We added the reference.

Section 3.2, Page 7, Line 18: !!!!

Authors: rephrased.

Section 3.2, Page 9, Line 11: very low uplift rate that you consider to be linear in time !!!!

Authors: There maybe misunderstanding about the used unit which is meter per year not millimeter per year. The uplift rate of 0.0007 m/yr or 0.7 mm/yr is a reasonable rate for the area and it matches with the vertical uplift in Kurdistan that has been presented by Tozer et al. (2019).

Section 4.1, Page 11, Lines 1-8: The structure of fold-faults varies laterally and not homogeneously. The Perat anticline is a pop-up structure whereas the Harir and Akre anticlines are fault-propagation folds. In total, the eroded volumes are not the same: the lower Cretaceous dissected on the anticlinal hinge of Akre (strong erosion) differs from Harir anticline where the Cretaceous is little eroded.

Authors: As we presented, the geometry of these anticlines varies laterally, but the shortening across, and vertical uplift along these anticlines does not vary significantly. The uplifted amount here is proportional to the shortening, which does not vary too much laterally. We calculated and added the shortening on Figure 10 to clarify this. The dissected amount of the Cretaceous carbonates is reflected by the landscape maturity. These carbonates are more dissected in the Akre anticline than in the other ones.

Regarding the eroded volume, both cross-sections across the Akre and Perat anticlines were constructed along Zinta and Bekhme gorges, respectively. Thus, the topographic profile cannot be used to estimate the eroded volume. Instead, we have plotted the topographic profiles across these two anticlines (dotted black line; Figure 10, Page 32) from nearby transects across the anticlines where topography is not affected by major rivers.

Section 4.2, Page 11, Lines 23-26: In the study of the recent deformation of the Folded zone of the Zagros Mts, the assumption of constant rock uplift and erosion seems too simplistic.

Authors: The relevant paragraph has been modified in the revised manuscript. We have used this assumption for the sake of simplicity and due to the lack of available data.

Section 5.2, Page 12, Line 20: What are your arguments? references?

Authors: Here we mean spatial variation in climate between these anticlines, which are located within the same climate zone. In such a local scale (less than 100 km), the climate (precipitation) does not vary significantly.

Section 5.2, Page 12, Line 23: What are your arguments?

Authors: the argument behind this sentence is explained by Andreani et al., (2014) and Andreani and Gloaguen (2016) as cited.

Section 5.2, Page 13, Lines 19-20: !!!

Authors: Rephrased; we mean the exposure of the Cretaceous carbonates in the Harir Anticline was later than in the Akre Anticline.

Section 5.2, Page 13, Lines 29-32: too simplistic

Authors: The paragraph is already rephrased in the newer version of the manuscript. We refer to the climate data that show that there was not much variation in precipitation in the last 300 kyr ago, which is the upper limit of our model. Regarding the absence of consideration for both rock fall and karstification, these are the limitations of the most landscape evolution model studies today (as it is explained in general comment no. 3 and references therein, which lack consideration for rock fall and karstification). Also, we explained that karstification does not have a significant impact on the landscape based on the field observations and remote sensing data (lack of caves, dolines, karren, etc.).

Section 5.3, Page 14, Lines 21-26: unclear

Authors: Rephrased.

Figure 4, Page 24: Indicate the shortening rates of the three folds

Authors: The shortening of each anticline is calculated and added to the corresponding cross sections in Figure 10.

Figure 12, Page 32: A systematic morphometric study (statistical computation) on all valleys using the same variables (elevation ...) was more relevant than the use of two insignificant examples. Why not use other parameters: longitudinal profiles of streams intersecting anticlinal flanks (knickpoints), Ksn, ...

Authors: As we explained in the main comments no. 1 and 4, here we assess the relative landscape maturity between these three anticlines in general. Based upon a variety of methods we tested, the results were very close; therefore, we think there is no need for presenting more analysis (e.g. Ksn, Topographic profiles and/or knickpoints). In the last version we even removed unnecessary swath topographic profiles based on the recommendation of a previous reviewer.

Figure 12, Page 34: blocking, Out-of-sequence.

Authors: We are mainly focusing on the tectonic geomorphology based on surface data and landscape maturity. We are afraid that including bold structural and tectonic terms in our map will require additional detailed structural reconstructions that should be justified by data at depth such as detachment levels through seismic profile interpretations, which are beyond the scope of our manuscript.

References:

Braun, J., and Sambridge, M.: Modelling landscape evolution on geological time scales: a new method based on irregular spatial discretization, *Basin Research*, 9(1), 27-52, <https://doi.org/10.1046/j.1365-2117.1997.00030.x>, 1997.

Braun, J. and Willett, S. D.: A very efficient O(n), implicit and parallel method to solve the stream power equation governing fluvial incision and landscape evolution, *Geomorphology*, 180–181, 170–179, <https://doi:10.1016/j.geomorph.2012.10.008>, 2013.

- Chen, A., Darbon, J. Ô. and Morel, J. M.: Landscape evolution models: A review of their fundamental equations, *Geomorphology*, 219, 68–86, <https://doi:10.1016/j.geomorph.2014.04.037>, 2014.
- Collignon, M., Yamato, P., Castellort, S. and Kaus, B. J. P.: Modeling of wind gap formation and development of sedimentary basins during fold growth: application to the Zagros Fold Belt, Iran, *Earth Surf. Process. Landforms*, 41(11), 1521–1535, <https://doi:10.1002/esp.3921>, 2016.
- Cowie, P. A., Attal, M., Tucker, G. E., Whittaker, A. C., Naylor, M., Ganas, A. and Roberts, G. P.: Investigating the surface process response to fault interaction and linkage using a numerical modelling approach, *Basin Res.*, 18(3), 231–266, <https://doi:10.1111/j.1365-2117.2006.00298.x>, 2006.
- Culling, W. E. H.: Soil Creep and the Development of Hillside Slopes, *J. Geol.*, 71(2), 127–161, 1963.
- Howard, A. D.: A detachment limited model of drainage basin evolution, *Water Resour. Res.*, 30(7), 2261–2285, <https://doi:10.1029/94WR00757>, 1994.
- Koons, P. O.: Modeling the topographic evolution of collisional belts, *Annual Review of Earth and Planetary Sciences*, 23(1), 375–408, <https://doi.org/10.1146/annurev.earth.23.050195.002111>, 1995.
- Maniatis, G., Kurfeß, D., Hampel, A., and Heidbach, O.: Slip acceleration on normal faults due to erosion and sedimentation—Results from a new three-dimensional numerical model coupling tectonics and landscape evolution, *Earth and Planetary Science Letters*, 284(3–4), 570–582, <https://doi.org/10.1016/j.epsl.2009.05.024>, 2009.
- Miller, S. R., Slingerland, R. L. and Kirby, E.: Characteristics of steady state fluvial topography above fault-bend folds, *J. Geophys. Res. Earth Surf.*, 112(4), 1–21, <https://doi:10.1029/2007JF000772>, 2007.
- Refice, A., Giachetta, E. and Capolongo, D.: SIGNUM: A Matlab, TIN-based landscape evolution model, *Comput. Geosci.*, 45, 293–303, <https://doi:10.1016/j.cageo.2011.11.013>, 2012.
- Sklar, L. and Dietrich, W. E.: River Longitudinal Profiles and Bedrock Incision Models: Stream Power and the Influence of Sediment Supply, in *Rivers Over Rock: Fluvial Processes in Bedrock Channels*, edited by K. J. Tinkler and E. E. Wohl, pp. 237–260, American Geophysical Union., <https://doi.org/10.1029/GM107p0237>, 1998.
- Tozer, R., Hertle, M., Petersen, H. I., and Zinck-Joergensen, K.: Quantifying vertical movements in fold and thrust belts: subsidence uplift and erosion in Kurdistan Northern Iraq, *Geological Society, London, Special Publications* 490 <https://doi.org/10.1144/SP490-2019-118>, 2019.
- Whipple, K. X. and Tucker, G. E.: Dynamics of the stream-power river incision model: Implications for height limits of mountain ranges, landscape response timescales, and research needs, *J. Geophys. Res. Solid Earth*, 104(B8), 17661–17674, <https://doi:10.1029/1999JB900120>, 1999.
- Wobus, C., Whipple, K. X., Kirby, E., Snyder, N., Johnson, J., Spyropolou, K., Crosby, B. and Sheehan, D.: Tectonics from topography: procedures, promise, and pitfalls, *Geol. Soc. Am. Spec. Pap.*, 398(04), 55–74, [https://doi:10.1130/2006.2398\(04\).](https://doi:10.1130/2006.2398(04).), 2006.
- Yanites, B. J., Becker, J. K., Madritsch, H., Schnellmann, M., and Ehlers, T. A.: Lithologic effects on landscape response to base level changes: A modeling study in the context of the eastern Jura Mountains, Switzerland, *Journal of Geophysical Research: Earth Surface*, 122. <https://doi.org/10.1002/2016JF004101>, 2017.